UNIVERSITY OF SOUTHAMPTON

FACULTY OF NATURAL AND ENVIRONMENTAL SCIENCES

School of Ocean and Earth Science

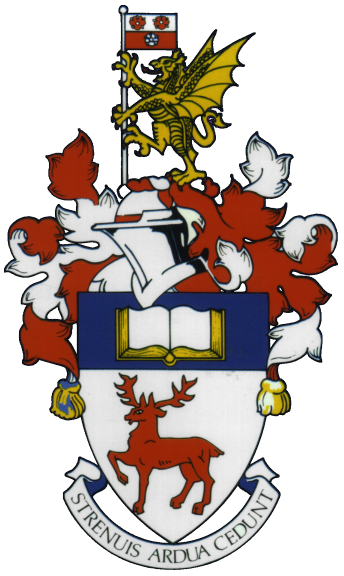

BORON ISOTOPES AS A PROXY FOR pH IN SILICEOUS AND CALCAREOUS MARINE ALGAE

by

Hannah Katie Donald

Thesis for the degree of Doctor of Philosophy

October 2017

UNIVERSITY OF SOUTHAMPTON

ABSTRACT

FACULTY OF NATURAL AND ENVIRONMENTAL SCIENCES
School of Ocean and Earth Science

Doctor of Philosophy

BORON ISOTOPES AS A PROXY FOR pH IN SILICEOUS AND CALCAREOUS MARINE ALGAE

by Hannah Katie Donald

Rising CO_2 in the atmosphere has directly led to a reduction in surface ocean pH - a process known as ocean acidification. There is a need to understand past climates in terms of ocean pH change in order to be able to relate these to the current effects of climate change on marine organisms. One way of doing this is by measuring boron isotopes in marine carbonates, such as foraminifera and corals, to estimate past ocean pH, and thus to infer past pCO_2. Key regions of atmospheric-ocean CO_2 exchange are the Southern Ocean and subarctic North Pacific, and they are also areas where modern ocean acidification is occurring fastest. The current application of the boron isotope proxy is restricted in these high latitude regions due to lack of calcareous organisms preserved in the sediment here. Therefore, there is a need to expand the boron isotope proxy into novel materials, such as diatoms and coralline algae, which are found in these key high latitude habitats in abundance.

This thesis aims to investigate whether the hard parts of marine algae (siliceous: diatoms; calcareous: coralline algae) are suitable archives for the boron isotope pH proxy. This is achieved by examining: (i) which boron species could be incorporated into the frustule/skeleton; (ii) the relationship between boron isotopic composition and seawater pH, and hence the sensitivity of boron isotopes in each organism to changes in seawater pH; (iii) the palaeo-archive potential of each organism. These aims are addressed by developing a method to measure boron isotopes and boron content of diatoms by MC-ICP-MS, calibrating the boron-pH relationships in a species of diatom using culturing experiments, applying this calibration to sedimentary diatoms collected from a core in the subarctic North Pacific, and also by investigating the relationship between boron isotopes and seawater pH in a species of coralline algae.

Contents

List of Figures

List of Tables

Declaration of Authorship

I, Hannah Katie Donald, declare that the thesis entitled ***'Boron isotopes as a proxy for pH in siliceous and calcareous marine algae'*** and the work presented in the thesis are both my own, and have been generated by me as the result of my own original research. I confirm that:

- this work was done wholly or mainly while in candidature for a research degree at this University;
- where any part of this thesis has previously been submitted for a degree or any other qualification at this University or any other institution, this has been clearly stated;
- where I have consulted the published work of others, this is always clearly attributed;
- where I have quoted from the work of others, the source is always given. With the exception of such quotations, this thesis is entirely my own work;
- I have acknowledged all main sources of help;
- where the thesis is based on work done by myself jointly with others, I have made clear exactly what was done by others and what I have contributed myself;
- part of this work has been published as:

  Donald, H.K., Ries, J.B., Stewart, J.A., Fowell, S.E., and Foster, G.L., (2017) Boron isotope sensitivity to seawater pH change in a species of *Neogoniolithon* coralline red alga. *Geochimica et Cosmochimica Acta* **217**, 240-253.

Signed:.....

Date:.....

"How inappropriate to call this planet 'Earth' when it is clearly 'Ocean'."
Arthur C. Clarke

"There are a whole lot of things in this world of ours you haven't started wondering about yet."
Roald Dahl

Acknowledgements

First of all I would like to extend huge thanks to my brilliant supervisor, Professor Gavin Foster, not only for taking a chance on a chemist who'd never even heard of diatoms before discovering this PhD project, but also for your instrumental guidance throughout my four years in Southampton. I am indebted to you for your advice and assistance, and I couldn't have asked for a better, more invested supervisor - thank you!

I would also like to say thank you to my co-supervisors Dr Alex Poulton and Professor Mark Moore for their help setting up all things biological, especially within very short time frames for the culturing experiments. Their guidance has been helpful and useful, and their discussions along with my panel chair Dr Steve Bohaty were invaluable. Thank you all. I would also like to thank Professor Heather Stoll and Professor Rachael James for examining my thesis and providing helpful comments in a great discussion to improve this work.

I have worked in so many different laboratories during this PhD project, and I want to acknowledge people who I've come across during these long, and often lonely, hours. Firstly to the wonderful B-team (Tom, Elwyn, Rachael, Eleni, Migue, Joe, Sara, Rosanna, Michael) - once in the B-team, always in the B-team! You all understand more than anyone else how much effort goes into working with boron, and I couldn't have wished for better people to spend all those days (and nights..!) on the Neptune with, or cleaning mounds of Teflon, or crawling on our hands and knees to ensure every last inch of the clean lab was boron-free. Next, special thanks go to Andy Milton, Matt Cooper and Agnes Michalik - the plasma lab and clean labs would not function without you! I'd also like to extend my gratitude to those who have helped me pretend to be a biologist - especially John Gittins (for helping me build gas rigs in the culture experiments), Mark Stinchcombe (for teaching me how to run nutrient samples), Matthew Humphreys (for running DIC samples), and Glaucia Fragoso, Chris Daniels and Lucie Munns (for teaching me how to culture diatoms from A to Z). I was also lucky enough to take on the responsibility of supervising Nico Fröhberg from Jacob's University in the final year of his undergraduate degree for 3 months. During this time, he worked incredibly hard and took everything in his stride, even when there were setbacks. I simply could not have completed the culture experiments without him, so thank you Nico - I predict a bright future in science ahead of you.

I would also like to thank my main collaborators during this PhD. I spent some time at the University of Nottingham with George Swann, who taught me so much about diatoms, and helped me turn a large blob of mud into pristine white diatoms. Justin Ries cultured the coralline algae samples I analysed in this project, and provided me with extensive feedback while writing my first peer-reviewed published paper (see Chapter 5). Kate Hendry not only provided me with several sponge samples for boron analysis, but also has been a very friendly and welcoming face at almost all of the conferences I have attended during my PhD - most notably at the annual Geochemistry Group Research

in Progress meetings. Thank you all for your help and guidance. I would also like to acknowledge the extended "boron family", who again I have come across regularly at conferences and meetings, and have provided me with very useful discussions - James Rae, Andrea Burke, Jess, Ben and Eloise.

To all of my friends (you know who you are): you've been brilliant during this rollercoaster ride! Thanks Cat, Lou and inflexible Tina for regular cups of tea and gossip, and wine and therapy. Thanks Heather for inspiring me, taking me on sunny sampling expeditions, and for being as obsessed with RuPaul's Drag Race as I am. Thanks Holly and Katie (and everyone else who's been through 166/03) for your wisdom and advice, and many baked goodies. Thanks Hannah, Juliette and Millie for delicious food and so much venting. Thanks Jen and Carolyn for our awesome time together on board the RRS James Clark Ross - I'll never forget it for as long as I live, I just wish I still had the muscles from all that exercising you made me do! Finally, thanks to all the girls in my Hoops netball team and Southampton University Chamber Choir - without singing and netball I would have been lost.

Will - how lucky it was to find you in our first week at NOC. Now, nearly four years later, I've found my total rock and best friend in you. Thanks for looking out for me this whole time, even though you had your own work to do too. Thanks for being my chauffeur, my chef, for taking me on adventures, and for letting me sail WAFI. You're the best.

Finally, my incredible family - mum, dad, Sophie you mean everything to me, and I literally could not have done this without you. I dedicate this work to you, mum and dad, for always believing in me, encouraging me in everything I take on, enabling me to seize every opportunity I can, for being genuinely and unwaveringly interested in my work, and for your endless love and support.

Chapter 1

Introduction

1.1 Project rationale

The high latitude oceans (subarctic North Pacific and North Atlantic, and Southern Ocean) play a crucial role in atmospheric CO_2 exchange on geological to human timescales (Takahashi et al., 1993), yet the full extent of this role remains to be completely understood. A powerful proxy method that has provided some key constraints in this regard (Martínez-Botí et al., 2015) is the boron isotope pH proxy. However, up to now, reconstructions of palaeo-atmospheric pCO_2 and past ocean pH using boron isotopes have almost exclusively been restricted to the well-preserved calcareous shells and skeletons produced by foraminifera and corals. However, there is a distinct lack of these organisms either inhabiting, or in the case of foraminifera, preserved at high latitudes. This geographic selectivity arises from the temperature restrictions on coral survivability (Freiwald et al., 2004; Orr et al., 2005) and the dominance of siliceous organisms such as diatoms in the surface waters of the high latitude oceans coupled with the corrosive nature of the bottom water in these regions (Figure 1.1). It is therefore required that the boron geochemistry of other substrates be explored, potentially facilitating the application of the boron paleo-proxies into these important, but currently understudied high-latitude regions. The central aim of this thesis is therefore to explore, largely for the first time, the boron isotopic composition of biogenic silica and the high-Mg skeleton of coralline algae.

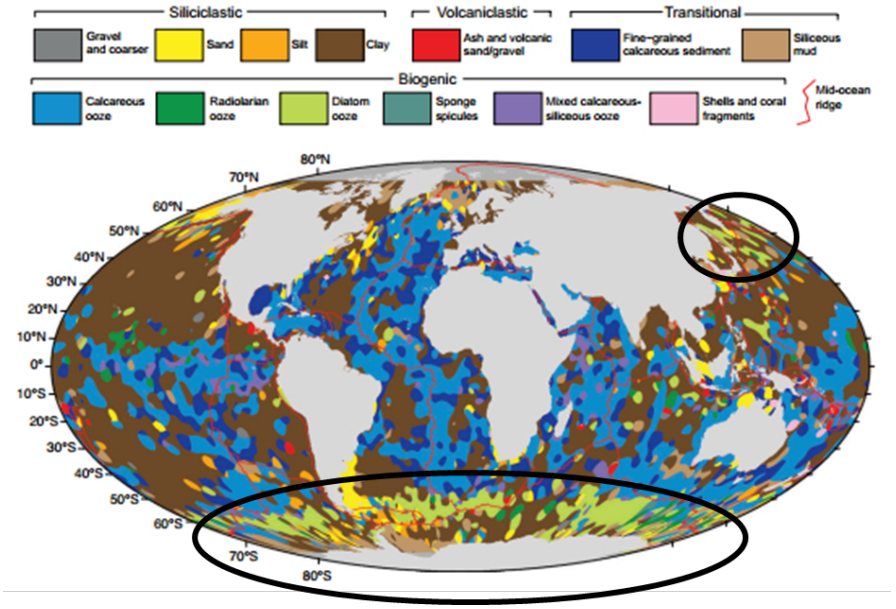

Figure 1.1: Digital map revealing major composition of global marine sediments adapted from Dutkiewicz et al. (2015). The black circles highlight that the Southern Ocean and North Pacific are dominated by siliceous sediments (greens), whereas the lower latitudes are dominated by calcareous material (blues).

While a number of studies are emerging examining the boron geochemistry of coralline algae (*e.g.* Feitzke et al., 2015; Cornwall et al., 2017), there are currently only a handful of studies involving the boron geochemistry of biogenic silica (Furst, 1981; Ishikawa and Nakamura, 1993; Mejía et al, 2013; de Leon, 2015), covering sponge spicules, siliceous ooze and diatoms. The current restriction of boron studies to organisms with calcareous shells and skeletons is largely driven by the available analytical techniques. Here, a new method is developed for measuring boron isotopes in diatom opal for the first time.

1.2 The importance and vulnerability of the high latitude oceans

The majority of the attention paid to the high latitude oceans concerns the fact that these regions are key areas of heat and carbon exchange between the ocean and atmosphere due to ocean circulation and the upwelling of deep water. In the following,

the key issues of ocean acidification over the last 100 years and atmospheric-ocean carbon exchange are discussed.

1.2.1 Ocean acidification

Since the beginning of the Industrial Revolution, humanity has released around 600 Gt of carbon through the burning of fossil fuel, deforestation, and cement making. Of this 600 Gt, around 35% has been absorbed by the ocean. The global ocean is able to capture this large portion of atmospheric CO_2 due to its buffering capability (equations 1.1 - 1.3).

$$CO_2 + H_2O \rightarrow H_2CO_3 \tag{1.1}$$

$$H_2CO_3 \rightarrow HCO_3^- + H^+ \tag{1.2}$$

$$HCO_3^- \rightarrow CO_3^{2-} + H^+ \tag{1.3}$$

However, as atmospheric CO_2 has been increasing rapidly since the Industrial Revolution, from 280 ppm to more than 400 ppm today (Doney et al., 2009; Bala 2013; Tans and Keeling, 2016), this has led to the imposition of changes upon ocean carbon chemistry (specifically an increase in protons), ultimately resulting in a reduction in seawater pH by 0.1 pH units (Figure 1.2). Climate models predict that by 2100, a high-end business as usual emission scenario (*i.e.* Intergovernmental Panel on Climate Change: Representative Concentration Pathway 8.5) will result in a global average surface pH_{sw} of ca. 7.8 (Figure 1.3), potentially reaching even lower levels at high latitudes. The cooler temperatures mean that CO_2 is more soluble in these high latitude regions than the rest of the global ocean. This has resulted, and will result, in a faster rate of ocean acidification at the high latitudes, making organisms that occupy these habitats vulnerable to large magnitude ocean acidification faster than organisms occupying warmer waters.

Ocean acidification affects biological processes within a number of marine organisms, such as the pH-dependent process of calcification, by reducing the $CaCO_3$ saturation state of seawater ($\Omega = [Ca^{2+}][CO_3^{2-}]/K^*_{sp}$; where K^*_{sp} is the stoichiometric solubility product of $CaCO_3$ at in situ conditions of temperature, salinity and pressure).

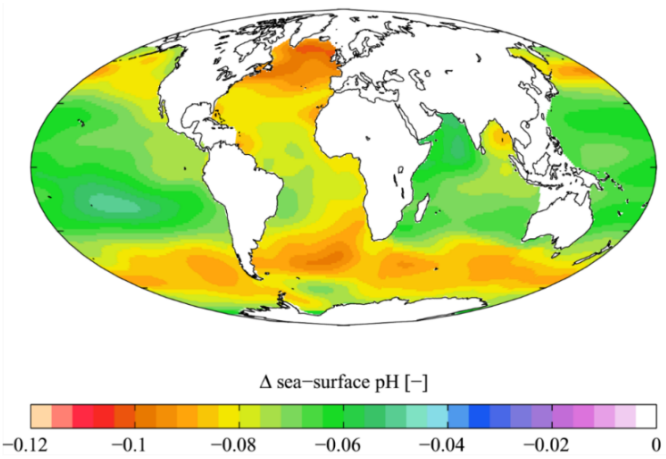

Figure 1.2: Map indicating surface ocean pH reduction between 1700 - 1990 (GLODAP and the World Ocean Atlas). The yellow and orange areas indicate a larger pH decrease, which are clearly concentrated at the high latitudes where CO_2 is more soluble in seawater.

Reductions in Ω of seawater have been shown to reduce calcification rates and increase solubility of the calcareous shells and skeletons of marine organisms (Sabine et al., 1995; Gattuso et al., 1998; Riebesell et al., 2000; Anthony et al., 2008; Hoegh-Guldberg et al., 2008; De'ath et al., 2009; Ries et al., 2009; Rodolfo-Metalpa et al., 2011; Ries et al., 2016), and some calcareous organisms have greater susceptibility to changes in Ω due to the increased solubility of their calcareous skeleton (*e.g.* high-Mg calcite of coralline algae; Ries et al., 2009). It is therefore perhaps unsurprising that the majority of ocean acidification research has focussed on investigating the reaction of calcifying organisms

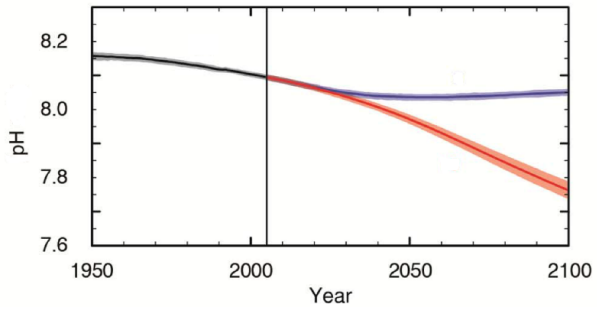

Figure 1.3: Figure from the most recent IPCC report, indicating potential future sea surface pH reduction. The blue line is indicative of a scenario involving immediate, large emission reductions, whereas the red line corresponds to the ocean acidification predicted during a business as usual scenario (IPCC RCP 8.5).

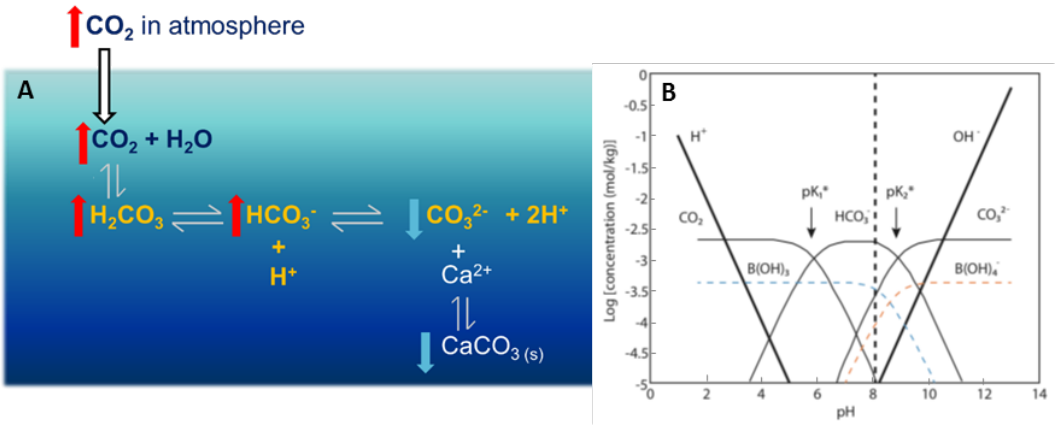

Figure 1.4: Carbon chemistry occurring in the ocean surface layers. As more CO_2 diffuses and dissolves into the surface ocean, more carbonic acid is formed (A). This affects the DIC equilibrium in the water column to produce more bicarbonate ions, and less carbonate ions, subsequently leading to dissolution of precipitated $CaCO_3$. (B) shows a Bjerrum plot of the equilibria associated with the oceanic carbonate system (Zeebe and Wolf-Gladrow, 2001).

to changing pH (Bach et al., 2011; Beaufort et al., 2011; Stoll et al., 2012). This multitude of studies agree, to different extents, that calcareous organisms are negatively affected by ocean acidification.

Despite this wealth of information regarding calcareous organisms, there has been a lesser focus on the response of siliceous organisms to a reduction in seawater pH, even though diatoms are one of the major primary producers in the oceans. They contribute approximately 45% of global primary production (Yang and Gao, 2012), and account for ca. 30% of carbon export to marine sediments (Smetacek, 1999), most notably in the northern and equatorial Pacific and in the opal-belt surrounding Antarctica (Figure 1.1, Figure 1.5). Only a small amount of the carbon that enters the biological pump is deposited to the seafloor, but diatoms play a vital role in this long-term carbon sequestration as they have a faster sinking velocity than other plankton (Miklasz and Denny, 2010). These phytoplankton also photosynthesise; a process which relies on the bioavailability of CO_2. In order to fully understand our future global carbon cycle and its associated biogeochemical feedbacks, it is therefore essential to understand the effects elevated pCO_2 and the associated reduction in surface pH will have on these marine algae.

Whilst palaeoceanography is a vital tool in determining reasons behind glacial-interglacial pCO_2 change, for example, new boron isotope measurements in marine algae

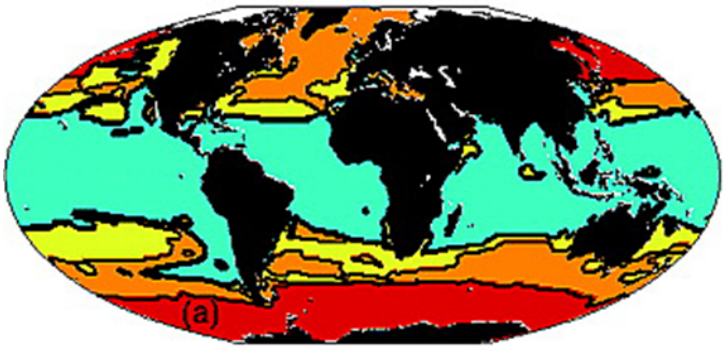

Figure 1.5: Map from Dutkiewicz et al. (2009) indicating dominance of diatoms (red colour) at high latitudes specifically in the Southern Ocean and North Pacific. Other dominant organisms are indicated by orange (other large phytoplankton), yellow (other small phytoplankton) and green (calcareous material) colours.

will also allow the effects of changing pCO_2 on these organisms to be resolved. Diatoms in particular represent a major source of primary production in the oceans, and consequently any environment changes they encounter will affect not only their internal biology, but also the ecosystems they are fundamental to. A decrease in oceanic pH may lead to amplified internal pH regulation, difficulties for transport proteins, and eventually evolutionary change. The current, unprecedented ocean acidification may also lead to changes in micro (and therefore macro) ecosystems, potentially disrupting oceanic food-chains as far as commercial fisheries, affecting humans domestically and economically on a global scale. It is therefore crucial to investigate and understand the effects of ocean acidification in these less-comprehensively studied marine organisms.

1.2.2 The exchange of CO_2 between the ocean and atmosphere in the high latitudes

High latitude oceans (namely the Southern Ocean, North Pacific and North Atlantic) are vital regions of gas exchange with the atmosphere (Figure 1.6). The modern Southern Ocean is a sink of CO_2 from the atmosphere where Antarctic Bottom Water (AABW) is formed, but deep waters also upwell in the Southern Ocean, acting as a source of CO_2. Seasonal stratification weakening in the subarctic North Pacific also allows sequestered CO_2 entrained in old, deep waters to upwell and be released to the atmosphere.

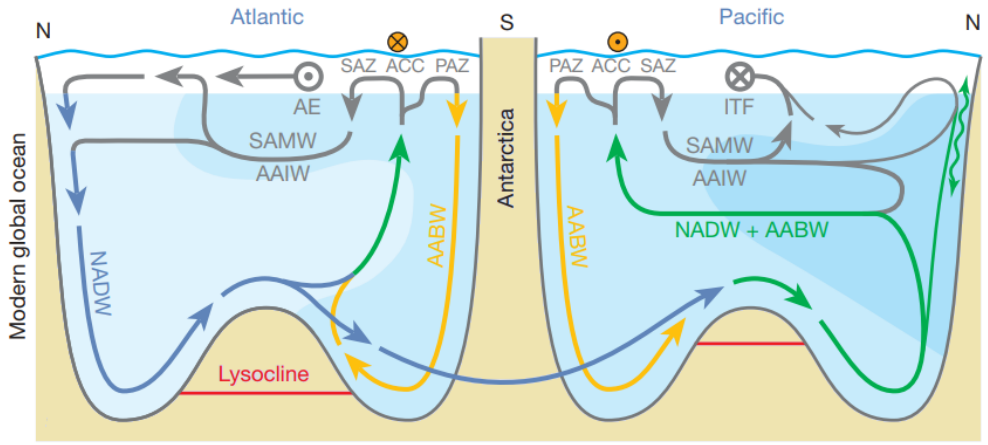

Figure 1.6: Cross section of the modern global ocean from Sigman et al. (2010) indicating the key high latitude regions of deep water upwelling and therefore CO_2 flux with the atmosphere are the Southern Ocean and the North Pacific. Abbreviations are as follows: SAZ (Subantarctic Zone), ACC (Antarctic Circumpolar Current), PAZ (Polar Antarctic Zone), AE (Agulhas Eddies), SAMW (Subantarctic Mode Water), AAIW (Antarctic Intermediate Water), NADW (North Atlantic Deep Water), AABW (Antarctic Bottom Water), ITF (Indonesian Through-Flow).

For example, the Southern Ocean alone absorbs ca. 1 billion tons of CO_2 per year, currently approximately half of all CO_2 absorbed by the global ocean per year. Where deep water upwells, these areas act as a source of CO_2 to the atmosphere, and allow ventilation of the deep ocean. Primary productivity is often stimulated in upwelling areas, as this leads to an influx of carbon- and nutrient-rich deep waters into the surface ocean, resulting in a positive feedback of algal blooms removing CO_2 from the atmosphere. The high latitude oceans play important roles in moderating global pCO_2 concentrations over glacial-interglacial cycles (Sigman and Boyle 2000; Sigman et al., 2010), such as the release of CO_2 to the atmosphere due to differences in water column stability and circulation. Nonetheless, the extent to which this regulation occurs and the link between these variations and other oceanic processes remains unclear (Sigman and Boyle 2000; Anderson and Archer, 2002; Fischer et al., 2010).

It is therefore clearly important to investigate high latitude oceans in more detail, and not only in terms of observing the current effects of ocean acidification. The use of geochemical proxies to investigate ocean sediments is a powerful palaeoceanographic tool, allowing reconstruction of past ocean conditions, and central to improving our understanding of why the high latitude oceans exert control over pCO_2 fluctuations are

palaeoceanographic archives of pCO_2 (*e.g.* Archer et al., 2000; Foster 2008). Boron isotope measurements in preserved organisms in high latitude sediments could allow us to infer pH of seawater in the past and therefore pCO_2 in these crucial regions (*e.g.* Spivack et al., 1993; Sanyal et al., 1996; Palmer, 1998; Martínez-Botí et al., 2015). However, these measurements have been restricted to mostly low latitudes due to the fairly large amount of well-preserved carbonate material they require, and the lack of this required material in high latitude sediments has precluded palaeo-pH reconstructions of these key areas (Figure 1.1).

1.3 Boron isotopes - a pH proxy

The boron isotope palaeo-pH proxy is based on the pH dependent relationship between aqueous species of boron in seawater and the subsequent uptake of boron by calcifying organisms. The proxy arises because (1) the abundance of the two major aqueous forms of boron in seawater are pH dependent (Dickson, 1990) and (2) there is boron isotope fractionation between these two boron species (Klochko et al., 2006). The following sections explain the aqueous chemistry of boron, and the analytical challenges that have been involved during the development of the proxy.

1.3.1 Aqueous chemistry of boron in seawater

Boron exists in seawater as two pH-dependent species; trigonal planar boric acid ($B(OH)_3$) and the tetrahedral tetrahydroxyborate anion (henceforth referred to as borate; $B(OH)_4^-$). Boric acid is dominant at low pH, and borate dominates at high pH in typical surface ocean conditions. The two species have been shown to be in equilibrium when pH = 8.60, where pK_B* (the dissociation constant) is measured at T = 25 °C and S = 35 (Figure 1.7; Dickson, 1990). Boric acid has a vacant p-orbital that is susceptible to nucleophilic attack, hence the neutral trigonal planar state can easily transform into an anionic tetrahedral species in an aqueous environment, where there is an excess of OH^-.

$$B(OH)_3 + H_2O \leftrightarrow B(OH)_4^- + H^+ \tag{1.4}$$

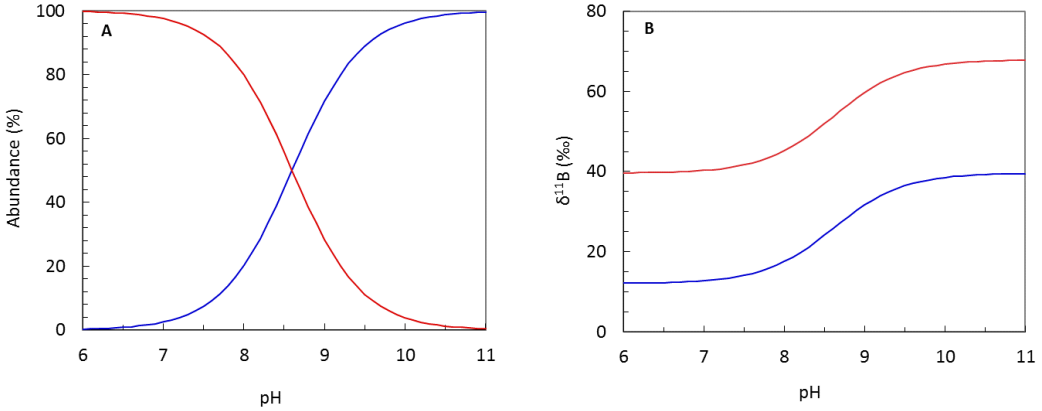

Figure 1.7: Plots describing (A) the pH-dependent relationship between the abundance of aqueous boron species, and (B) the isotopic fractionation observed between boric acid (red) and borate (blue) at T = 25 °C and S = 35.

The two stable isotopes of boron (^{10}B and ^{11}B) occur roughly in a 1:4 ratio, and the structural difference between the aqueous species leads to an enrichment of ^{11}B in boric acid of approximately 27.2 ‰ (Klochko et al., 2006; Nir et al., 2015). This fractionation is attributable to difference in bond strengths, as the more stable trigonal structure of boric acid has the stronger B-O bonds. When a hydroxide oxygen donates its electrons to form tetrahedral borate, these electrons enter a high energy π^* orbital, which reduces bond order and therefore weakens all four B-O bonds, and typically, heavier isotopes are more likely to be found in more stable molecules (equation 1.5).

$$^{10}B(OH)_3 + ^{11}B(OH)_4^- \leftrightarrow ^{11}B(OH)_3 + ^{10}B(OH)_4^- \tag{1.5}$$

Boron isotopic composition is described using the delta notation δ^{11}B relative to a boric acid standard (NIST SRM 951 boric acid according to Catanzaro et al., 1970) shown in equation (1.6).

$$\delta^{11}B(‰) = \left[\left(\frac{(^{11}B/^{10}B_{sample})}{(^{11}B/^{10}B_{standard})}\right) - 1\right] \times 1000 \tag{1.6}$$

Since the δ^{11}B of total boron in seawater (boric acid and borate) is constant at 39.61 ± 0.04 ‰ (Foster et al., 2010), as the proportions of boric acid and borate change with pH_{sw}, the δ^{11}B composition of each species also varies as a function of pH, with borate δ^{11}B increasing with pH_{sw} as described in equation (1.7), and boric acid δ^{11}B as

described in equation (1.8).

$$\delta^{11}B_{B(OH)_4^-} = \frac{\delta^{11}B_{sw} + \left(\delta^{11}B_{sw} - 1000(\alpha_B - 1)\right)10^{pK*_B - pH}}{1 + \alpha_B 10^{pK*_B - pH}} \tag{1.7}$$

$$\delta^{11}B_{B(OH)_3} = (\delta^{11}B_{B(OH)_4^-}.\alpha_B) + \varepsilon_B \tag{1.8}$$

Where pK^*_B is the dissociation constant (dependent on temperature and salinity; Dickson, 1990), $\delta^{11}B_{sw}$ is the δ^{11}B composition of total boron in seawater, $\delta^{11}B_{B(OH)4-}$ is the δ^{11}B composition of aqueous borate, and α_B is a constant (1.0272 ± 0.0006; Klochko et al., 2006; ε_B is 1000.α_B-1) describing the equilibrium boron isotope fractionation between boric acid and borate. In previous measurements, δ^{11}B has been shown to vary in different materials (Figure 1.8).

Boron is a conservative element in seawater with a concentration of 432.6 μmol L^{-1} (Lee et al., 2010). The major sources and sinks of boron in seawater were recently detailed in Greenop et al. (2017; Figure 1.9). As boron is a conservative element, and the modern sources and sinks are almost equal, modern δ^{11}B is in steady-state and well-mixed (Lemarchand et al., 2002).

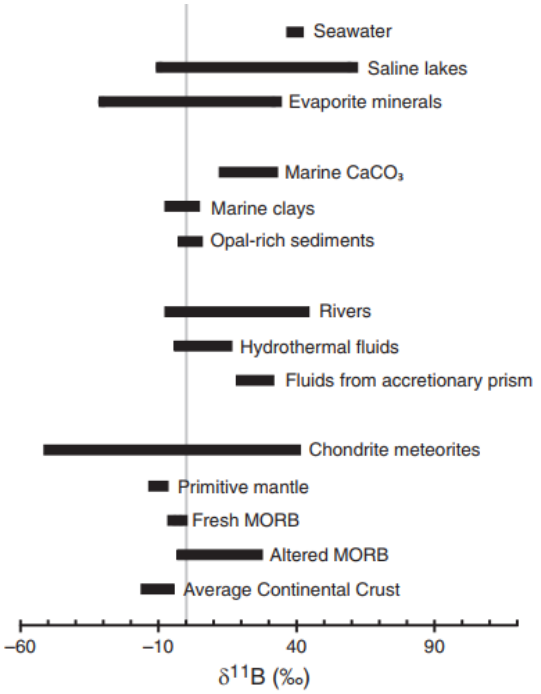

Figure 1.8: Compilation of various δ^{11}B values previously measured (Foster et al., 2016).

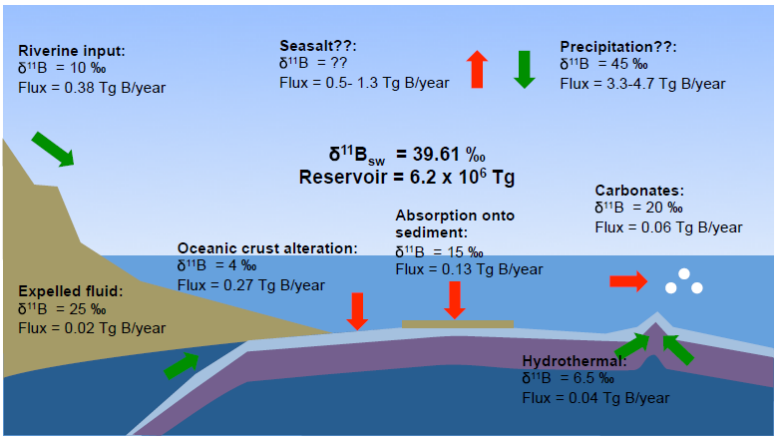

Figure 1.9: Major sources and sinks of boron in the modern ocean (Greenop et al., 2017).

1.3.2 Boron isotopes in marine carbonates

Marine carbonates, specifically foraminifera and corals, have been used in the development and progression of the boron isotope proxy for past ocean pH. One of the major assumptions involved with the boron proxy is that only the borate anion is incorporated into the calcium carbonate ($CaCO_3$) lattice (equation 1.9; Hemming and Hanson, 1992).

$$CaCO_{3(s)} + B(OH)_{4(aq)}^{-} \leftrightarrow Ca(HBO_3)_{(s)} + HCO_{3(aq)}^{-} + H_2O \tag{1.9}$$

The δ^{11}B of the carbonate sample can therefore replace the $\delta^{11}B_{B(OH)4-}$ in equation (1.10) in order to reconstruct the seawater pH that the organism was grown in. This has been fundamentally corroborated by culture studies that have examined the relationship between δ^{11}B of biogenic carbonate and seawater pH (*e.g.* Sanyal et al., 1996; Sanyal et al., 2001; Henehan et al., 2013).

$$pH = pK_B^* - log\left(-\frac{\delta^{11}B_{sw} - \delta^{11}B_{B(OH)_4^-}}{\delta^{11}B_{sw} - \alpha_B\delta^{11}B_{B(OH)_4^-}1000(\alpha_B - 1)}\right) \tag{1.10}$$

Although borate is assumed to be the most likely form of aqueous boron incorporated into $CaCO_3$, this assumption has led to contention. Whilst many examples of carbonate δ^{11}B have been shown to lie on or near to the aqueous borate line in Figure 1.7 (*e.g.* Sanyal et al., 1996; Sanyal et al., 2001; Foster, 2008; Henehan et al., 2013), there are

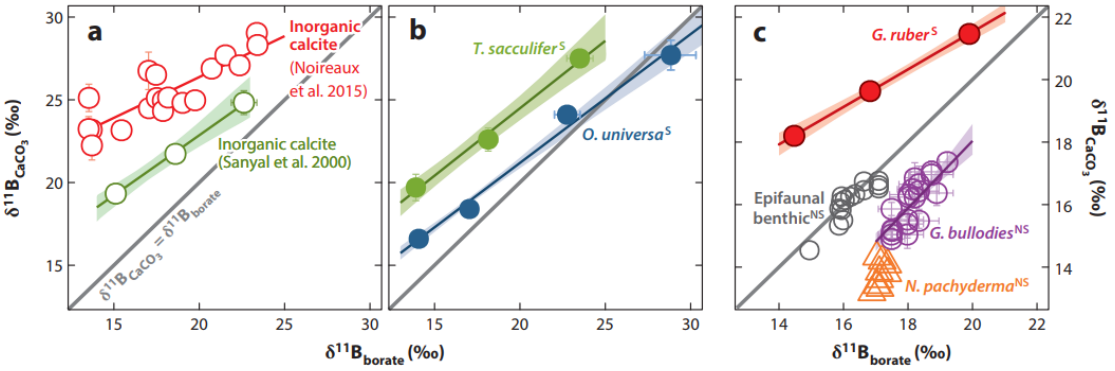

Figure 1.10: Plot showing calibrations between δ^{11}B of $CaCO_3$ and of aqueous borate investigated in several foraminifera species as well as inorganic calcite (Sanyal et al., 2000; Noireaux et al., 2015; Sanyal et al., 2001; Sanyal et al., 1996; Henehan et al., 2013; Rae et al., 2011; Yu et al., 2013; Martínez-Botí et al,. 2015).

also δ^{11}B examples of many biogenic carbonates that are elevated relative to the δ^{11}B of seawater borate (*e.g.* Vengosh et al., 1991; Gaillardet and Allègre, 1995; Anagnostou et al., 2012; McCulloch et al., 2012; Henehan et al., 2013; Holcomb et al., 2014) as observed in Figure 1.10. Some studies have attributed this offset from the δ^{11}B borate line to the incorporation of boric acid as well as borate (Klochko et al., 2009; Noireaux et al., 2015). Several ^{11}B magic angle spinning nuclear magnetic resonance (MAS NMR) spectroscopy studies have concluded that there are both tetrahedrally- and trigonally-co-ordinated boron species observed within the $CaCO_3$ lattice (Rollion-Bard et al., 2011; Cusack et al., 2015; Noireaux et al., 2015; Balan et al., 2016). However, the presence of trigonal boron species alone does not corroborate their origin; these boron species may not originate from boric acid, but instead be derived from a co-ordination change and deprotonation of borate (Balan et al., 2016). Offsets in biogenic carbonate δ^{11}B (especially in corals) are therefore thought to be predominantly caused by the elevation of internal pH in order to aid calcification (*e.g.* McConnaughey and Falk, 1991; McCulloch et al., 2012). In this case, the pH of the calcifying fluid can be calculated using boron isotopes rather than seawater pH in equation (1.10).

1.3.3 Boron isotopes: pCO_2 reconstruction

Being able to reconstruct palaeo-pH accurately and precisely using boron isotopes is required for the subsequent step of pCO_2 reconstruction. This is important as

ice core pCO_2 records are limited to the last ca. 800 kyr, and in order to understand our potential future climate change, we must be able to examine data from further back in time in order to identify patterns and links between systems, as well as examine analogues for the near future precedent of > 400 ppm atmospheric pCO_2.

In reconstructions, sea surface pH must be known from the boron isotope measurements (using equation 1.10), along with one other carbonate system variable (*i.e.* alkalinity or total dissolved inorganic carbon) to calculate aqueous CO_2 and hence atmospheric pCO_2 (Pearson and Palmer, 2000). Care must therefore be taken, as alkalinity and DIC also vary throughout geological time, so the more accurate and precise the boron isotopes and second carbonate system parameter, the better the reconstruction. The boron proxy has been shown to be able to reproduce pCO_2 measured in ice cores, and it is this accuracy that affords its reliability in reconstructing older pCO_2 (*e.g.* Pearson and Palmer, 2000; Pagani, 2002; Honisch and Hemming, 2005; Pagani et al., 2005; Foster, 2008; Honisch et al., 2009; Badger et al., 2013; Martínez-Botí et al., 2015).

1.4 Boron in plants

Boron is known to be an essential element for terrestrial plants, as well as diatoms (Marschner, 1995), as it is thought to be involved in the plant metabolism, cell wall synthesis and structural integrity (Goldbach et al., 2001; Goldbach and Wimmer, 2007). The absence of boron in soils causes deficiency problems in plants, but boron toxicity has also been shown to limit growth (Camacho-Cristóbal et al., 2008). This balance between deficiency and toxicity is exacerbated as boron has limited mobility within higher plants (Brown and Shelp, 1997). As in most biological processes, the lighter ^{10}B is able to move faster within plants, although boric acid has been revealed as the likely source of boron to terrestrial plants as it is able to passively diffuse through plant roots (Brown and Shelp, 1997).

1.5 Marine algae

Marine algae differ from corals and foraminifera used previously in boron proxy reconstructions as they photosynthesise and utilise carbon concentrating mechanisms (CCMs), and do not build their hard parts from vacuolised seawater. CCMs vary between species, but the primary mechanism of interest is that some marine phytoplankton (including diatoms) can actively uptake bicarbonate ions and convert this carbon into CO_2 if seawater pCO_2 is too low in order to perform photosynthesis efficiently. These biological processes have the potential to produce unexpected δ^{11}B-pH relationships as studies are sparse in which marine plants have been examined in detail with regards to boron uptake and boron isotopic fractionation (*e.g.* Mejía et al., 2013). This thesis aims to expand current knowledge of boron systematics within marine algae - specifically diatoms and coralline algae.

1.5.1 Biogenic silica

Biogenic silica is abundant in high latitude sediments, most notably in the opal-belt of the Southern Ocean, and in the North Pacific, and the biogenic silica found in these areas is largely from diatom origin. However, the only previous study measuring boron isotopes in biogenic silica is Ishikawa and Nakamura (1993), in which they measure δ^{11}B in bulk siliceous ooze (Figure 1.8). There are currently no studies in the literature investigating δ^{11}B of diatoms where pH is known and/or controlled, or of the diatom fraction preserved in sediment cores.

Interest in the use of biogenic silica in palaeo-proxies has increased recently, most notably focussing on silicon and nitrogen isotopes as a proxy for silicon and nitrogen utilisation (*e.g.* De La Rocha, 2006; Leng and Swann, 2010; Egan et al., 2012; Hendry et al., 2014). This is especially the case where well-preserved carbonate organisms are sparse but, despite this recent attention, biogenic silica remains an under-used resource when compared to marine carbonates in palaeoceanography. Diatoms play a large role in numerous biogeochemical cycles in the global ocean, and they are especially important in documenting changes in the high latitudes, including attributing some of

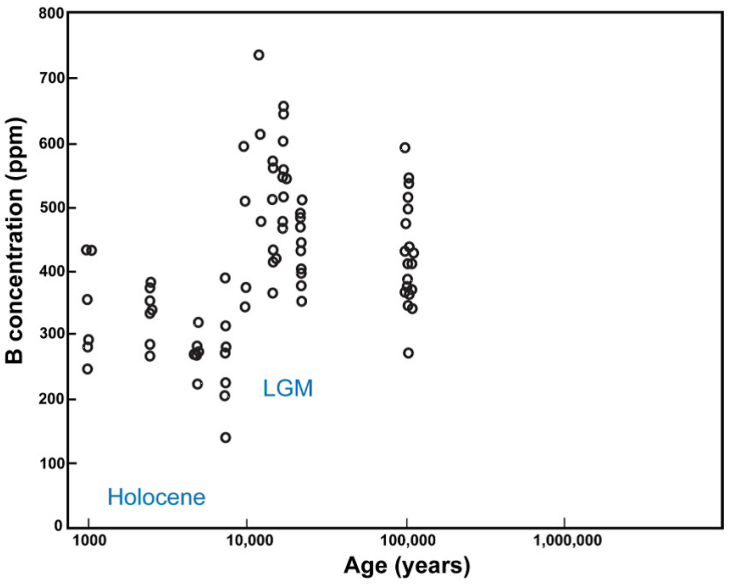

Figure 1.11: Boron concentration of sponge spicules plotted against age from Furst (1981).

the difference between glacial and interglacial pCO_2 levels to an increased marine silica input, leading to increased diatom and reduced coccolith populations during glacial periods.

Palaeoceanographic studies of the boron content of sedimentary opal are extremely limited (Furst, 1981; de Leon, 2015). Figure 1.11 shows this study that determined the boron content of glacial and interglacial sponge spicules from sediments in the North Atlantic. Furst found that there was a distinction between glacial (ca. 350 - 750 ppm) and interglacial (ca. 150 - 450 ppm) boron concentrations. No boron isotope or concentration data exists for sedimentary diatom opal but diatoms belonging to the species *T. weissflogii* and *T. pseudonana* were shown by Mejía et al. (2013) to have a higher boron content at higher pH_{sw}. These authors concluded that this feature indicated borate active transport into the cell with bicarbonate ions. This suggests that, as in marine carbonates, boron in diatoms is at least partially controlled by pH_{sw}.

1.5.1.1 Diatoms

Diatoms remove silicon from seawater to construct their outer cell walls (frustules), and the largest fluxes in the oceanic silicon cycle are primarily driven by diatom biological activity (Tréguer et al., 1995). The dissolution rate of diatom frustules within

the water column balanced with the rate of silica burial also plays a large role in the silicon cycle in returning silicon to solution. Frustule dissolution rates are higher in seawater diatoms than freshwater diatoms, indicating the catalytic effect of ions found in seawater on silica dissolution (*e.g.* Na^+ and Mg^{2+}; Loucaides et al., 2008). The alkaline nature of seawater consequently enhances oceanic silicon recycling ability, with only ∼5 - 7% sediment burial occurring on average (Loucaides et al., 2008). Silicon is present in seawater as dissolved amorphous silica (SiO_2; Dove et al., 2008). Its speciation is controlled by the kinetics of hydrolysis, as shown by equations 1.11 - 1.13. $Si(OH)_4$, or orthosilicic acid, is a diprotic acid according to equations 1.12 and 1.13 (Exley and Sjöberg, 2014). It is widely reported in the literature that silicon principally exists as $Si(OH)_4$ in solution at pH lower than 9.47 (*e.g.* Isshiki et al., 1991; Hammad and Ibrahim, 2012; Exley and Sjöberg, 2014). Silica can only complex Na^+ under certain conditions (Tanaka et al., 2014), ensuring that this ionic interaction does not interfere with the speciation process. Since silica is hydrolysed in seawater, there has been much debate concerning which species is utilised by diatoms to construct their frustules. Previous studies of silicon uptake in diatoms proposed that $SiO(OH)_3^-$ was transported across the membrane (Tanaka et al., 2013). However, this dissolved form of silicon only accounts for approximately 3% of the total dissolved silicon in seawater (Del Amo and Brzezinski, 1999). As $Si(OH)_4$ is far more bioavailable, it seems likely that evolutionary adaptation would have favoured the use of the more abundant $Si(OH)_4$, ultimately requiring less energy input.

$$SiO_{2(s)} + 2H_2O \rightarrow Si(OH)_4 \tag{1.11}$$

$$Si(OH)_4 \rightarrow SiO(OH)_3^- + H^+ \tag{1.12}$$

$$Si(OH)_4 \rightarrow SiO_2(OH)_2^{2-} + 2H^+ \tag{1.13}$$

Diatoms polymerise $Si(OH)_4$ to construct their frustules out of biogenic silica. $Si(OH)_4$ is taken up by diatoms *via* active transport through silicon transporter (SIT) proteins (Del Amo and Brzezinski, 1999) because the silicic acid concentration in seawater is typically low at ∼3-70 μM (Tréguer et al., 1995). Transmembrane SITs require Na^+ to function, aiding active uptake by introducing a charge difference (Figure 1.12; Del Amo

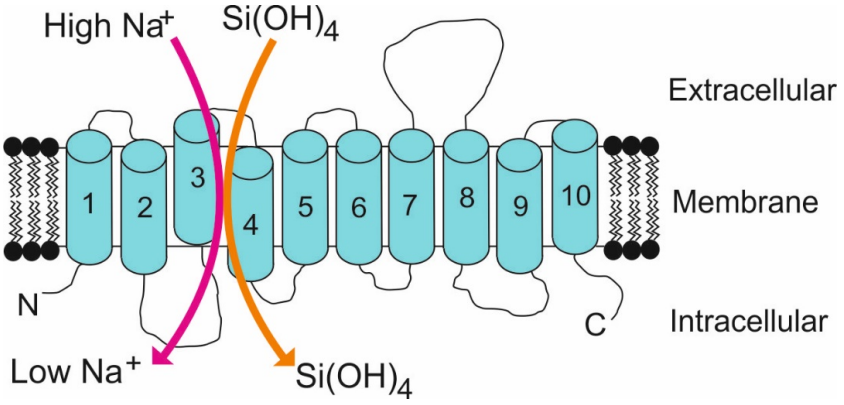

Figure 1.12: Silicic acid transport across the diatom membrane (adapted from Kröger and Poulsen, 2008).

and Brzezinski, 1999).

Once $Si(OH)_4$ has entered the cell, it is believed to accumulate in storage vacuoles. These tend to have relatively high pH in order to prevent polycondensation of $Si(OH)_4$ at its higher concentration inside the vacuole (Vrieling et al., 1999). The accumulated $Si(OH)_4$ is transported to the silicon deposition vesicle (SDV) - an acidic compartment where formation of biogenic silica and construction of the frustule occurs.

The low pH of the SDV encourages polycondensation, but also prevents dissolution of biogenic silica. This acidity also helps to avoid Ostwald ripening, where fewer larger molecules are formed in favour of many smaller molecules, disrupting frustule construction (Vrieling et al., 1999). Low pH within the SDV encourages polymerisation of $Si(OH)_4$, but this reaction is also kinetically favoured (Figure 1.13). Siloxane bonds (Si-O) are shown to be shorter than expected (1.64 ± 0.03 $\AA$; Oberhammer and James, 1980) indicating some ionic character. Shorter bonds indicate stronger interactions, and release of a small molecule (in this case water) is kinetically favoured. These characteristics demonstrate the spontaneity of this reaction, and show that biogenic silica formation is favoured.

During biosilicification, biogenic silica combines with matrix proteins, such as silaffins and silacidins (Richthammer et al., 2011; Otzen, 2012; Pamirsky and Golokhvast, 2013). Due to their zwitterionic nature, both proteins undergo supramolecular self-assembly, and are rich in phosphorylated serine residues that aid silica precipitation. The amount of these proteins within the frustule has been shown to depend on the aqueous environment, with a greater number of silacidins present in silicic acid limited

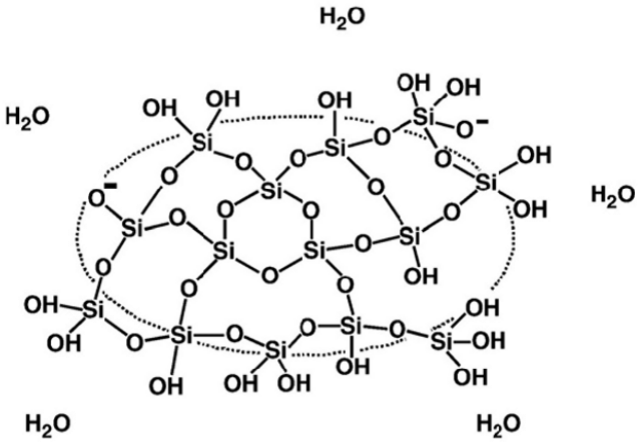

Figure 1.13: The lattice formation of biogenic silica in diatom opal, indicating tetrahedral silica polymer and amorphous silica.

conditions (Richthammer et al., 2011). This demonstrates a natural feedback mechanism within the diatom to allow it to survive in silicon-deficient environments. Long chain polyamines (LCPAs) are also involved in the biosilicification process. LCPAs stabilise the highly concentrated $Si(OH)_4$ as a sol because they are amphiphilic (Brunner et al., 2009). During biogenesis, the frustule is constructed within the SDV, which expands to contain the new cell wall. Exocytosis occurs in preparation for the separation of the two daughter cells in the final stage in the biosilicification cycle (Figure 1.14; Baeuerlein, 2000).

Although silica speciation in seawater is pH dependent, $Si(OH)_4$ is the only known bioavailable form of soluble silicon (Exley, 1998; Exley and Sjberg, 2014). As $Si(OH)_4$ accounts for 94.6% of the silicon species in seawater (Exley and Sjöberg, 2014), a change in pH will not affect this speciation enough to change the Si species taken up by diatoms. However, during the process of ocean acidification, a decrease in pH of ocean surface layers may lead to a positive or negative effect on the biological processes of diatoms.

A decrease in pH means an increase in the concentration of protons, $[H^+]$, in seawater. Many transmembrane proteins require proton pumps, so the intrinsic physiology of the diatom cell may be affected. As H^+ is transported into the SDV in diatoms for frustule construction, maintaining this acidic pH may become easier at lower pH, as more H^+ are bioavailable, resulting in a lower energy cost for the diatom. Biogenic silica is indeed formed in an acidic environment (Vrieling et al., 1999), suggesting that

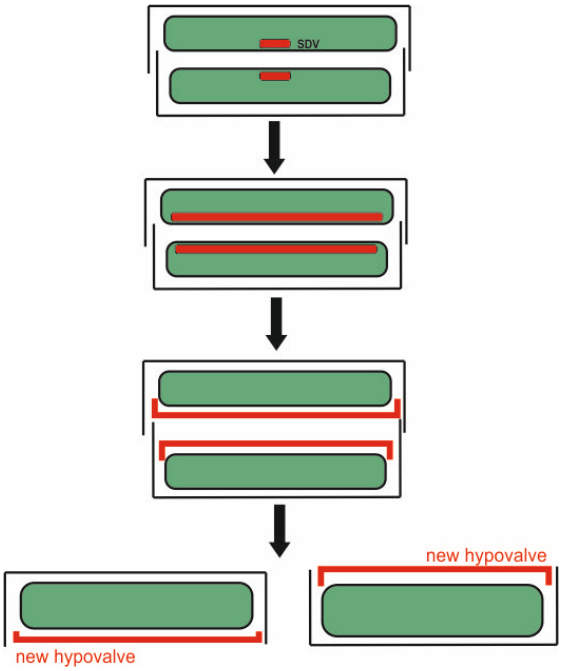

Figure 1.14: Division of a diatom cell involving the SDV (adapted from Kröger and Poulsen, 2008).

low pH is favourable for frustule maintenance. Ocean acidification may therefore benefit diatoms in the short-term by reducing frustule dissolution. As a result of this, diatoms may outcompete other phytoplankton, leading to alterations in marine ecosystems.

If frustule dissolution is also reduced with reducing pH_{sw}, eventually less silicon will be efficiently recycled within the water column. The amount of silicon reaching sediments will increase, lengthening the time taken to re-enter the silicon cycle, possibly instigating a global silicon deficiency if reduced pH_{sw} is maintained for longer than the residence time of Si in the oceans. This has significant implications for many processes, including diatom phosphate uptake for instance, where essential biological processes will be disrupted during growth and the buffering capability of diatoms in the surface ocean will be reduced, exacerbating ocean acidification (Exley, 1998). Ultimately however, diatoms may then export more carbon to ocean sediments, altering the carbonate chemistry of the surface ocean in such a way as to encourage CO_2 drawdown from the atmosphere, mediating further ocean acidification. Regardless, the importance of pH to diatoms and global biogeochemical cycles is yet to be fully explored, and is rarely considered on human or geological timescales.

As noted above, there is relatively little dissolved CO_2 in the oceans so in order

to photosynthesise efficiently, diatoms utilise CCMs (Hopkinson et al., 2011). CO_2 is a small uncharged molecule, and can therefore diffuse across lipid bilayers easily. This diffusion accounts for some carbon acquisition by diatoms, but the rest is achieved by active uptake of bicarbonate. Bicarbonate is transported into diatoms through transmembrane proteins of the solute carrier (SLC4) family, which use Na^+ and Cl^- ions in exchange and co-transport (Nakajima et al., 2013), and this transport increases when pH_{sw} increases due to CCMs.

Although boron has been measured in clean diatom frustules in one previous study (Mejía et al., 2013), how it is co-ordinated within the silica lattice structure is unknown. The borate anion has a very similar size and tetrahedral structure to $Si(OH)_4$, but despite this complementary shape, SIT proteins cannot transport borate into the cell as it is a charged species. Bicarbonate has a single negative charge, so if active transport is involved in boron uptake in diatoms, bicarbonate SLC4 transporters are the most likely point of entry to the cell (Mejía et al., 2013).

Boron could gain entry to the diatom cell *via* two mechanisms; either the passive diffusion of boric acid or the active uptake of the borate anion. Since diffusion of boric acid will occur regardless, and is unlikely to be associated with the increasing boron content of the diatom frustule with increasing pH_{sw} (Mejía et al., 2013), this could indicate that both boron species are involved, invoking a change in dominance at different pH_{sw}. Since the isotopic composition of these two species is very different, $\delta^{11}B$ of diatom opal is likely a sensitive tracer of which species is indeed incorporated, and hence also to pH_{sw}, upon which the initial $\delta^{11}B$ ultimately depends.

Measuring $\delta^{11}B$ of diatoms may therefore provide valuable insights into the following; (i) how boron enters the diatom cell; (ii) what relationship boron isotopes within diatoms have with seawater pH, and therefore whether $\delta^{11}B_{diatom}$ can be used to reconstruct past oceanic pH in $CaCO_3$ deficient regions; and (iii) whether $\delta^{11}B$ can be used to examine internal pH modification, and therefore the effect of ocean acidifcation on biosilicification in diatoms.

1.5.2 Coralline algae

Coralline algae are a vital primary producer found in coral reefs, and crucially occupy high latitude habitats (McCoy and Kamenos, 2015). These marine algae are composed of high-Mg calcite, which is more soluble than other $CaCO_3$ (Ries et al., 2016), and this combined with the increased solubility of CO_2 in cooler waters means ocean acidification therefore poses a serious threat to coralline algae and the ecosystems that depend on them (Kuffner et al., 2008; Gao and Zheng, 2009; Ragazzola et al., 2012).

Several studies have investigated the influence of ocean acidification on the nature and rate of calcification in a variety of coralline red algae (Hall-Spencer et al., 2008; Martin and Gattuso, 2009; Roleda et al., 2015; Cornwall et al., 2017). The responses recorded differ in extent, but all coralline algae showed negative effects conferred as a result of a reduction of seawater pH. Despite the varied responses between species, a common result was that the organism was able to continue to calcify at reduced seawater pH, even if the rate of calcification was vastly reduced (Borowitzka, 1981; Semesi et al., 2009; Comeau et al., 2013). This shows calcifying algae have mechanisms similar to corals with which to increase their internal pH (pH_{cf}) to aid calcification. Therefore, coralline algae are able to mitigate moderate ocean acidification, which has been shown to lead directly to coralline algae survival in natural ecosystems affected by a reduction in seawater pH (Kamenos et al., 2016). This resilience mechanism may stem from biological processes within the algae, as they perform both calcification and photosynthesis (*e.g.* Buitenhuis et al., 1999). The balance between these processes may explain why they are able to continue to calcify at high pCO_2 despite the decrease in seawater pH, as more photosynthesis is able to occur, providing extra energy for calcification and increasing local pH through the removal of dissolved CO_2 (*e.g.* Smith and Roth, 1979; Bowes, 1993; Gao et al., 1993; Hurd et al., 2011; Martin et al., 2013; Castillo et al., 2014).

Only two recent studies have previously investigated $\delta^{11}B$ of coralline algae. Fietzke et al. (2015) measured *Clathromorphum nereostratum via* laser ablation inductively coupled plasma mass spectrometry (LA-ICP-MS) and revealed that skeletal $\delta^{11}B$

within this species is consistent with a pH_{cf} that is significantly higher than measured ambient seawater pH as seen in corals (by ca. 0.6 pH units), suggesting an increase of internal pH may play a similarly important role in coralline algal calcification. However, skeletal $\delta^{11}B$ data for coralline algae species cultured under a range of controlled seawater pH conditions that demonstrate the response of internal pH to changes in seawater pH are currently sparse. The only other such study to date by Cornwall et al. (2017) measured the $\delta^{11}B$ of three species of coralline algae (the crustose *Neogoniolithon* sp. and *Sporolithon durum*, and the branching *Amphiroa anceps*) using MC-ICP-MS. This study also revealed the internal pH of all three species was elevated compared with seawater pH, and the $\delta^{11}B$ measurements showed a similar relationship with seawater pH as with other marine carbonates.

1.6 Thesis outline

The key objective for this PhD project is to expand the utility of the boron isotope palaeo-pH proxy by measuring $\delta^{11}B$ in organisms that have not been typically used in reconstructing past pH and pCO_2 before. This work includes the investigation of diatoms and coralline algae, which both crucially occupy high latitude habitats. Ultimately, this work could allow high-resolution pH and pCO_2 records to be reconstructed in the key high latitude regions where well-preserved carbonates are scarcely found in sediments.

1.6.1 Chapter 2: Developing a method to measure boron isotopes in diatom opal by MC-ICP-MS

Chapter 2 describes the method development for measuring boron isotopes in diatoms using MC-ICP-MS for the first time. Key questions addressed:

Q1. Can boron isotopes be measured in diatoms using MC-ICP-MS?

Q2. If so, can $\delta^{11}B$ be measured in diatoms accurately and with comparable reproducibility to marine carbonates?

1.6.2 Chapter 3: Investigating the relationship between seawater pH and boron isotopes in cultured diatoms (*Thalassiosira weissflogii*)

In chapter 3, a species of diatom (*T. weissflogii*) is batch cultured at five different pH values (controlled using bubbled pCO_2). The new MC-ICP-MS method to measure δ^{11}B is applied, and the relationship between seawater pH and δ^{11}B is assessed. Key questions addressed:

Q3. How could ocean acidification affect T. weissflogii diatoms?

Q4. What is the relationship between $\delta^{11}B$ and seawater pH in diatoms?

Q5. By what mechanism could this relationship occur?

1.6.3 Chapter 4: Boron isotopes in sedimentary diatoms (*Coscinodiscus marginatus* and *C. radiatus*) from 2.85 - 2.52 Ma in the subarctic Northwest Pacific (ODP Site 882)

Chapter 4 explores the application of the new method to measure δ^{11}B and B/Si in biogenic silica to reconstruct surface water pH in diatoms from sediment ODP Site 882 in the subarctic Northwest Pacific. Key questions addressed:

Q6. Can $\delta^{11}B$ measured in diatoms be used to accurately reconstruct past ocean pH?

Q7. What can the new $\delta^{11}B_{diatom}$ data tell us about the effect of the onset and intensification of Northern Hemisphere Glaciation in the subarctic Northwest Pacific?

1.6.4 Chapter 5: Boron isotope sensitivity to seawater pH change in a species of *Neogoniolithon* coralline red alga

Chapter 5 investigates the relationship between seawater pH and δ^{11}B measured in coralline red algae (*Neogoniolithon* sp.) in order to test the palaeo-archive potential of coralline algae. Key questions addressed:

Q8. How could coralline algae (Neogoniolithon sp.) be affected by ocean acidification?

Q9. Does $\delta^{11}B$ measured in coralline algae behave in a similar way to that measured in coral?

Q10. Do coralline algae hold potential as palaeo-archives?

1.6.5 Chapter 6: Concluding remarks

Chapter 6 is a synoptic chapter in which the conclusions of chapters 2-5 are synthesised. The questions listed above are revisited, and future avenues to explore following the work described in this thesis are also discussed.

Chapter 2

Developing a method to measure boron isotopes in diatom opal by MC-ICP-MS

Acknowledgements:

Gavin Foster (Monte Carlo simulation for standard addition, discussion and feedback)

George Swann (delivered training in diatom extraction from sediment)

Michael Henehan and Luz Maria Mejía (discussion about diatom cleaning method)

Claus-Dieter Hildebrand (collected sample TC460 from core PC460)

2.1 Introduction

The boron isotope palaeo-pH proxy has been used extensively to reconstruct past ocean pH and the oceanic carbon cycle (*e.g.* Spivack et al., 1993; Sanyal et al., 1996; Palmer, 1998; Foster, 2008; Henehan et al., 2013; Martnez-Bot et al., 2015). However, measuring boron isotopes is well recognised as a challenge. The methods used in this proxy have developed rapidly since the first high-precision boron isotope analysis using positive thermal ionisation mass spectrometry in the 1980s (PTIMS; *e.g.* Ramakumar et al., 1985). A method using negative thermal ionisation mass spectrometry was developed in the late 1980s (NTIMS; *e.g.* Vengosh et al., 1991; Hemming and Hanson, 1992; Hemming and Hanson, 1994) allowing smaller sample sizes to be measured, and finally,

boron isotopes measured by multi-collector inductively coupled plasma mass spectrometry (MC-IPC-MS) was pioneered in marine carbonates by Lécuyer et al. (2002) and developed further by Foster (2008). This method involves separating the sample from the matrix, removing the risk of any potential analytical mass bias, but with additional complexities relating to boron purification and memory in the ICP-MS (see Foster et al., 2013 for full discussion). These developments in analytical procedure in particular have improved accuracy, precision and utility of boron isotope measurements, leading to a growth in the application of the methodology to reconstruct past ocean pH, and in some cases, past atmospheric pCO_2.

Boron isotope- and boron concentration-based reconstructions of past climate are usually carried out on biogenic $CaCO_3$, and extensive boron isotope work has been carried out in particular on foraminifera and deep-sea and tropical corals (*e.g.* Hemming et al., 1998; Foster, 2008; Krief et al., 2010; Rollion-Bard et al., 2011; Rae et al., 2011; Anagnostou et al., 2012; McCulloch et al., 2012; Henehan et al., 2013; Holcomb et al., 2014; Martínez-Botí et al., 2015). Carbonates, however, are not the only bio-mineral produced by marine organisms. In order to fully exploit the boron isotope-pH proxy, organisms that precipitate biogenic opal, such as diatoms, need to be explored as this will open up a number of regions to study. The high latitude oceans are of particular importance, and currently contain little or no calcifying organisms.

Diatoms are generally under-utilised in palaeoceanography with respect to the commonly applied proxies (such as oxygen and carbon isotopes), due to a number of analytical difficulties. This group of siliceous organisms has understandably been extensively used for silicon isotope analysis where past productivity related to silicic acid utilisation has been explored (*e.g.* De La Rocha et al., 1998; Wischmeyer et al., 2003; Leng et al., 2009; Egan et al., 2012; Hendry and Brzezinski, 2014). Carbonates have been historically used for palaeo proxy development as calcareous organisms are directly involved in the carbon cycle. Whilst diatoms occupy the same habitats and are involved in similar global cycles as foraminifera, diatoms tend to dominate export production due to their fast growth and high nutrient uptake rates (Smetacek, 1999). However, before diatoms can be used for boron isotope work, analytical methods developed for carbonates need to be adapted to a siliceous matrix, and this novel method is outlined

in the following chapter.

2.2 Methods

Following previous boron isotope studies, here all sample handling and analyses were carried out in boron-free class 100 HEPA (high efficiency particulate air) filtered clean laboratories at the University of Southampton. All sample preparation took place entirely in over-pressured laminar flow hoods with individual boron-free HEPA filters fitted. Clean suits and gloves were worn at all times, and great care was taken with the preparation and handling of all samples to reduce any possibility of physical contamination; for example, pipette tips were always handled using acid-cleaned plastic tweezers and never allowed to touch any surface. The rinsing of labware and preparation of lab reagents required the use of MilliQ distilled water (EMD Millipore Q-Gard, 18.2 Ω, <5 ppb TOC), removing boron-based impurities from impacting sample analysis. Contamination potential was frequently monitored using total procedural blanks (TPB) measured in every batch of columns run. The TPB comprised an equivalent volume of sodium hydroxide (NaOH, 0.5 M) as used in the addition of samples to columns within a particular batch (ca. 0.2 - 4 mL). This is analysed following the sample analysis protocols detailed below, and typically the TPBs for this work contained less than 40 pg of boron. This equates to a blank correction of ca. 0.015%, which is smaller than our analytical precision and is therefore ignored here.

2.2.1 Sampling

In order to develop a method for measuring boron isotopes and boron concentration in biogenic silica a British Antarctic Survey core catcher sample (TC460) from core PC460 in the Southern Ocean (-60.81534 N, -50.9851 E, water depth 2594 m) was used (supplied by Dr Claus-Dieter Hildebrand). A pure diatom sample was separated from the bulk sediment and cleaned at the University of Nottingham with Dr George Swann following an established diatom separation technique (Swann et al., 2006). The bulk sample underwent organic removal and carbonate dissolution (using 30% H_2O_2 and 5%

HCl), heavy liquid separation in several steps at different specific gravities using sodium polytungstate (SPT; Morley et al., 2004), and visual monitoring throughout the process to ensure the sample was free from non-diatom material, such as clay particulates. After the final SPT separation, samples were rinsed thoroughly with MilliQ and sieved at 10 μm to remove all SPT traces.

2.2.2 Cleaning

2.2.2.1 Equipment cleaning

All plastic and Teflon were thoroughly cleaned using trace element grade reagents (including all acids) before use to minimise any possible contamination using established and robust protocols within the boron-free clean laboratory at the University of Southampton. Specifically, all plastic-ware, including pipette tips and centrifuge vials, was submerged without air bubbles in hydrochloric acid (HCl, 3 M) at 90°C for no more than 24 hours, rinsed thoroughly with MilliQ in a boron-free HEPA filtered over-pressured hood within the clean lab, and stored sealed in Teflon jars (pipette tips) or plastic boxes (centrifuge vials). The final cleaning stage for all plastic involved rinsing with 10% Teflon-distilled nitric acid (HNO_3) and then MilliQ immediately before use. Plastic-ware was considered 'single-use', and disposed of correctly (recycled if rinsed with MilliQ).

Teflon beakers (2 -7 mL) were cleaned after use using the following protocol. Firstly, ensuring the used empty beakers were kept closed, outer ink labels were removed using acetone and the outside of the beaker rinsed thoroughly with MilliQ. Beakers were then opened and the last traces of the used sample was physically removed by wiping the insides of the beaker and accompanying lid with acetone, and again thoroughly rinsing with MilliQ. Beakers were partially filled with HNO_3 (7 M), sealed with sufficient head space, and heated standing on a hotplate to reflux (140°C) for at least 2 h. Once the reflux stage was complete, the beakers were emptied and rinsed along with their lids thoroughly with MilliQ. From here, the beakers were only handled using plastic tweezers when open. Beakers and lids were all arranged submerged in HNO_3 (7 M) in a 1 L Teflon jar with openings facing upwards, and this jar was sealed with sufficient head space to be

heated to reflux overnight (140°C). The Teflon jar was emptied and rinsed thoroughly with MilliQ, and this step was repeated, but using 2% HNO_3 instead of 7 M HNO_3 as a sequential reflux cleaning procedure. After this final reflux, the beakers were rinsed with MilliQ three times, shaken to remove remaining water droplets, sealed tightly and stored in an airtight plastic box. Immediately prior to use, the cleaned Teflon beakers were filled with 10% Teflon-distilled HNO_3 and heated to reflux (140°C) for at least 1 hour, and rinsed thoroughly with MilliQ (also inside the over-pressured hoods).

It should be noted that in the following procedures, all HNO_3 was Teflon-distilled unless otherwise stated.

2.2.2.2 Sample cleaning

During this PhD project, three types of marine diatom biogenic silica were prepared for analysis:

1. TC460 in-house standard; bulk sedimentary diatom opal from core catcher material from the Southern Ocean (core PC460). Discussed in chapter 2.
2. Cultured diatom opal from *Thalassiosira weissflogii*. Discussed in chapter 3.
3. Preserved sedimentary diatom opal comprising species *Coscinodiscus marginatus* and *C. radiatus* from the Northwest Pacific (core ODP Site 882). Discussed in chapter 4.

Cultured diatoms have high organic content compared to diatoms preserved in sediment, and as the boron targeted for measurement is that which is incorporated into the frustule, it is important that these organics are removed from both sediment and cultured samples in the cleaning stage. The TC460 samples, and all other biogenic silica samples analysed herein, were cleaned thoroughly at the University of Southampton using the following procedure, based on a method described by Mejía et al. (2013) and Horn et al. (2011).

The samples were placed in 50 mL centrifuge tubes and acidified (2 mL H_2SO_4). Potassium permanganate ($KMnO_4$) was added incrementally, 1 mL at a time, until there was no further colour change (total ca. 8 mL; Figure 2.1) and the sample remained deep purple. The sample was ultra-sonicated briefly (no more than 15 s), and if the colour

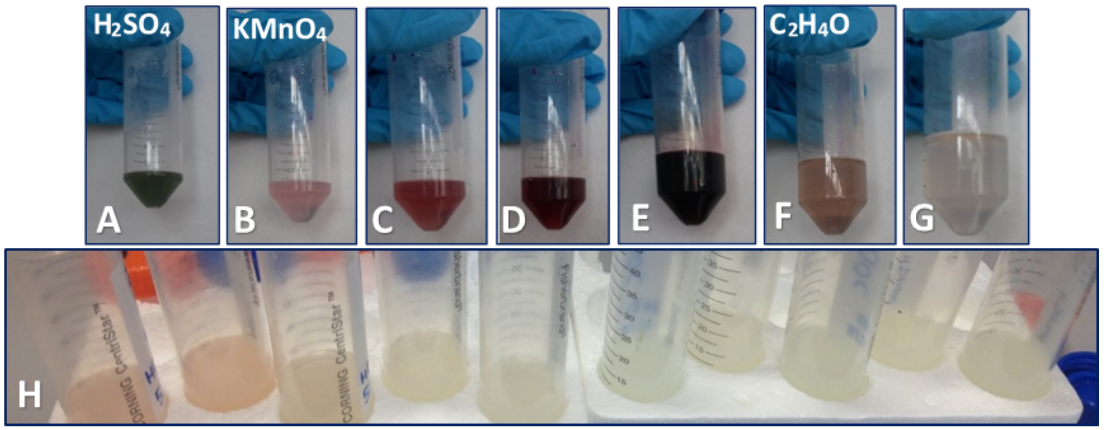

Figure 2.1: A shows an acidified sample, then B - E depict the addition of $KMnO_4$ (purple colour intensifying), and F - G show the addition of $C_2H_2O_4$ (becoming gradually colourless) during oxidation. In H, the difference between samples is evident in slight differences in colour at the same stage of oxidation - darker colours indicate a higher level of organics are present to oxidise, therefore requiring a larger volume of both oxidants. All samples were processed to full oxidation until they became deep purple following sufficient addition of KMnO4, and then completely colourless following sufficient addition of $C_2H_2O_4$.

changed (indicating further oxidation of organic material), an additional 1 mL $KMnO_4$ was added. Oxalic acid ($C_2H_2O_4$) was then added in 0.5 mL increments (total ca. 1 mL) until the sample remained colourless (Figure 2.1). The samples were topped up to 50 mL with MilliQ water, centrifuged and the supernatant was disposed of. The samples were rinsed in this way with MilliQ a further two times.

The rinsed samples were then transferred to Teflon beakers, and ca. 1 mL perchloric acid ($HClO_4$) was added to each sample. They were then heated for one hour, with inversion at 30 minutes. The samples were allowed to cool, diluted with 4 mL MilliQ and then passed through a 2 μm polycarbonate filter, ensuring the filtration system used a wet trap (Figure 2.2). Once on the filter, the samples were rinsed with at least 50 mL MilliQ, and then the cleaned samples were transferred manually to fresh Teflon beakers.

The aim of this procedure is similar to the established cleaning procedure for carbonate samples (Rae et al., 2011) in terms of using an oxidative approach to remove organic material that has the potential to contain boron. In contrast to carbonate samples, the diatoms require a stronger oxidiser to remove any organics within the frustule, hence the use of perchloric acid in the final stage. This extra step is possible

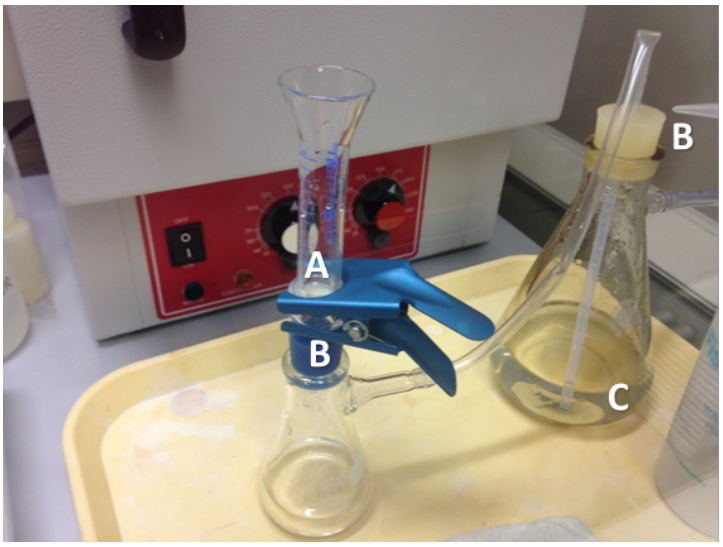

Figure 2.2: The experimental set up for rinsing the oxidised diatoms after the perchloric acid leach. This included a 0.2 μm polycarbonate filter (A), silicone bungs (B), and a wet trap (C).

because the opal frustule is able to withstand dissolution by acid.

2.2.3 Dissolution

In contrast to carbonates that are readily soluble in acid, marine biogenic silica is dissolved in a basic solution. To this end, all cleaned samples were completely dissolved in a known volume of NaOH determined gravimetrically of known concentration (0.5 M). A measure of the Si/Na ratio therefore allowed an accurate determination of the Si concentration of the sample. Each sample was then ultra-sonicated for ca. 30 minutes and then heated to 140°C until fully dissolved (6 - 72 hours). The dissolution time differed for each sample depending on sample volume, and consequently the cultured diatoms were more easily dissolved than sediment samples. Dissolved samples were briefly centrifuged prior to the boron purification procedure to ensure no insoluble particles were added to the column.

2.2.4 Purification

The anion exchange columns used to separate the boron fraction from the total dissolved sample were hand-made from Teflon tubing, and heated and moulded using

a specially made stainless steel mould. The reservoir containing the resin was set to a volume of ca. 20 μL, and resin was held in place by a Teflon frit. The resin used in these columns was Amberlite IRA 743 - a boron-specific anionic resin that has an optimum working pH of 9 (Kiss, 1988; Lemarchand et al., 2002), and was hand-crushed to a sieve size of 63 - 120 μm.

For the traditional carbonate-based methods used at the University of Southampton, once samples are dissolved in HNO_3, it is normal for boron concentration determination to take place prior to loading onto the Amberlite micro-columns by measuring a small aliquot ($< 10\%$) of the dissolved sample using ICP-MS. However, as diatom samples are dissolved in 0.5 M NaOH, the dilution required to reach suitably low sodium concentrations for determination by ICP-MS results in the boron concentration reaching blank levels. Therefore, for opal samples, column separation and purification of the boron must take place prior to the determination of its concentration.

Column exposure to the laboratory air was kept minimal, even though the columns remained within the boron-free laminar flow hoods throughout the purification procedure. To aid in the reduction of fall-in blank, the columns were placed in a plastic holder, and covered by an upturned plastic beaker (Figure 2.3). To clean the column prior to use, ca. 1.5 mL of 0.5 M HNO_3 was added to each in order to fill the entire column and reservoir. This was followed by 1 mL of 0.5 M HNO_3, and two subsequent

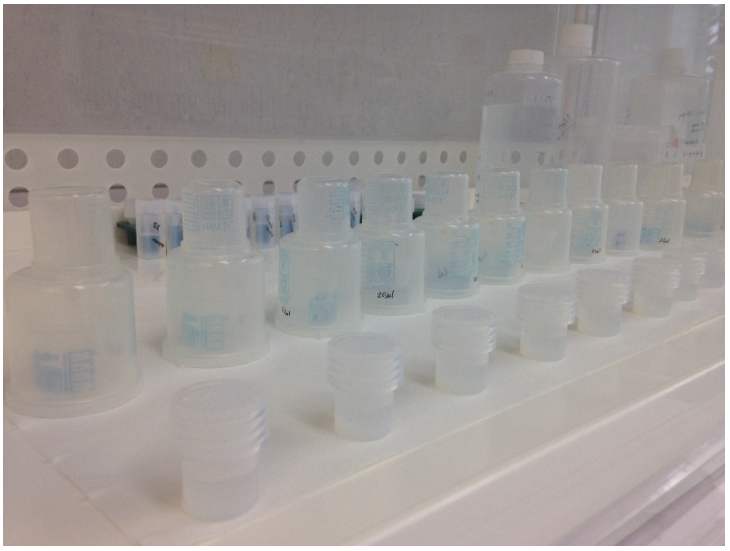

Figure 2.3: Columns in plastic holders inside the boron-free laminar flow hoods.

additions of 1 mL of MilliQ were added to the column to complete the cleaning procedure, and to equilibrate the column and wash off the 0.5 M HNO_3. The dissolved and centrifuged diatom sample was then added to the column (gradually and specifically no more than 300 μL at once to avoid overloading). The partition coefficient for boron on Amberlite resin is dependent on solution pH (Lemarchand et al., 2002), with an optimum at approximately pH 9.5. The carbonate procedure at the University of Southampton (Foster et al., 2013) involves a buffering step where 100 - 200 μL of buffer (sodium acetate - acetic acid; pH ca. 5) is added to the dissolved carbonate sample. The pH of the 0.5 M NaOH used to dissolve the opal samples here was ca. 13, therefore requiring no buffering prior to loading. The wash and elution procedure is shown in Figure 2.4. The sample matrix washed off the column in 1800 μL MilliQ (9 x 200 μL) was collected in an acid cleaned Teflon beaker (3 mL, 10% HNO_3) for determination of the Si content (see below). The purified boron was then eluted in 550 μL HNO_3 (0.5 M, 5 x 110 μL; Figure 2.5) in a clean 5 mL beaker. As a check that all boron was collected, a final acid cleaned beaker (3 mL) was used to collect an additional 110 μL 0.5 M HNO_3,

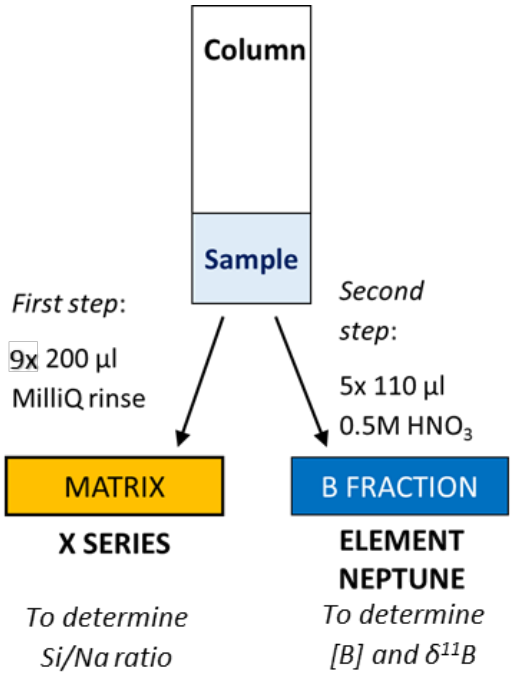

Figure 2.4: Schematic identifying the purification procedure. The matrix fraction is measured on the X-Series ICP-MS to ascertain the Si/Na ratio, and the boron fraction is measured on the Element ICP-MS to find the boron concentration, and the Neptune MC-ICP-MS to determine δ^{11}B.

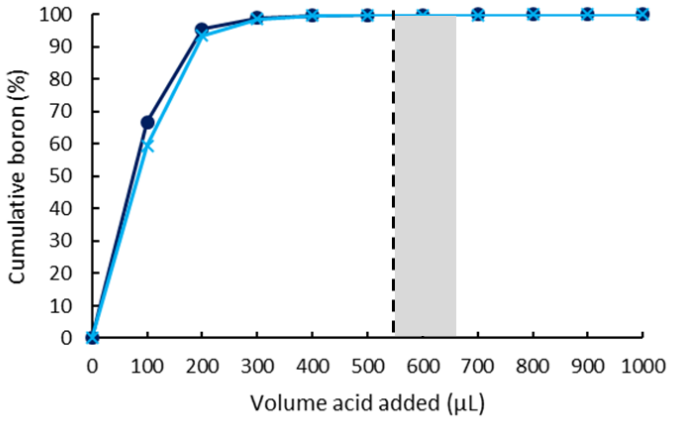

Figure 2.5: Elution curves of two columns, showing 100% of boron within the sample tested is collected after 550 μl of 0.5 M HNO_3 is added to the column. The black dashed line indicates the total sample volume (*i.e.* 550 μL), and the grey shaded area indicates the volume of 0.5 M HNO_3 collected for the tail (110 μL).

hereon known as the sample "tail" (Figure 2.5). The column was then cleaned using the same procedure prior to sample loading (fill 0.5 M HNO_3, 1 mL 0.5 M HNO_3, 1 mL MilliQ, 1 mL MilliQ), and stored in fresh MilliQ.

2.2.5 Boron isotope analytical procedure

The boron isotopic composition of the biogenic silica samples was determined on a Thermo Scientific Neptune MC-ICP-MS, also situated in a boron-free HEPA filtered laboratory at the University of Southampton, following the established method from (Foster, 2008). The Neptune comprises a sample introduction system and argon plasma to ionise the sample, sample and skimmer cones (X cones) and lenses to focus the ion beam. The sample is then accelerated, and electromagnets deflect the beam to the collector array of Faraday detectors (Figure 2.6).

Following Foster (2008), a Teflon nebuliser (ESI; uptake = ca. 70 μL min^{-1}) was connected to a Teflon barrel spray chamber for sample introduction (Figure 2.7). For a 50 ppb solution, ^{11}B signals of 600-800 mV were typically measured using $10^{12}\Omega$ resistors, with ^{10}B and ^{11}B detected using Faraday cups L3 and H3 respectively. A secondary gas line was attached to the spray chamber after this introduction system containing additional argon gas (ca. 0.16 L/min) and ammonia (0.02 - 0.05 L/min).

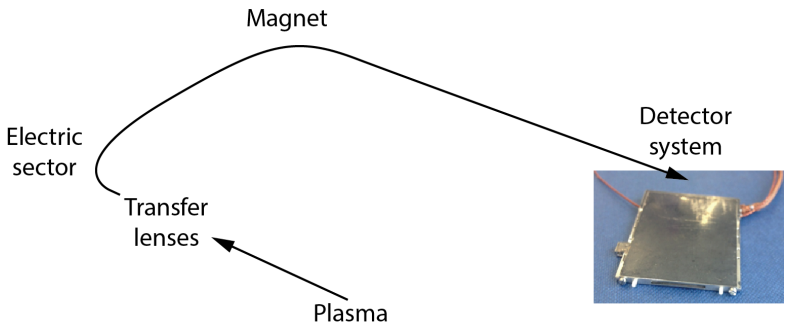

Figure 2.6: A schematic of the Thermo Scientific Neptune MC-ICP-MS detailing the main sectors of the instrument, and inset is a Faraday detector showing the slit that the sample eventually reaches at collection.

The ammonia was added to improve wash-out of boron in between samples (Al-Ammar et al., 2000). Ammonia reacts with any boron remaining in the spray chamber after sample analysis to form ammonium borate, which is easily washed into waste.

Typical tuning conditions during boron isotope analysis using the Neptune MC-ICP-MS are shown in Table 2.1. Boron isotopic composition is described using the delta notation δ^{11}B relative to a boric acid standard (NIST SRM 951 boric acid according to Catanzaro et al., 1970; equation 2.1), and tuning was completed using this standard made up to 50 ppb.

Instrument induced fractionation of the $^{11}B/^{10}B$ ratio was corrected using a sample-standard bracketing routine with NIST SRM 951 and following Foster (2008). This allows a direct determination of δ^{11}B without recourse to an absolute value for NIST SRM 951 (Foster, 2008) using the following equation, where $^{11}B/^{10}B_{standard}$ is the

Inlet system		**Lenses**	
Cool gas	15.50 L/min	Extraction	-2000
Auxiliary gas	0.90 L/min	X deflection	2.36
Sample gas	1.075 L/min	Y deflection	-3.99
Ammonia	0.02 L/min	Focus	-604
X	2.550	Shape	237
Y	4.260		
Z	2.060		

Table 2.1: Typical tuning parameters during an analytical session on the Neptune MC-ICP-MS. These values are used as a guide, as each analytical session required fine-tuning and the parameters were therefore different for each run.

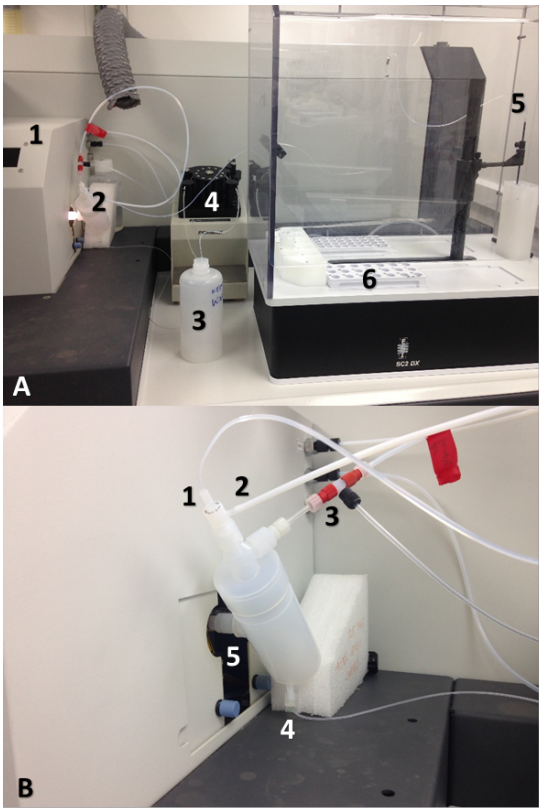

Figure 2.7: The experimental set up of the Neptune introduction system, including ESI autosampler. (A) shows the argon plasma window (1), the spray chamber introduction system (2), the waste beaker (3), the peristaltic pump (4), the autosampler probe (5), and the sample rack (6). (B) shows a close-up of the Teflon barrel spray chamber. This detail includes the Teflon nebuliser (1), sample gas line (2), additional gas and NH_3 line (3), waste line (4), and injector (5).

mean $^{11}B/^{10}B$ ratio of the standards bracketing the sample of interest.

$$\delta^{11}B(‰) = \left[\left(\frac{(^{11}B/^{10}B_{sample})}{(^{11}B/^{10}B_{standard})} \right) - 1 \right] \times 1000 \tag{2.1}$$

Mass fractionation stability was optimised by measuring NIST SRM 951 at variable sample gas flows (successively tested from low to high; Foster, 2008). Bracketing standards were made up to a similar concentration to the samples, although 50 ppb boron was typically aimed for in all analyses. Vials of blanks, comprising the same 0.5 M HNO_3 that was used to make up samples and of the same volume, were also used to bracket each sample block to act as on-peak-zeros and correct for fall-in blank throughout the analytical session. Figure 2.8 lists a typical block of samples and standards.

Blank
NIST SRM 951
Sample 1
NIST SRM 951
Sample 2
NIST SRM 951
Sample 3
NIST SRM 951
Blank

Figure 2.8: Example of an analytical sequence for the Neptune, where each sample is bracketed by a 951 boric acid standard, and each sample block is bracketed by blank (0.5 M HNO_3).

Every sample was analysed 60 times in one measurement with a two second integration time (120 seconds total), which was completed twice for each sample. This is why the stability of the bracketing standards is so important to maintain throughout the analytical run. The reported δ^{11}B was an average of the two analyses once every sample had had an independent repeat measured (*i.e.* the two measurements did not share blanks or bracketing standards). To minimise the length of each analytical session, and hence the fall-in blank, analytical runs were maintained at a maximum of 15 samples (ca. 9 hours). Machine stability and accuracy was monitored throughout the analytical session using many repeats of NIST SRM 951, as well as boric acids of gravimetrically determined δ^{11}B (including those of Vogl and Rosner, 2012).

2.2.6 B/Si concentration analytical procedure

All boron fractions were collected in pre-weighed acid cleaned Teflon beakers and their mass was recorded using a Precisa balance. Due to the amount of diatom material required to obtain a high enough boron concentration for accurate δ^{11}B measurements, a large amount of NaOH was required to dissolve the diatoms. This high matrix therefore precluded the use of a multi-element method to measure both B and Si on the Element ICP-MS without large dilution, which would have reduced the boron signal to within blank levels. In order to ascertain boron concentration, a 10 μL aliquot was taken and diluted with 490 μL 0.5 M HNO_3 in acid cleaned plastic centrifuge tubes (2 mL). This was then analysed using a Thermo Fisher Scientific Element 2XR ICP-MS, with boron concentration determined using standard approaches and a gravimetric

Standard 1 ppb
Standard 5 ppb
Standard 10 ppb
Standard 1 ppb
Sample 1 (1 ppb)
Sample 2 (1 ppb)
Sample 3 (1 ppb)
Standard 1 ppb
Standard 5 ppb
Sample 4 (5 ppb)
Sample 5 (5 ppb)
Sample 6 (5 ppb)
Standard 5 ppb
Standard 1 ppb
Standard 5 ppb
Standard 10 ppb

Figure 2.9: Example of a typical analytical sequence for the Element, where lines between the standards and samples represent a blank measurement (0.5 M HNO_3). The standards are shown at example concentrations of 1 and 5 ppb boron, and bracketing standards are concentration matched to the samples within each block. Standards are made up to approximately match the boron concentration of samples. The full standard block (1, 5 and 10 ppb boron) is repeated throughout the sequence, as well as at the end to ensure stability during each analytical session.

standard containing boron, silicon, sodium, and aluminium (made up to 1 ppb, 5 ppb and 10 ppb depending on sample concentration). The sample introduction system was the same set up as the Neptune described above. Tuning was performed to optimise for counts of B (typically 30000 - 50000 cps for 1 ppb B), In and U (typically 80000 - 100000 cps and 100000 - 150000 cps respectively), and minimise UO:U ratios (less than 7 %). Analyses were also carried out using standard blocks to monitor instrument performance throughout the run, but every standard and sample analysed on the Element was bracketed by a blank (0.5 M HNO_3) rather than a standard (Figure 2.9).

In order to determine the B/Si ratio, and hence the B concentration of the opal samples, the Si concentration must also be quantitatively measured. This is achieved here by using a known concentration and mass of NaOH to dissolve each sample, and therefore by measuring the Si/Na ratio, the exact Si concentration of each opal sample can be determined. During the purification procedure, sample matrix was washed off the column using MilliQ, which were collected in pre-weighed acid cleaned Teflon beakers.

Blank (10 % HNO_3)
Blank (3% HNO_3 + Be, In, Re)
Blank
Standard 1 (1 ppb)
Standard 2 (20 ppb)
Standard 3 (60 ppb)
Standard 4 (120 ppb)
Sample 1
Sample 2
Sample 3
Blank
Standard 1
Standard 2
Standard 3
Standard 4
Blank

Figure 2.10: Example of an analytical sequence for the X-Series, where the standards are made up gravimetrically and calibrated through the run, and the samples are diluted in order to be comparable to the bracketing standard concentrations. Typical standard concentrations are shown in brackets in terms of Si concentration.

These samples were used to determine silicon concentration, and were measured using the ThermoScientific X-Series 2 ICP-MS.

Samples were prepared in acid cleaned plastic vials, and diluted with 3 % HNO_3 enriched with Be, In and Re for the X-Series internal standardisation. Sequences written for the X-Series analyses utilised quantitative standard blocks to bracket the entire sample run, in which a block of standards was run before and after all of the samples in order to check instrument stability, and to maintain the internal calibration for these known element concentrations (Figure 2.10). The standards run on the X-Series consisted of varied concentrations of the gravimetric standard also used on the Element, containing B, Si, Na and Al.

2.3 Analysis of boron isotopes by MC-ICP-MS

2.3.1 Purification check

In order to ensure that Amberlite IRA743 resin is compatible with biogenic silica, it was required that the matrix fraction did not contain significant levels of boron, and that the B fraction did not contain significant levels of other elements (in this case sodium, silicon and aluminium). Several replicates of TC460 underwent the entire cleaning, separation and analytical procedure, and both fractions of each replicate were measured for B, Si, Na and Al. Figure 2.11 shows the matrix fractions measured on the X-Series contained an average of 265 ppm Na and 114 ppm Si, with minor Al of an average of 13 ppb (range = 5 - 25 ppb) and blank levels of B (average 2.6 ppb).

Figure 2.12 shows there were elements other than boron recorded in the B fractions measured on the Element, but at an average of 1.7 ppb Na and 1.9 ppb Si, these elements are vastly reduced from the hundreds of ppm observed in the matrix fraction (both observed at less than 0.002 % of the matrix concentration). However, Al is more

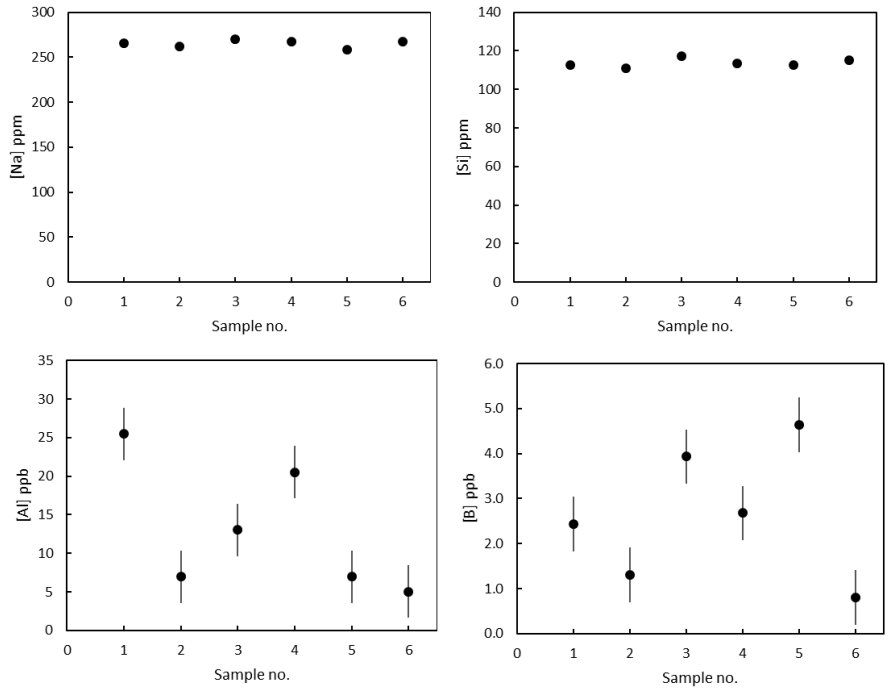

Figure 2.11: Matrix fraction ICP-MS measurements indicating blank levels of B are present in the matrix washed off the Amberlite IRA 743 resin-based column.

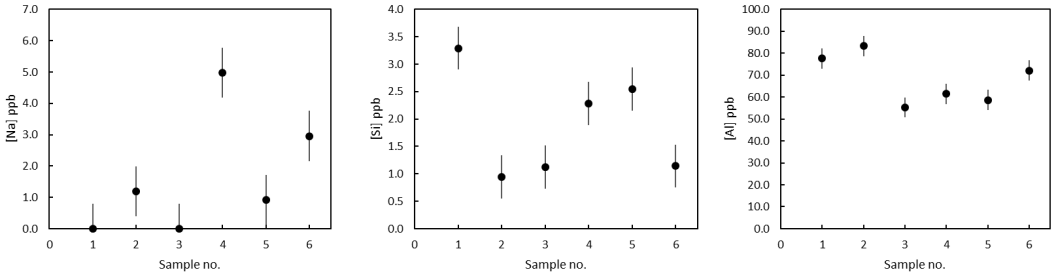

Figure 2.12: B fraction MC-ICP-MS measurements indicating blank levels of Na (ca. 1.7 ppb) and Si (ca. 1.9 ppb), and a higher concentration of Al (ca. 68 ppb) are all present.

concentrated in the B fractions than in the matrix fraction (ca. 68 ppb compared with ca. 13 ppb respectively).

It has been shown that diatoms utilise Al for structural purposes in their frustules (Stoffyn, 1979; Van Bennekom et al., 1991; Gehlen et al., 2002), and the apparently enhanced Al concentration observed in the B fraction also suggests Al is present as $Al(OH)_4^-$. It is likely that, even though up to 70 ppb Al was detected in the B fraction, these levels of contamination will not be a significant issue (Foster, 2008).

2.3.2 Reproducibility of δ^{11}B

The ability to reproduce δ^{11}B in diatom opal is a crucial test of the novel method described here. In order to assess this reproducibility, multiple repeats of the diatom in-house standard TC460 were performed over several analytical sessions. External uncertainty was determined by the reproducibility of δ^{11}B when a single sample of TC460 was processed multiple times via the entire method described above, including cleaning, dissolution, purification and analysis. Internal uncertainty was determined by the measurement uncertainty of the δ^{11}B of TC460 during an analytical session.

In total, TC460 was measured 18 times in separate analyses at a number of different concentrations in order to assess external reproducibility of this method. Carbonates generally have a reproducibility of $\pm$ 0.2 ‰ (2σ) at 50 ppb boron using MC-ICP-MS methods (Foster and Rae, 2016). The repeated measurements of TC460 revealed a reproducibility of $\pm$ 0.28 ‰ (2σ) over 18 samples, ranging from 19 ppb to 61 ppb (11 to 34 ng) boron. All of these repeat analyses of TC460 were within error of the mean δ^{11}B

of 5.98 ‰ (Figure 2.13).

Figure 2.14 confirms that the Al levels observed in the B fractions did not cause a mass bias effect, as there is no correlation between δ^{11}B and [Al].

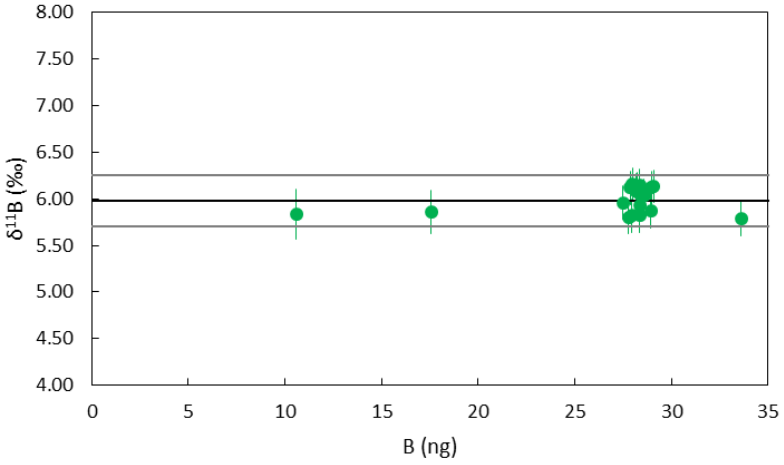

Figure 2.13: The reproducibility of the TC460 diatom core catcher in-house standard. This shows all samples lie within error of the mean (5.98 ‰ ± 0.28 ‰, 2σ) at varied concentrations. This compares well to carbonates (2σ = 0.2 ‰). The error bars also show how 2σ increases when the amount of boron analysed (ng) decreases, also similar to carbonates.

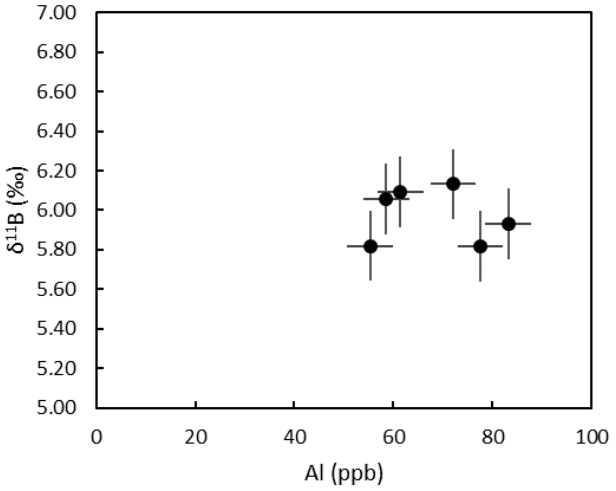

Figure 2.14: Aluminium concentration of the B fraction shows no correlation with δ^{11}B, likely suggesting there is no obvious mass bias effect and that the enhanced Al concentration is not sufficient to influence δ^{11}B isotopic measurements.

2.3.3 Accuracy of $\delta^{11}B$

Whilst the reproducibility (2σ) of TC460 has been shown to be similar to that regularly achieved using marine carbonates, it is also important to assess the accuracy of this novel method, as we must be able to reproduce the correct $\delta^{11}B$ during analysis. Following Tipper et al. (2008) and Ni et al. (2010) this was achieved here using a standard addition technique. Assessment of accuracy by standard addition was achieved by gravimetrically mixing known amounts of a boric acid standard and a sample with a biogenic silica based matrix to obtain a range of different fractions. In this case, the standard used was the well-characterised NIST SRM 951 boric acid ($\delta^{11}B = 0$ ‰), and the sample was TC460 ($\delta^{11}B = 5.98 \pm 0.28$ ‰; Figure 2.14). Two standard addition experiments were completed; one using equal initial boron concentrations of 951 and TC460, and one using a 1:4 ratio (951:TC460) to test the effect of a larger relative matrix concentration. All mixtures were passed through the entire separation and analytical procedure, including aliquots of pure standard and sample. A sodium acetate - acetic acid buffer was added to all 951 boric acid used (buffer volume = double the volume of 951) to ensure the pH was high enough for the column separation procedure. The amount of biogenic silica matrix added to the columns for each mixture was kept constant, so the volume added to the column was altered for each mixture accordingly.

Figure 2.15 shows the results of the standard addition where the uncertainty on individual data points was determined using a Monte Carlo approach. Specifically, 1000 realisations of the calculated $\delta^{11}B$ of each mixture were generated by resampling the normally distributed uncertainty in each component. This included (with 95% confidence): the mass of sample added (± 6%), the concentration of end members (± 0.5%), and the $\delta^{11}B$ of TC460 (± 0.3%). The mean and 2 standard deviations of the 1000 realisations thus provides a measure of the uncertainty in the calculated $\delta^{11}B$ of each mixture.

When uncertainty in the mixture $\delta^{11}B$ is considered, it is clear that nearly all the mixtures lie within error of the 1:1 line, indicating that there is a lack of a matrix effect when analysing the $\delta^{11}B$ of biogenic silica as described herein. A least squares linear regression of the mixtures, considering only the scatter of the central values and

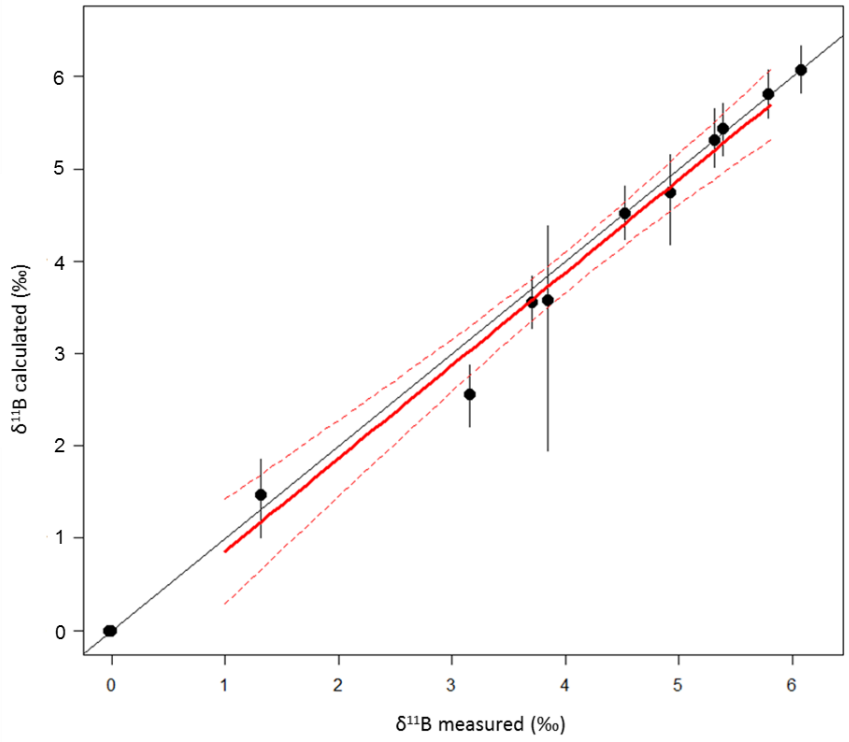

Figure 2.15: The linear regression (red line) between the measured δ^{11}B of each mixture and the theoretical δ^{11}B, with $R^2 = 0.97$, $p < 0.0001$, slope = 1.01 ± 0.07 and intercept = -0.15 ± 0.29 is shown compared to the 1:1 line (black).

not their uncertainties, has a slope of 1.01 ± 0.07 and an intercept of -0.15 ± 0.29 ‰, implying the approach is accurate to ± 0.29 ‰, which is close to the stated reproducibility of TC460 (± 0.28 ‰ at 2σ).

2.4 Analysis of B/Si by ICP-MS

B and Si content were measured separately and combined post-analysis in order to determine the B/Si ratio for each sample. As discussed in section 2.3.1, measuring both fractions for B, Si, Na and Al allowed a purification check, to ensure the matrix fraction was B-free, and to check the B fraction contained only boron. The reproducibility of this method was tested using six repeats of the afore-mentioned TC460 bulk sediment diatom sample.

All samples lie well within 2σ error of the mean (6.90 ± 1.47 ppm; Figure 2.16),

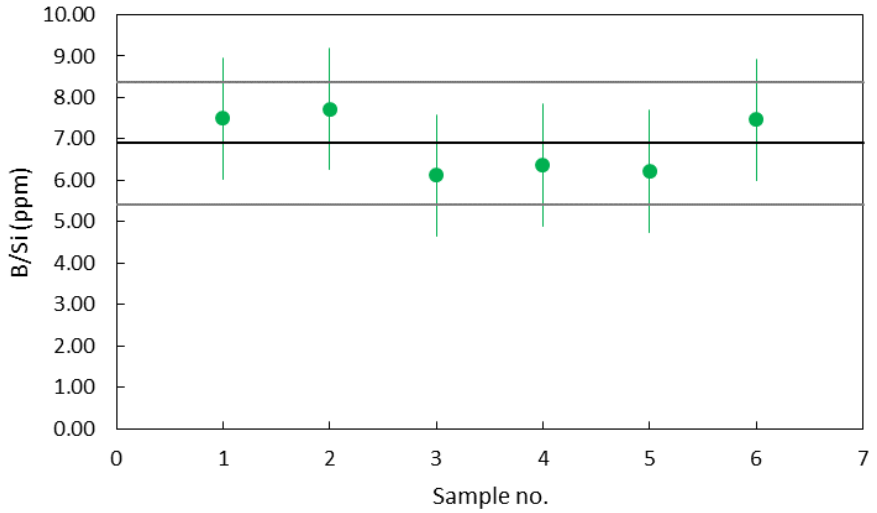

Figure 2.16: B/Si ratios of six repeat samples of the sediment diatom "standard" TC460. The black line indicates the mean value, and the grey lines show 2σ, of 6.90 ± 1.47 ppm.

implying the reproducibility of this method to determine B/Si ratios in diatoms is precise to ± 20 %. Improvements could be made to the reproducibility by measuring a larger volume of samples of different concentrations in order to increase confidence.

2.5 Summary

This novel method development demonstrates that boron isotopes can be measured accurately (2σ = 0.29 ‰) and with good reproducibility (2σ = 0.28 ‰) by MC-ICP-MS in diatom opal. These results compare well to robust, established methods measuring boron isotopes in carbonates. Whilst there are still areas to build on, specifically in terms of obtaining a commonplace reference material for long-term reproducibility tests and inter-laboratory comparisons, this is a solid basis for expanding the measurement of boron isotopes into diatoms, sponges and other biogenic siliceous organisms.

Chapter 3

Investigating the relationship between seawater pH and boron isotopes in cultured diatoms (*Thalassiosira weissflogii*)

Intended co-authors:

Nico Fröhberg (helped with culturing and sampling, analysed samples for biogenic Si and POC/PON, took SEM pictures, discussion about ocean acidification effects on diatoms)

Gavin Foster (assisted with R models describing potential boron species uptake, general discussion, guidance, feedback)

Alex Poulton, Mark Moore (discussion, feedback)

Acknowledgements:

John Gittins (helped set up the gas lines and provided strain of *T. weissflogii*)

Matthew Humphreys (analysed samples for DIC on the VINDTA)

Mark Stinchcombe (analysed samples for nutrients on the QuAAtro)

Lucie and Chris Daniels (supervised and instructed Nico during SEM analysis)

The high latitude oceans are key areas of carbon and heat exchange between the atmosphere and the ocean. As such, they are a focus area for both modern oceanographic and palaeoclimate research. However, most palaeoclimate proxies that could provide a long-term perspective are based on calcareous organisms such as foraminifera that are scare, or entirely absent, in deep-sea sediments south of 50° latitude in the Southern Ocean and north of 40° in the North Pacific. As a result, proxies need to be developed

in the opal-based organisms (*e.g.* diatoms, sponges, radiolaria) that are found at these high latitudes and dominate the biogenic sediments that are recovered from these regions. Here, we evaluate for the first time the relationship between seawater pH (pH_{sw}) and $\delta^{11}B$ in the frustules of the diatom *Thalassiosira weissflogii* cultured at a range of pCO_2/pH_{sw}, in order to contribute towards efforts to determine the effects of ocean acidification on diatom physiology, as well as to assess the applicability of the boron isotope pH proxy in diatoms. Our results suggest that a reduction in pH_{sw} has little effect on growth rates and carbon acquisition in diatoms, although nitrogen uptake increased with increasing pH_{sw}, and cell size also marginally increased. In agreement with existing data, we find that the boron content of the cultured diatom frustules increases with increasing pH_{sw} (Mejía et al., 2013), but their $\delta^{11}B$ shows a relatively well defined negative trend with increasing pH_{sw} - a completely distinct relationship from any that have been measured in biominerals previously. This relationship has implications for how boron is incorporated into diatom opal and we explore the potential of our new B/Si- and $\delta^{11}B$-pH calibrations for palaeo-pH reconstruction high latitude marine sediments that have, up until now, eluded study due to the lack of suitable carbonate material.

3.1 Introduction

Marine carbonates are excellent substrates for use in palaeoclimate research, particularly seawater proxies such as the boron isotope palaeo-pH proxy, as they are directly involved in the seawater carbon equilibrium (*e.g.* Sanyal et al., 2001; Hönisch and Hemming, 2004; Kasemann et al., 2009). As seawater pH (pH_{sw}) changes, the equilibrium shifts to oppose the change imposed upon it, as described by Le Chatelier's principle, so carbonate ion concentration in seawater, and therefore the precipitation of $CaCO_3$, is dependent on pH_{sw} (and saturation state, Ω). Any Ω reduction will therefore lead to the eventual dissolution of precipitated $CaCO_3$.

Carbonate preservation in sediments is reduced by its increasing solubility with increasing pressure at depth. Preservation is also affected by carbonate ion concentration in the overlying water, which is a function of nutrient and carbon content, and carbonates tend to dissolve in cold, corrosive deep water. This results in the carbonate

compensation depth (CCD) - the depth at which carbonates are no longer preserved in marine sediments - occurring at a shallower depth of ca. 3.5 - 4.5 km in the deep North Pacific (Bickert, 2009), as this water at the end of the ocean conveyor is rich in carbon and nutrients. Carbonate distribution in marine sediments also depends on production in the overlying water, hence biogenic silica largely dominates marine sediments in the "opal-belt" in the Southern Ocean, as well as the subarctic North Pacific, as diatoms occupy these high latitude habitats where they out-compete calcareous organisms in this nutrient-rich water. The relatively high-density frustules of diatoms have a high sinking velocity (Smetacek, 1999), and the opal that reaches the deep ocean is then preserved better in corrosive cold water than carbonates.

The high latitude regions, such as the Southern Ocean and the subarctic North Pacific, are key areas of gas exchange with the atmosphere. Both are areas where upwelling of deep nutrient-rich water occurs, which promotes primary productivity, and in turn draws down CO_2 from the atmosphere. The balance of processes involved in determining whether the ocean is a source or sink of CO_2 are poorly understood, to the extent that their contribution to glacial-interglacial pH and pCO_2 changes is a subject of vigorous debate (*e.g.* Martin, 1990; Sigman and Boyle, 2000; Doney et al., 2009). Recently, several studies have shown how the boron isotope pH proxy has tracked surface water CO_2 content, and thus documented changes in air-sea CO_2 flux (*e.g.* Martínez-Botí et al., 2015). However, the lack of preserved marine carbonates in those areas thought to be key in glacial-interglacial CO_2 change (*e.g.* the polar Antarctic zone; Sigman et al., 2010) represents a currently unsurmountable problem. There is therefore a requirement for the boron isotope palaeo-pH proxy to be developed in biogenic silica in order to study these high latitude regions more thoroughly.

3.1.1 Ocean acidification and diatoms

Atmospheric CO_2 dissolves in seawater to form carbonic acid, and forms an equilibrium with bicarbonate and carbonate anions that, when combined with alkalinity, determine pH_{sw} (see Figure 1.4). As phytoplankton require CO_2 for photosynthesis,

this equilibrium is vital in determining the amount of carbon available to phytoplankton, as primary production can be carbon-limited for large organisms in the modern ocean (Wu et al., 2014a). When $CO_{2(aq)}$ is limited, carbon concentrating mechanisms (CCMs) can convert bicarbonate to CO_2 in certain species (Riebesell et al., 1993; Chen and Durbin, 1994) and diatoms employ strict internal pH regulation to assist these biological processes. Ocean acidification therefore represents a carbon-enrichment for many photosynthesising species, as with a higher pCO_2 comes a reduced requirement for energy-demanding CCMs (Wu et al., 2014a).

As a direct result of increasing atmospheric pCO_2, ocean acidification is occurring in the global ocean (Doney et al., 2009). Primary production takes place in the surface ocean (<100 m), which is also the area currently most affected by increasing atmospheric pCO_2. It is therefore important to understand the effects that increasing atmospheric pCO_2, and hence reducing pH_{sw}, will have on these marine organisms in the surface ocean. Despite displaying some resilience to moderate ocean acidification, marine carbonates have been shown to be negatively affected by ocean acidification, and a reduction in pH_{sw} leads to reduced calcification in many organisms, and eventually the dissolution of precipitated $CaCO_3$ due to a reduction in carbonate saturation state in seawater (Sabine et al., 1995; Gattuso et al., 1998; Hoegh-Guldberg et al., 2007; Anthony et al., 2008; Ries et al., 2009; Rodolfo-Metalpa et al., 2011; Beaufort et al., 2011; McCulloch et al., 2012c).

Though diatoms are siliceous phytoplankton that may account for ca. 45% of all marine primary productivity (*e.g.* Nelson et al., 1995), relatively few studies compared to those undertaken using calcareous organisms have explored how ocean acidification will affect diatoms (*e.g.* Riebesell et al., 1993; Thornton, 2009; Wu et al., 2010; Hervé et al., 2012; Mejía et al., 2013; Gao and Campbell, 2014; Wu et al., 2014; Passow and Laws, 2015; Li et al., 2016). Crucially, ocean acidification is occurring in high latitude diatom-dominated communities faster than the global average as CO_2 is more soluble at low temperatures. Organisms that occupy these areas are therefore more likely to experience physiological changes as a result of large magnitude ocean acidification faster than organisms occupying warmer waters.

3.1.2 Boron isotopes

As noted above, the boron isotopic composition has been used extensively in marine carbonates for the reconstruction of past ocean pH, and past atmospheric CO_2 (*e.g.* Hemming and Hanson, 1992; Pearson and Palmer, 2000; Hönisch and Hemming, 2005; Foster, 2008; Henehan et al., 2013). Comprehensive calibration work has been completed for species of (*e.g.*) foraminifera that are currently used in palaeoceanographic reconstruction, and it has been shown that whilst $\delta^{11}B$ compositions are fairly similar among carbonates, they do have species-specific calibrations involving slightly different offsets from the boron isotopic composition of aqueous borate (Figure 1.10). It is therefore important to investigate the relationship between $\delta^{11}B$ and pH_{sw} by analysing organisms grown at controlled pH_{sw}. Once this relationship is known, this $\delta^{11}B$-pH calibration can be applied to fossils found in deep-sea sediment cores, reliably reconstructing pH and pCO_2 (*e.g.* Hönisch and Hemming, 2005; Foster, 2008). Beyond the use of boron isotopes as a tracer of ancient ocean pH, and analogous to how boron is used in corals (McCulloch et al., 2012b), boron isotopes measured in diatoms could also be used as a tool to assess how diatoms will respond to future ocean acidification.

Here, the relationship between $\delta^{11}B$ in diatom frustules and pH_{sw} is investigated for the first time using a batch culturing technique and different air-CO_2 mixtures to ensure a wide range of pH_{sw} (8.54 ± 0.57 to 7.48 ± 0.06), with the aim to investigate the effects of ocean acidification upon the diatom *Thalassiosira weissflogii* (*T. weissflogii*), as well as to explore the response of the boron based proxies in diatom frustules to changing pH_{sw}. Ultimately, we show how boron isotopes measured in diatom frustules provide further insight into boron uptake and physiological activity within the diatom, as well as test whether $\delta^{11}B$ and B content in diatoms hold potential as palaeo-proxies for the ocean carbonate system.

3.2 Methods

3.2.1 Experiment set up

The diatom species *T. weissflogii* was grown at the University of Southampton in dilute batch cultures (inoculation = 1000 cells mL^{-1}) for a maximum of one week for each experiment, with the carbonate system controlled by CO_2 bubbling (Figure 3.1). All culture handling was completed within a laminar flow hood to ensure sterility. The flow hood surfaces were cleaned with ethanol before and after handling, as well as all labware entering the laminar flow hood such as bottles and pipettes.

Target pCO_2 (ppm)	**Measured pCO_2 (ppm)**	**2σ (ppm)**
200	125	8
280	244	73
400	267	28
800	809	62
1600	2117	40

Table 3.1: Target pCO_2 and measured pCO_2 for each culture batch (see Figure 3.1). Each culture treatment is henceforth referred to by its target pCO_2 concentration.

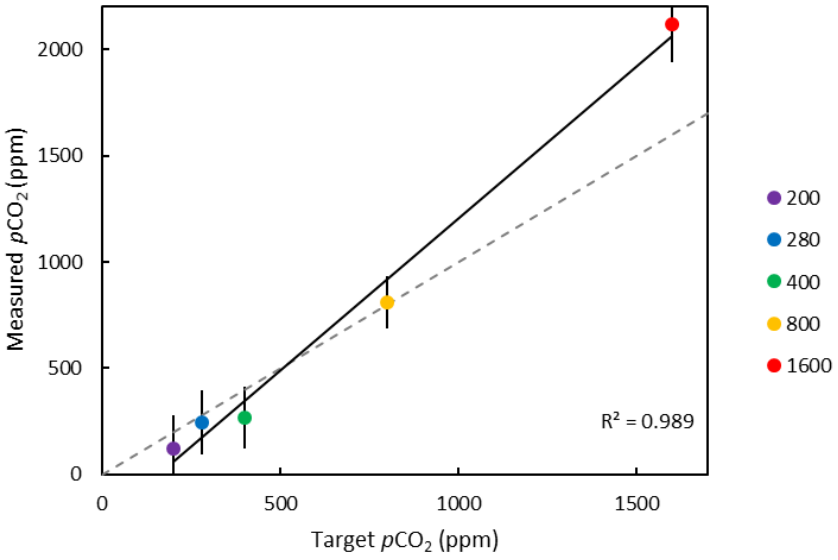

Figure 3.1: Plot of target pCO_2 based on bubbled CO_2 concentration *vs.* measured CO_2. Also shown is the 1:1 line (dashed grey line).

The centric diatom *T. weissflogii* (Grunow in van Heurck, PCC 541, CCAP 1085/1; Fryxell and Hasle, 1977) was grown in triplicate in K/1 enriched sterile and filtered seawater (0.2 μm; seawater sourced from Labrador Sea; Keller et al., 1987) in the culture experiment flasks (3 L glass Erlenmeyer flasks). The culture experiments were bubbled with air-CO_2 mixtures in different concentrations (sourced from BOC; Table 3.1) to provide a wide pH range at constant bubble rates, and every flask was agitated by hand twice daily to limit algal settling and aggregation (Figure 3.2). The unialgal cultures were grown in replete conditions at constant temperature (20°C) and a 12h:12h light:dark cycle (with 191.7 μmol photons m^{-2} s^{-1}, or 8.3 mol photons m^{-2} d^{-1} during the photoperiod), and cell counts were performed daily to ensure the batch cultures remained in the exponential phase throughout the experiment. The diatoms were acclimated to each pCO_2 for at least 10 generations before inoculating the culture experiment flasks with these pre-grown cells (Figure 3.3).

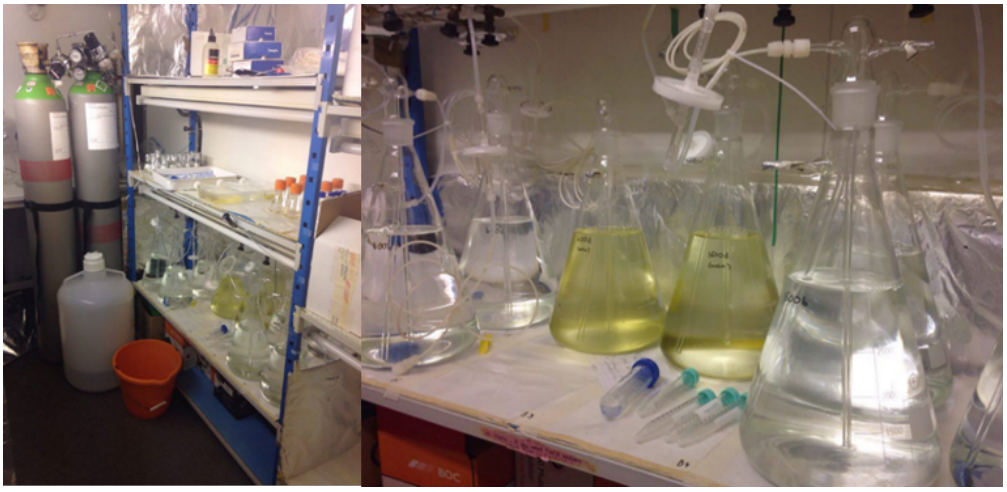

Figure 3.2: Experiment acclimation involved inoculating one flask to grow at least 10 generations of *T. weissflogii* and bubbling all four flasks attached to each gas line to ensure the media was held at the correct pH. Here, inoculated acclimation flasks can be identified by the green colour of the media originating from the algal growth.

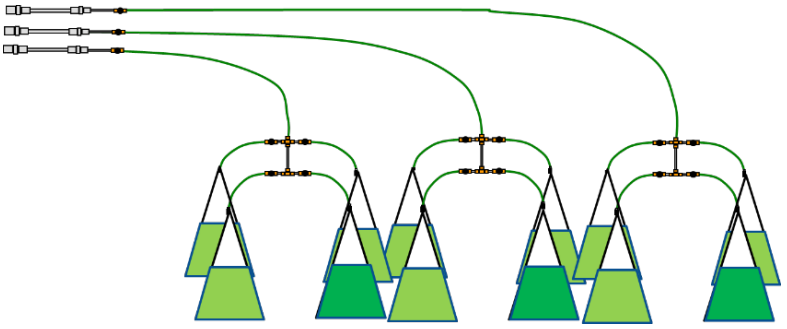

Figure 3.3: Schematic of the experimental set up, indicating four flasks attached to each gas line (one for acclimation, and three for running the experiment in triplicate).

3.2.2 Growth rate and cell size

A 5 mL sub-sample was taken from each culture flask through sterilised Nalgene tubing into sterile syringes, and sealed in sterile 15 mL centrifuge tubes. A Multisizer 3 Beckman Coulter Counter was used to acquire cell density and cell size distributions, and 3% NaCl was used as the diluent. Cell density was calculated using integration and averaging over three measurements of each culture experiment flask. Growth rates were calculated using equation 3.1:

$$\mu = (lnN_t - lnN_i)/(t - t_i) \tag{3.1}$$

Where N_i is the initial cell density at the start of the experiment (t_i) and N_t is the cell density at time t. Cell size was also determined using the Coulter Counter, similarly using three replicates of each culture experiment to determine the mean cell size and distribution in each flask.

3.2.3 pH, DIC and alkalinity

A pH meter (Orion 410A) was calibrated using standard National Bureau of Standards (NBS) buffers prior to sample extraction at pH 10.01, 7.00 and 4.01. A 3 mL sub-sample was taken from each culture flask through sterilised Nalgene tubing into sterile syringes, and sealed in sterile 15 mL centrifuge tubes to prevent atmospheric equilibration. The samples were then analysed using the calibrated pH probe, ensuring

the time lag between sampling and measuring was less than 5 minutes.

These pH electrode measurements were made daily to monitor the evolution of pH through the experiment. For quantitative constraints on the carbonate system of the culture media, DIC/TA (Dissolved Inorganic Carbon/Total Alkalinity) measurements were made (± 1 μmol kg^{-1}). 500 mL stoppered glass flasks were first rinsed with hydrochloric acid (HCl) and MilliQ, and dried at 60°C before using for samples. Samples were taken every other day in triplicate for each pH_{sw} treatment (*i.e.* one per experiment flask) using sterilised Nalgene tubing, ensuring no air bubbles were present throughout the tubing and the flask. The bottles were filled to overflowing and immediately stoppered, then uncapped to be poisoned with 1 mL mercury chloride ($HgCl_2$) to prevent any further biologically-induced changes in DIC and stored sealed in complete darkness until analysis. Analysis was performed at the University of Southampton using a VINDTA (Versatile INstrument for the Determination of Total inorganic carbon and titration Alkalinity). Carbonate system parameters, including pH_{sw}, were calculated using measured alkalinity and DIC values, temperature and salinity with the CO_2SYS programme (Van Heuven et al., 2011; using constants from Dickson, 1990; Lueker et al., 2000; Lee et al., 2010).

3.2.4 Nutrients

In order to monitor the evolution of the composition of the culture media through the experiment, nutrient samples were taken every day for the 400 and 1600 ppm treatments, and every other day for the 200, 280 and 800 ppm treatments. 15 mL sub-samples were taken in triplicate for each treatment using sterilised Nalgene tubing and sterilised plastic syringes. The sample was gently filtered through sterile 0.2 μm polycarbonate filters to remove biological particulates, and frozen at -20°C until analysis. Nutrient analysis for nitrate and nitrite, silicic acid, nitrite, and phosphate (NO_3 + NO_2, $Si(OH)_4$, NO_2 and PO_4^-) was carried out using a QuAAtro analyser at the National Oceanography Centre, Southampton (ca. ± 7 mmol kg^{-1}). This system uses UV/vis spectroscopy analysis to determine nutrient contents, and different reagents are

used for each separate channel. Thawed samples were diluted by a factor of 10, and run using calibrated standards.

3.2.5 Biogenic silica and POC/PON

Biogenic silica and particulate organic carbon (POC) and nitrogen (PON) were all measured at Jacobs University in Bremen, Germany (ca. ±10 %). For biogenic silica analysis, a 30 mL sub-sample was taken from each culture flask at the point of cell harvesting and filtered through a 0.2 μm polycarbonate filter. The samples were dried at 40°C overnight, and Si analysis followed the method described by Grasshoff et al. (1983) and Brown et al. (2003). The samples were digested in sodium hydroxide (NaOH, 0.2 M) at 85°C for 2 hours, and neutralised with HCl (0.1 M). Ammonium heptamolybdate in sulphuric acid was added to the sample to form silicomolybdic acid, and this reaction was stopped after 20 minutes by the addition of oxalic acid. Ascorbic acid was also added to ensure the stability of the product. Concentrations were determined using a spectrophotometer measuring the absorbance of silicomolybdic acid at 810 nm.

For POC/PON analysis, Whatman glass-fibre filters (GF/F) were pre-combusted (6 hours) in a muffle furnace oven at 450°C, and a 3 mL sub-sample was passed through the filter to collect the cells at the point of harvesting. The filters were then fumed with HCl for 24 hours under vacuum, dried overnight at 40°C, and the pellets were encapsulated in tin. POC/PON analysis was carried out using a CNHS analyser (Eurovector Euro EA 3000 Elemental Analyzer), calibrated with acetanilide and a certified soil standard (*Bodenstandard 1*).

3.2.6 SEM

Scanning electron microscopy (SEM) analysis was undertaken at the University of Southampton. Following a method described in Daniels et al. (2012), 5 x 5 mm subsections of Nucleopore 0.8 μm polycarbonate filter samples were fixed on aluminium stubs, sputter-coated with gold using a Hummer VI-A gold coater, and examined using a Leo 1450VP scanning electron microscope (x 5000 magnification). Images were then analysed for visual differences between the diatoms from each culture treatment.

3.2.7 Preparing cultured diatoms for δ^{11}B and B/Si analysis

The cultured diatom samples were collected by centrifugation at 96 h, during the exponential phase. Each flask was simultaneously disconnected from the gas supply, and the culture was immediately split between 500 mL sterilised centrifuge tubes, and centrifuged at 3700 rpm for 30 minutes and the supernatant extracted to waste. Once the contents of each culture flask was centrifuged into a pellet, it was rinsed with MilliQ and frozen at -20°C in sterile plastic 50 mL centrifuge tubes.

The cleaning, separation and analytical protocols are as described in Chapter 2. Briefly, the culture samples were defrosted and acidified (H_2SO_4), and the organics were oxidised using potassium permanganate and oxalic acid (following Horn et al., 2011 and Mejía et al., 2013). The samples were rinsed thoroughly using MilliQ water *via* centrifugation and transferred to acid-cleaned Teflon beakers. A secondary oxidation was completed under heat using perchloric acid. Finally, the organic-free samples were rinsed thoroughly with MilliQ *via* filtration.

In the boron-free HEPA filtered clean laboratory at the University of Southampton, each sample was dissolved completely in a gravimetrically known amount of NaOH (0.5 M) at 140°C for 6 to 12 hours, and briefly centrifuged prior to boron separation to ensure no insoluble particles were added to the column. Anion exchange columns containing Amberlite IRA 743 resin were used to separate the matrix from the boron fraction of each sample. 1800 μL MilliQ was used to collect the matrix fraction, and the pure boron fraction was eluted in 550 μL of 0.5 M HNO_3 acid.

The δ^{11}B of each sample was determined using a Thermo Scientific Neptune MC-ICP-MS following an established method from Foster (2008). to an accuracy of $\pm$ 0.29 ‰ and a precision of $\pm$ 0.28 ‰ (as derived from standard addition experiments; Chapter 2). A Teflon nebuliser was connected to a Teflon barrel spray chamber introduction system, and ^{11}B and ^{10}B was measured using 10^{12} Ω resistors, and detected using Faraday cup H3 and L3 respectively. Ammonia was also used in order to improve washout of boron between samples (following Al-Amar et al., 2001). Instrument-induced fractionation of the ^{11}B/^{10}B ratio was corrected using a sample-standard bracketing sequence with NIST SRM 951 boric acid, allowing a direct determination of δ^{11}B using the

following equation, where $^{11}B/^{10}B_{standard}$ is the mean $^{11}B/^{10}B$ ratio of the bracketing standards adjacent to the sample of interest. The $\delta^{11}B$ of the culture media was also determined as 38.8 ± 0.19 ‰, which is marginally lighter than that of seawater (39.61 ± 0.04 ‰ Foster, 2008).

$$\delta^{11}B(‰) = \left[\left(\frac{(^{11}B/^{10}B_{sample})}{(^{11}B/^{10}B_{standard})} \right) - 1 \right] \times 1000 \tag{3.2}$$

For B/Si analysis, an aliquot of the boron fraction was taken and diluted with 0.5 M HNO_3, and analysed using a Thermo Fisher Scientific Element 2XR ICP-MS. B concentration was determined using comparison to a gravimetric standard containing boron, silicon, sodium and aluminium, and each sample was blank bracketed. The Si concentration of the matrix fraction was determined by measuring the Si/Na ratio having added a known concentration and mass of NaOH to each sample. The same gravimetric standard was used for this, and samples were analysed using a Thermo Scientific X-Series 2 ICP-MS. B/Si was analysed to a precision of ± 20 % (Chapter 2). Statistical analysis on all variables was undertaken using R (version 3.4.0).

3.3 Results

3.3.1 Media composition

All flasks were initially filled with media from the same large batch, and all culture treatments therefore started with the same initial pH_{sw}. The pH_{sw} for all treatments was then altered using bubbling from the different air-CO_2 mixtures, ranging from low pH_{sw} (1600 ppm, high pCO_2) to high pH_{sw} (200 ppm, low pCO_2). These differences in pH_{sw} were brought about by the changes in DIC within the media due to the differences in the bubbled pCO_2. Mean pH and pCO_2 for each culture treatment were calculated based on the number of cells grown per 24 hours, and the pH measured in that 24 hours, in order to adjust for exponential growth of *T. weissflogii*. Almost all treatments held constant DIC and pH_{sw} until the final 24 hours, where an evolution of DIC and pH_{sw} in all culture treatments was observed (Figure 3.4). This change is due

to the growth of diatoms, and a net removal of DIC due to diatom growth despite the constant addition of pCO_2 (those treatments with higher pCO_2 exhibit an increase in DIC towards the end of the experiment).

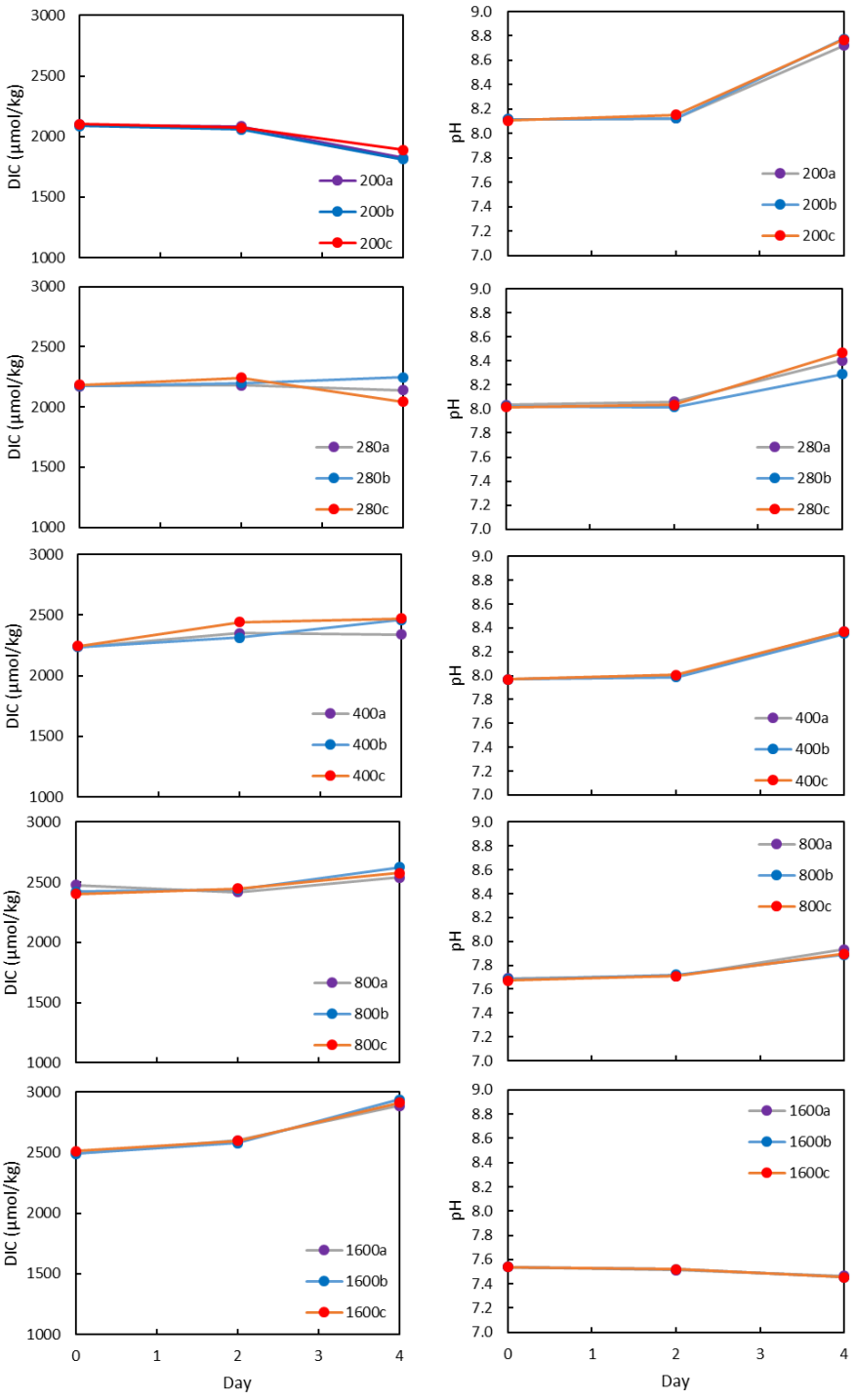

Figure 3.4: Each culture treatment shows evolution in the culture media depending on diatom growth. All treatments exhibit changes in DIC due to diatom growth balanced with the input of pCO_2. The higher pCO_2, the more DIC increases towards the end of the experiment.

Treatment	pCO_2	2σ	pH	2σ	DIC	2σ	HCO_3^-	2σ
200	125	8	8.53	0.73	1925	61	1091	59
280	244	73	8.25	0.41	2165	113	1521	260
400	267	28	8.25	0.44	2400	115	1728	107
800	809	62	7.83	0.24	2525	56	2206	69
1600	2117	40	7.48	0.08	2791	21	2628	22

Table 3.2: Mean carbonate system parameters calculated for each culture treatment, based on the number of cells grown in each 24 hour period of the batch experiment.

3.3.2 Ocean acidification effects on *T. weissflogii*

The relationship between growth rates, mean cell size, and C, N and Si per cell, and pH_{sw} was determined using least squares linear regression (Figure 3.5). This treatment indicated that no significant relationship was found between pH_{sw} and growth rate, and a reduction in pH_{sw} also appears to have no effect on biogenic silica quota per cell, despite the slight reduction in mean cell size (Figure 3.5). Any further correlations observed are therefore not influenced by growth rate variation.

Significant relationships were observed between cell size and pH_{sw} ($p > 0.001$, $R^2 = 0.68$; Figure 3.5), and C/N and pH_{sw} ($p > 0.001$; Figure 3.5). Mean cell size is therefore dependent upon the reduction in pH_{sw} with smaller cells present at lower pH_{sw}, although this change appears to be within error over 1.2 pH units (Figure 3.5). C/N ratios decrease with reducing pH_{sw}, which arises due to a constant (within error) carbon concentration per cell relative to a N/cell increase with decreasing pH_{sw} ($p > 0.001$), suggesting a dependence of N/cell on pH_{sw}. Si/C ratios show no significant trend, as both Si/cell and C/cell appear to be unaffected by changing pH_{sw} (Figure 3.5).

A similarity in cell size is also observed in SEM images of a sub sample from each culture treatment (Figure 3.6). However, the SEM images also indicate that the diatoms grown in the 1600 ppm treatment are more robust to vacuum treatment, and therefore likely have more robust frustules, than the cells grown at 200 ppm.

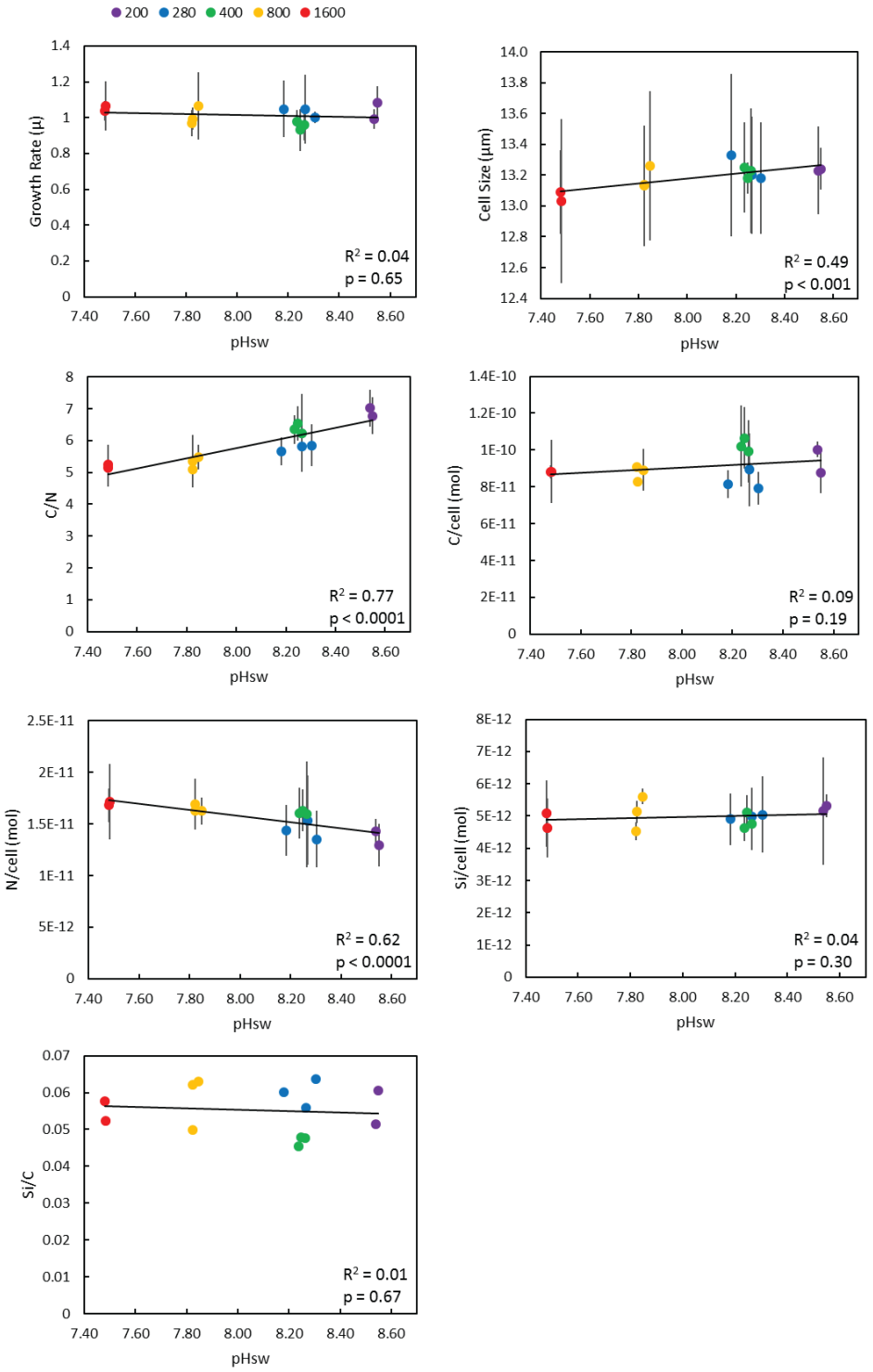

Figure 3.5: Linear least squares regressions of parameters measured in *T. weissflogii* cultures as a function of pH_{sw}. The diatom growth rate appears to be unaffected by pH_{sw}, but cells grown at lower pH_{sw} were smaller than those grown at higher pH_{sw} The only other relationships of significance with pH_{sw} are those involving N (N/cell and consequently C/N), indicating cells grown at lower pH_{sw} contain more N/cell. Error bars shown are 2σ.

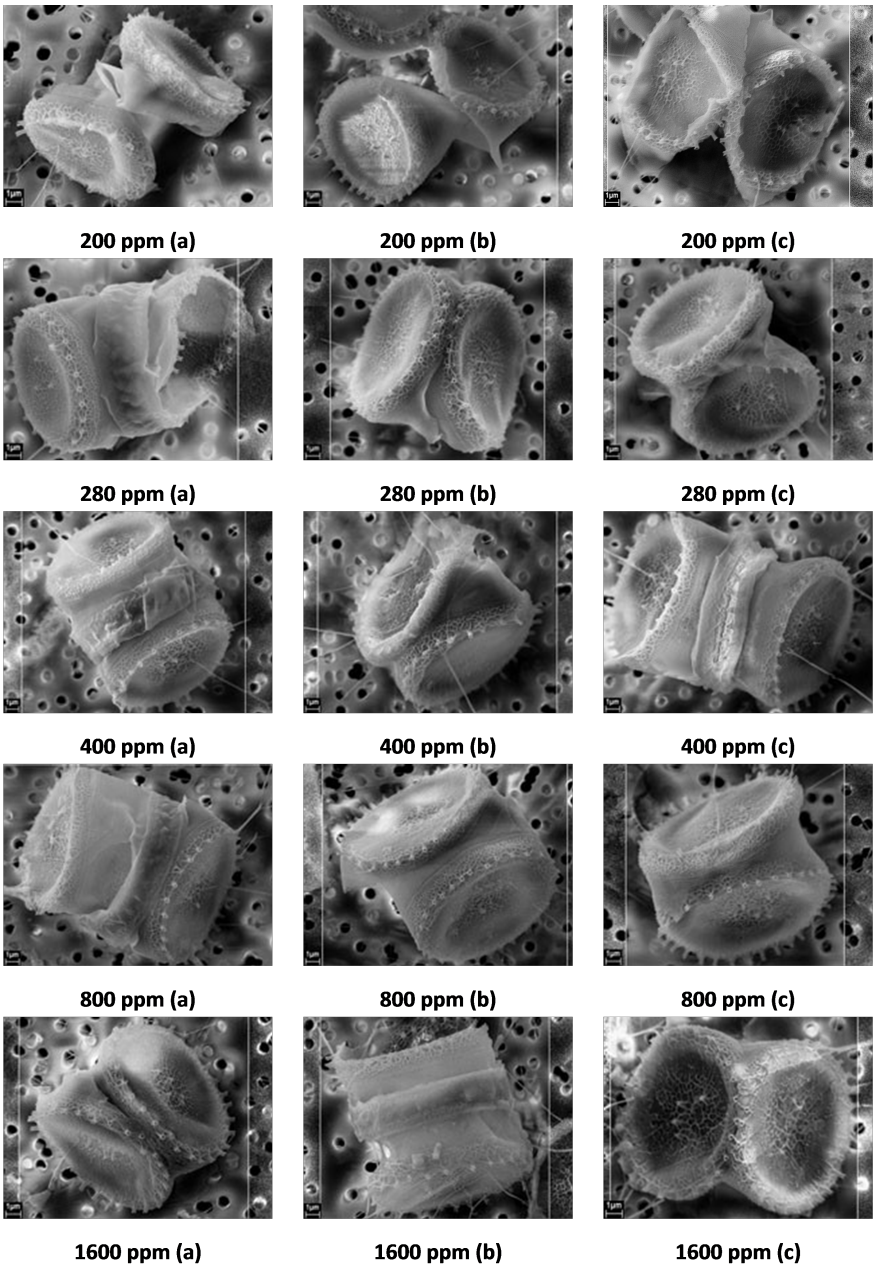

Figure 3.6: SEM images of subsamples from all five culture treatments of *T. weissflogii* grown at 200, 280, 400, 800 and 1600 ppm pCO_2 (top to bottom).

3.3.3 Boron in diatoms

Boron content of diatom frustules was measured as B/Si, which increased with increasing pH_{sw} significant to the 95% level ($R^2 = 0.71$, $p < 0.05$; Figure 3.7). Both boron and nitrogen content per cell appear to be the two variables measured most affected by the reduction in pH_{sw}, with both elements increasing with increasing pH_{sw}, and inherently with increasing cell size.

Parameter 1	**Parameter 2**	**Gradient**	**Intercept**	**R^2**	**p**
Growth rate	pH_{sw}	-0.03	1.23	0.04	0.65
Cell size	pH_{sw}	0.16	11.9	0.49	< 0.001
C/N	pH_{sw}	1.59	-6.96	0.77	< 0.0001
C/cell	pH_{sw}	7E-12	3E-11	0.09	0.19
N/cell	pH_{sw}	-3E-12	4E-11	0.62	< 0.0001
Si/cell	pH_{sw}	2E-13	4E-12	0.04	0.30
Si/C	pH_{sw}	-0.002	0.07	0.01	0.67
B/Si	pH_{sw}	3.92	-26.9	0.71	< 0.05
$\delta^{11}B$	pH_{sw}	-2.62	17.3	0.43	< 0.01
C/N	$\delta^{11}B$	-0.21	5.05	0.20	< 0.05
C/cell	$\delta^{11}B$	2E-12	1E-10	0.11	0.24
N/cell	$\delta^{11}B$	9E-13	2E-11	0.82	< 0.0001
Si/cell	$\delta^{11}B$	-6E-14	5E-12	0.06	0.23
Si/C	$\delta^{11}B$	-0.002	0.05	0.16	0.11
$\delta^{11}B$	B/Si	-0.37	2.21	0.25	0.39

Table 3.3: Statistical analysis results based on least squares linear regressions for all variables measured. Significant relationships at the 95% level are indicated by a p value of < 0.05.

The $\delta^{11}B$ for cultured *T. weissflogii* are isotopically light with an average value across all treatments of -3.95 ‰. Figure 3.8 shows there is also a clear relationship between $\delta^{11}B$ of the diatom frustule and pH_{sw} ($R^2 = 0.43$, $p < 0.01$), albeit one that is negative rather than positive as seen in carbonates, as well as much lighter.

As $\delta^{11}B$ measured in *T. weissflogii* and pH_{sw} have a strong relationship, a number of variables shown to have a relationship with pH_{sw} also have a significant relationship with $\delta^{11}B$. This is true for mean cell size and C/N ratios (both increasing with heavier $\delta^{11}B$; Figure 3.9), as well as nitrogen content (decreases with heavier $\delta^{11}B$; Figure 3.9), which again clearly drives the C/N ratio relationship with $\delta^{11}B$ rather than the carbon content. No clear trends are observable for $\delta^{11}B$ plotted against growth rate or Si/cell, suggesting boron uptake in diatoms is not directly dependent on growth rate and silicic acid uptake (Table 3.3).

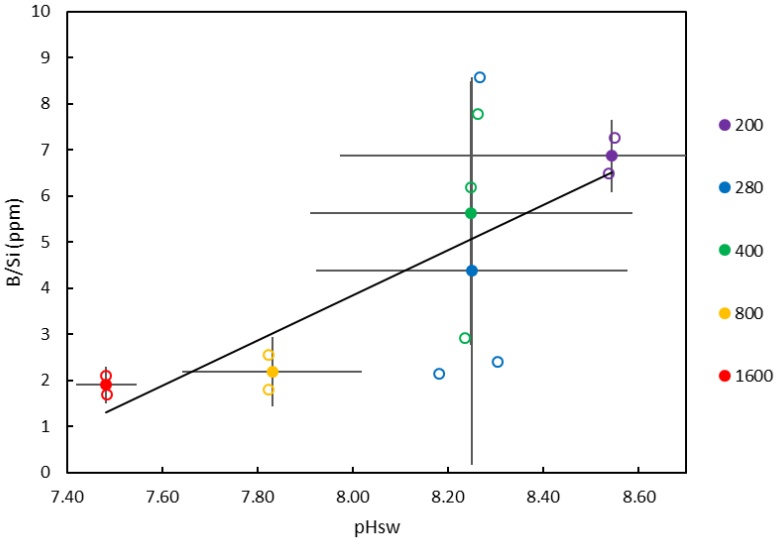

Figure 3.7: Boron content of diatoms frustules in each treatment shows a positive relationship (hollow points indicate individual culture treatments, and solid points indicate treatment means), where increasing pH_{sw} results in increased boron content of the frustule.

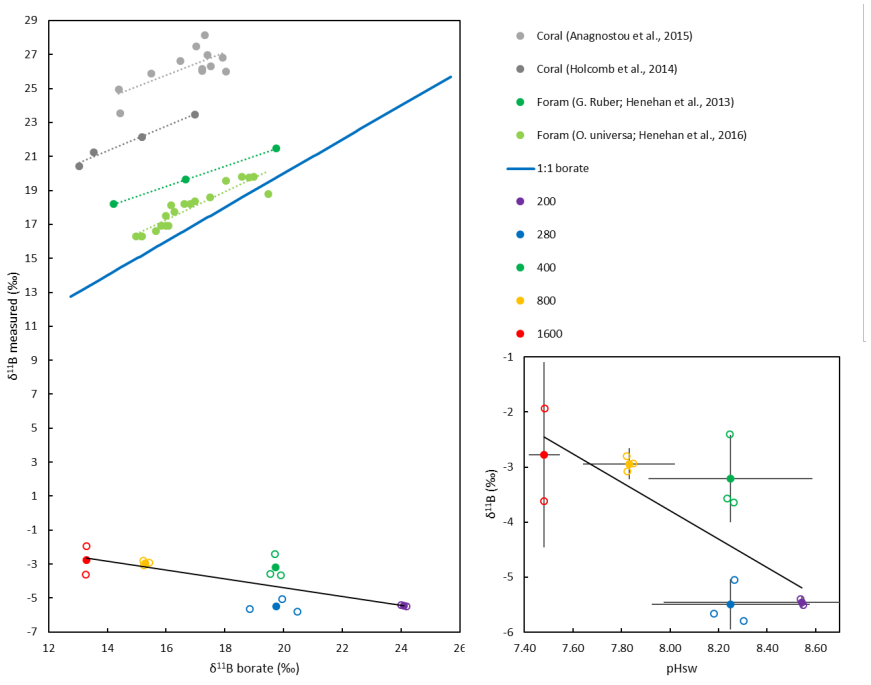

Figure 3.8: δ^{11}B of aqueous borate plotted against previously measured coral δ^{11}B (Anagnostou et al., 2012; Holcomb et al., 2014) and foraminifera δ^{11}B (Henehan et al., 2013; Henehan et al., 2016) shown in grey and green points respectively. The diatom δ^{11}B results for each culture treatment are plotted in coloured points, and show a distinctive negative relationship with δ^{11}B borate, as well as their unusually light absolute δ^{11}B compared with previously measured carbonates.

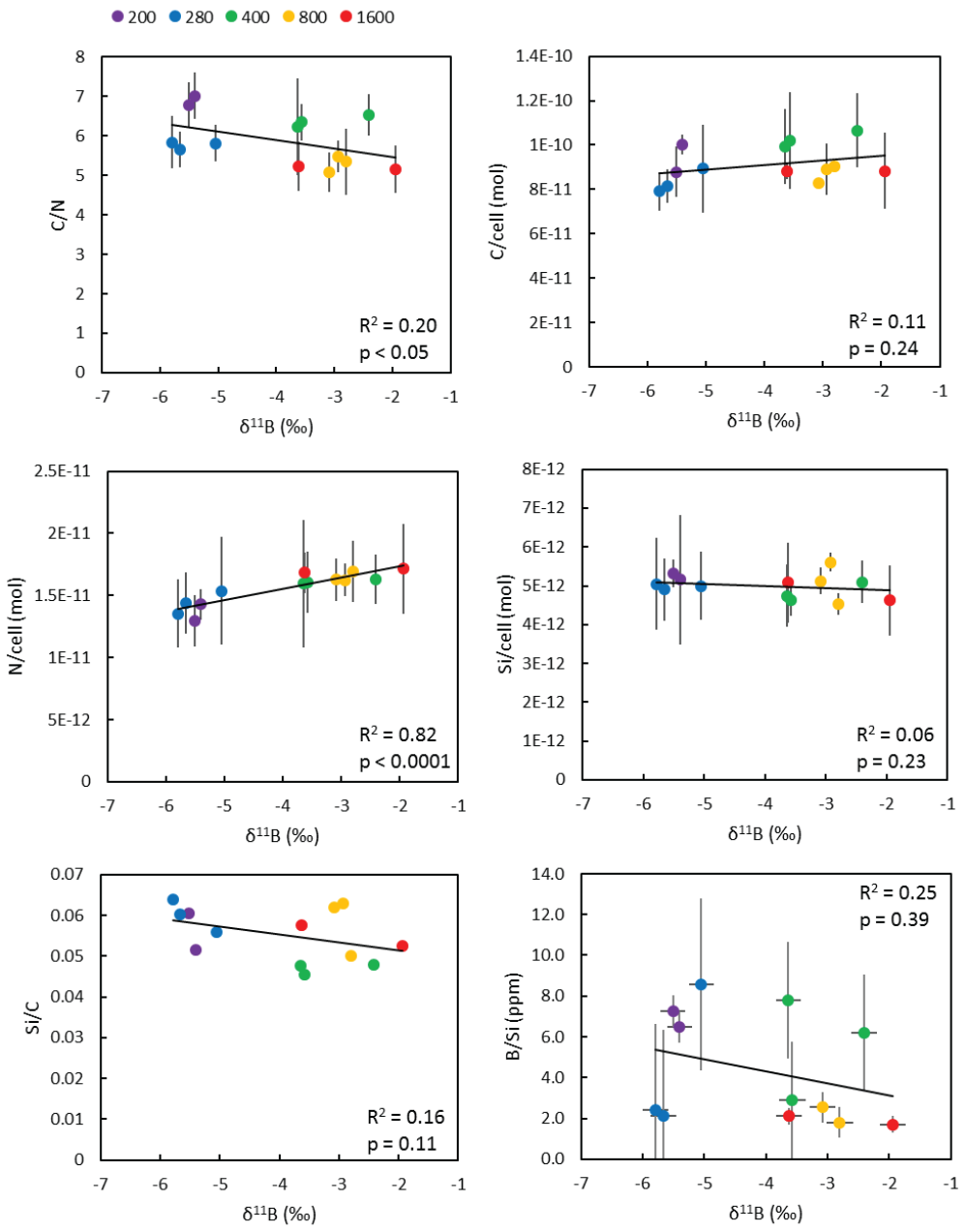

Figure 3.9: Linear least squares regressions of parameters measured in *T. weissflogii* cultures as a function of δ^{11}B.

3.4 Discussion

3.4.1 Ocean acidification effects and implications for diatoms

The growth rates of *T. weissflogii* in this study appear to be unaffected by variable pH_{sw}, with no significant differences revealed between growth rates at either

of the extreme culture treatments of 200 and 1600 ppm (Figure 3.5). Previous ocean acidification studies have shown that diatoms exhibit divergent growth responses in the face of changing pH (Gao and Campbell, 2014), including growth stimulation, growth inhibition, and also unaffected growth observed within the same species (note particularly *T. pseudonana*; *e.g.* Yang and Gao, 2012). Some previous studies investigating *T. weissflogii* have found that a reduction in pH_{sw} led to an increased growth rate (*e.g.* Hervé et al., 2012; Mejía et al., 2013), although others are in agreement with this study; where a pH_{sw} reduction has negligible effect on *T. weissflogii* growth rate (Li et al., 2016). No effect on *T. weissflogii* growth rate was also observed at elevated pCO_2 by Passow and Laws (2015), but only in the absence of other environmental stressors: under light and temperature stress, Passow and Laws (2015) found high pCO_2 resulted in a decline in growth rates as a result of increased energy requirements and slower metabolic processes. Whilst other environmental variables are also important factors in influencing diatom growth rate, light and temperature were not investigated as variables for this study, as both were maintained throughout the experiments at a mean of ca. 8.3 mol photons m^{-2} d^{-1} and 20°C respectively, ensuring the only influence on the culture treatments was *via* pCO_2 and hence pH_{sw}.

3.4.1.1 Silica

Diatom frustules are not affected by the same destabilisation that calcareous organisms encounter during a reduction in pH_{sw}, as silica availability in seawater depends upon the solubility of amorphous silica rather than pH_{sw} as for carbonates, and silica dissolved in seawater is predominantly present as $Si(OH)_4$ at pH_{sw} below 9.47 (pK_a of $Si(OH)_4$; Exley and Sjöberg, 2014). In this study, silica per cell does not appear to vary significantly between each treatment, even though cell size decreases slightly with a reduction in pH_{sw} (Figure 3.5). The slight decrease in mean cell size is within error, so in terms of silicification, there appears to be no difference between *T. weissflogii* grown at higher pH_{sw} and that grown at lower pH_{sw}. This in turn implies that *T. weissflogii* diatoms are resilient against this magnitude of ocean acidification. This is also qualitatively inferred from the SEM imagery (Figure 3.6), where diatoms grown at

higher pH_{sw} visually exhibit a larger collapse under vacuum than those diatoms grown at reduced pH_{sw}

3.4.1.2 Cellular carbon and nitrogen

Under elevated pCO_2, it might be expected that growth rate of larger diatoms would increase compared to those grown at lower pCO_2 due to increased rates of photosynthesis and carbon acquisition, however this was not observed in this culture experiment. The C/N ratio shows an increase with decreasing pH_{sw}, but the carbon content of the cells in all treatments appears to be constant when normalised to cell volume. Hence, it is the nitrogen content per cell that increases with decreasing pH_{sw} that then drives this change in the C/N ratio. This suggests ocean acidification could affect the nitrogen metabolism in diatoms by altering enzyme activity and protein structure (Huergo et al., 2013; Wu et al., 2014b).

The observation that organic carbon content of the diatoms remained constant implies that none of the culture treatments were carbon limited. This reflects the typical marine environment, where phytoplankton are more likely to be limited by another essential nutrient than by carbon (more likely to be N or Si limited). *T. weissflogii* supports a CCM involving the active uptake of both CO_2 and HCO_3^- directly from seawater (Burkhardt et al., 2001), which suggests the constant trend may simply be due to efficient CCMs supplying adequate carbon to the diatoms at lower pCO_2 as HCO_3^- at a similar rate to those diatoms grown at elevated pCO_2 that are able to use CO_2 directly from seawater (Thornton, 2009).

In terms of the increase in cellular nitrogen with a reduction in pH_{sw}, several studies have reported an increase in cellular nitrogen concentration with decreasing cell size (Verity et al., 1992; Montagnes and Franklin, 2001), which also correlates with lower pH_{sw} in this study (Figure 3.5). However, when combined with temperature, light and other nutrient stressors, a variety of factors influence cellular nutrient concentrations (including nitrogen and growth rates; *e.g.* Burkhardt et al., 1999). Consequently, in the context of a future acidic ocean, whilst *T. weissflogii* diatoms appear to be fairly

resilient with regards to their growth rates, carbon requirements and silica content, however, future blooms could use more nitrogen per unit of Si, leaving less available for the rest of the phytoplankton community when the diatoms become Si-limited.

3.4.2 Boron content of diatom frustules

Boron is an essential micronutrient involved in structural stability, especially for organisms that photosynthesise (Marschner, 1995; Tanaka and Fujiwara, 2008). In this study, the boron content of diatom frustules increased with increasing pH_{sw}, corroborating a study completed by Mejía et al. (2013), in which they also found this positive relationship in *T. weissflogii* (Figure 3.10). Not only is this relationship replicated here, but the absolute boron content is also shown to be similar between the two studies (ca. 2 - 10 ppm compared with 1.7 - 8.6 ppm in this study), despite the different analytical methods used (LA-ICP-MS in Mejía et al., 2013 *vs.* MC-ICP-MS in this study). This strongly suggests that pH_{sw} is a controlling factor in boron uptake in diatom frustules. Mejía et al. (2013) concluded that the uptake of boron in diatoms is likely to be independent to that of silicic acid, as although their results showed boron content and Si/C (degree of silicification) were both dependent upon pH_{sw}, there was no significant relationship between boron content and Si quotas. The results of this study appear to corroborate the assumption that these two uptake processes are independent, as in this study there is also the lack of a significant trend between Si quota and pH_{sw} (Figure 3.5), and Si quota and $\delta^{11}B$ (Figure 3.9).

Brown et al. (2002) noted that boron can react with many biological molecules, and that it is likely that a large proportion of boron found within an organism could be complexed with biological molecules. For example, N-containing molecules provide stability to boron species through additional H bonding (Woods, 1996). This suggests that the boron concentration of the cytoplasm could be highly variable (Raven, 1980; Dordas and Brown, 2000), however these complexed boron molecules have been shown to have no effect on cellular metabolism. It has also been shown that boron passively diffuses into higher plants, but can potentially undergo active uptake (Pfeffer et al., 2001), contributing to large variation in internal boron concentration (Dordas and Brown, 2000;

Brown et al., 2002). This is to ensure a lack of boron deficiency in boron-limited environments, as this can affect cell wall structure, and lead to an imbalance between carbon and nitrogen metabolisms causing carbohydrate excess.

Mejía et al. (2013) proposed that boric acid may also passively diffuse across the cell wall and through the apoplast, ensuring the cell obtains enough boron to meet its biological needs in organic parts of the organism. However, as an increase in boron content of the diatom frustule with increasing pH_{sw} is observed in both this study and that of Mejía et al. (2013), it is likely that borate is also actively transported across the cell wall, due to the reduction of aqueous boric acid concentration with increasing pH_{sw}. As borate is an anion, this must occur through transport proteins, and then the borate is transported to the silicon deposition vesicle (SDV) when the cell undergoes biosilicificiation *via* silicon transport vesicles (STV) (Vrieling et al., 1999). As a result of the strict internal pH regulation of diatoms, borate found within the cytosol could also be internally transported into STVs or the SDV to a greater extent at high internal pH, which could subsequently lead to more borate being fixed in the inorganic matrix of the diatom frustule.

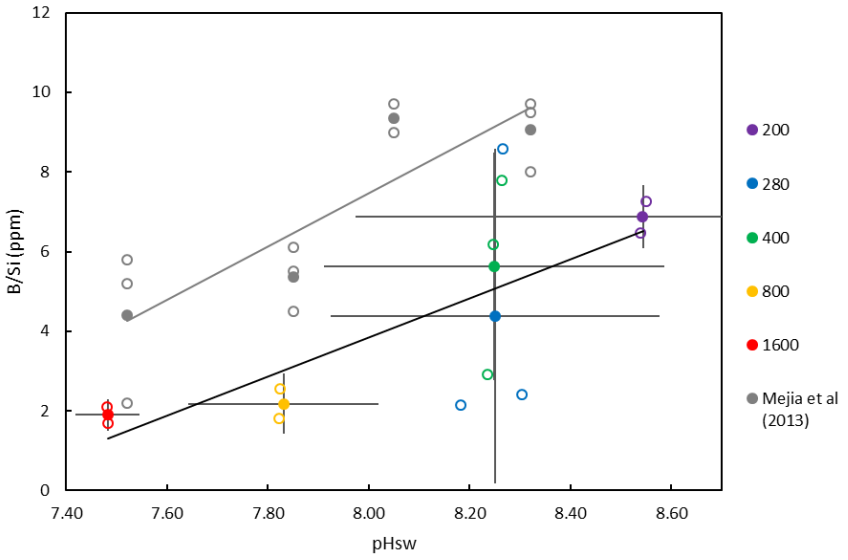

Figure 3.10: Boron content of cultured *T. weissflogii* diatoms as a function of pH_{sw}. Coloured symbols are from this study (open are individual culture treatment flasks, and closed are mean values), and grey symbols are from Mejia et al. (2013). Both studies show an increase in boron content with increasing pH, and although the linear regressions are slightly different, the absolute B/Si values are similar.

Mejía et al. (2013) suggest that bicarbonate transporter proteins (BTR1) that are phylogenetically similar to BOR1 borate transporters, and have poor selectivity of similar anions, could actively co-transport borate with bicarbonate. As the pCO_2 in seawater decreases (pH_{sw} increases), there is less bioavailable CO_2 for diatoms to use in photosynthesis, so CCMs become more active. This involves actively transporting more bicarbonate anions into the cell, potentially leading to more borate being taken up either due to an increased $B(OH)_4^-/HCO_3^-$ ratio at high pH_{sw}, or due to increased CCM activity at higher pH_{sw}.

3.4.3 $\delta^{11}B$ relationship with pH_{sw} in diatom opal

Diatoms silicify internally, so the components required for biomineralisation are taken up into isolated internal vesicles, ensuring silicification occurs from a closed system at reduced internal pH within the SDV (Del Amo and Brzezinski, 1999; Vrieling et al., 1999). Since boric acid can passively diffuse through the cell membrane, and borate is likely transported into the cell with bicarbonate, it is probable that both aqueous boron species are present in the Si deposition environment. Both boron species therefore need to be considered in modelling the potential mechanisms of boron uptake in diatoms, in an attempt to explain the negative trend observed between $\delta^{11}B$ of diatom opal and pH_{sw}.

Since the lowest energy option for the diatom to obtain boron is the passive diffusion of boric acid, this was considered in a model where the boric acid concentration inside the diatom was in equilibrium with that of the seawater. This led to a predicted reduction in diatom boron concentration with increasing pH_{sw} - the opposite to the observed relationship from the culture experiment (Figure 3.11). Therefore, combined with the measured $\delta^{11}B$, which indicate that borate must be involved as incorporation of boric acid would result in the frustule being far too isotopically heavy, this suggestion can be ruled out.

The second model explored builds on the model of borate active uptake suggested by Mejía et al. (2013), and proposes that borate is transported into the diatom

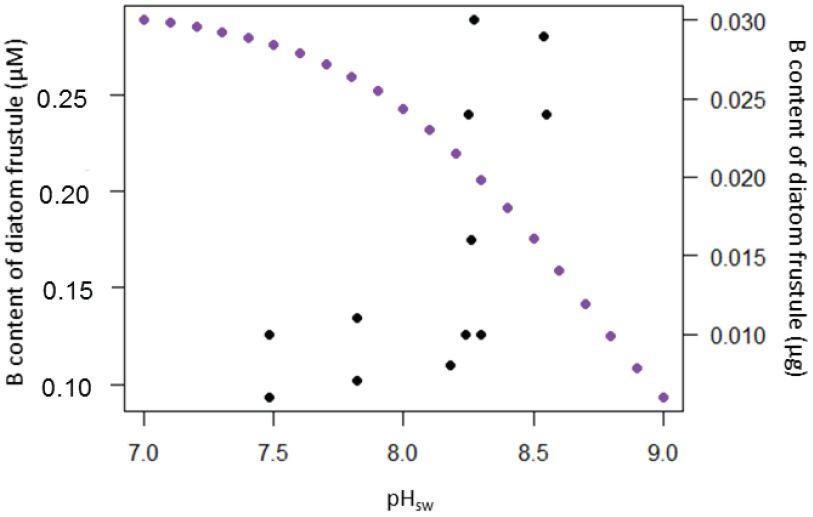

Figure 3.11: Model showing the disparity between boron concentration of diatom frustules if boric acid is in equilibrium with seawater concentration (purple) and the boron concentration observed in culture experiments (black) with increasing pH$_{sw}$.

as an inverse function of pCO_2 in addition to the passive diffusion of boric acid in equilibrium from seawater (Figure 3.12). Once inside the diatom, the borate is eventually transported into the SDV and after a further re-speciation at a pH of ca. 5.5 (Mejía et al., 2013), the remaining borate is incorporated into the silica polymer forming the new frustule hypovalve.

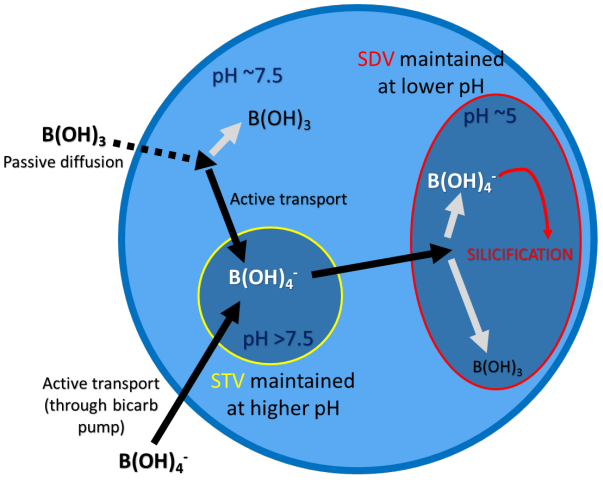

Figure 3.12: Schematic showing visually how boron enters the diatom cell, based on a suggestion by Mejía et al. (2013). Active transport and passive diffusion both play roles in boron transport into the diatom, while only borate is incorporated into biogenic silica in the SDV.

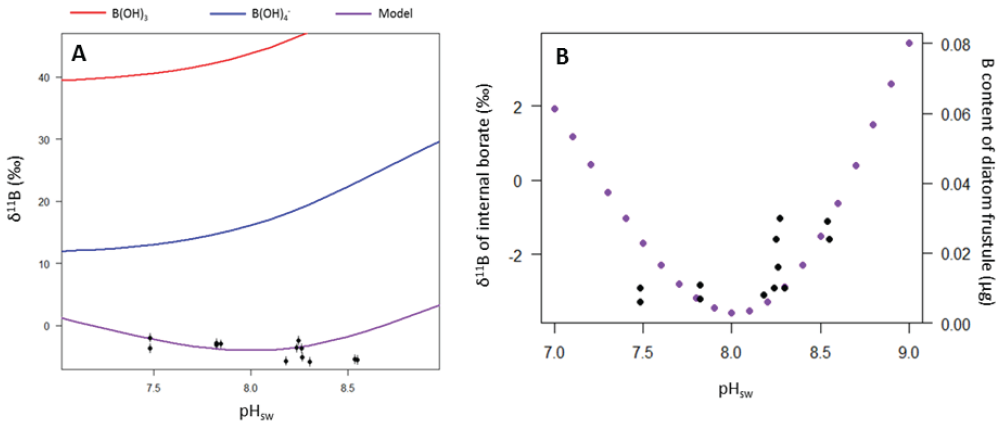

Figure 3.13: Model showing δ^{11}B (A) and boron content (B) dependent on an inverse relationship with pCO$_2$ involving active borate co-transport with bicarbonate. The black circles are the data measured in this study, and the purple line (A) and circles (B) is the model based on an exponential increase in borate/bicarbonate uptake, which can describe the data observed at all pH$_{sw}$ well, apart from the highest pH$_{sw}$ of 8.53. This simplistic model fixes boric acid content of the diatom as equal to that of seawater, depending on pH$_{sw}$, and therefore the increasing borate content as a result of increasing bicarbonate pumping can explain this negative δ^{11}B-pH$_{sw}$ relationship observed in cultured *T. weissflogii* diatoms. This trend has never been seen before in marine carbonate δ^{11}B. The red line is δ^{11}B of aqueous boric acid, and the blue line is δ^{11}B of aqueous borate.

As the amount of borate actively taken in depends on the bicarbonate concentration, the boron content, and hence δ^{11}B, of the diatom is therefore dependent on pCO$_2$ rather than the absolute concentration of boron species in seawater. As pCO$_2$ declines, the photosynthetic demand of the diatom results in more bicarbonate taken up using the CCM, and hence an exponential increase in active borate uptake (Figure 3.13) due to the increasing $B(OH)_4^-/HCO_3^-$ ratio.

As some discrepancies are observed between the measured and modelled δ^{11}B, this model is not perfect, and some key caveats include: (i) isotopic fractionation during passive boric acid diffusion is unlikely (Nir et al., 2015), but any isotopic fractionation occurring during active borate uptake is unknown; and (ii) beyond the SDV, the location and transport of borate once it enters the cell is unknown.

However, a basic model check can be completed by calculating the total δ^{11}B and boron content of a solution (*i.e.* the internal fluid) that would allow a diatom to be capable of reducing δ^{11}B to less than that of the δ^{11}B of aqueous borate in seawater. Figure 3.14 shows these δ^{11}B predictions are valid apart from for the culture treatment

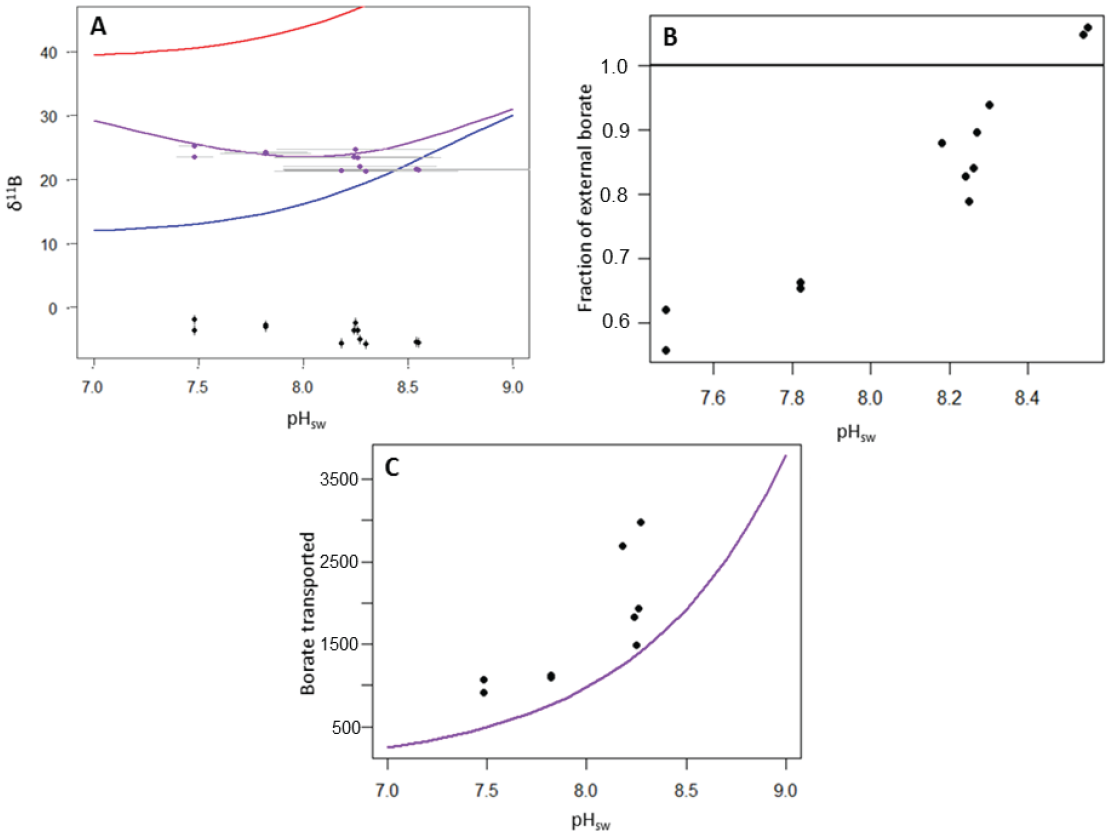

Figure 3.14: Model check based on determining the δ^{11}B of the internal fluid where biosilicification occurs in a diatom. These panels show experiment data in black, the model check in purple, and aqueous boron species are depicted as before (red: boric acid, blue: borate). Panel A shows the required δ^{11}B of the internal fluid to obtain the observed δ^{11}B values, and all are theoretically possible based on the passive diffusion of boric acid and active uptake of borate. As pH increases, the δ^{11}B of the internal fluid tends towards external borate δ^{11}B to a point where a value below the borate line is impossible to reproduce (confirmed in panel B using fraction of external borate required; more than 100% cannot be achieved). Panel C reveals a final confirmation in terms of the trend of boron concentration, with the measured data compared to the increasing borate content of the internal fluid, assuming borate undergoes active co-transport with bicarbonate.

at the highest pH_{sw} of 8.53. However, as indicated by the error bars in Figure 3.14A, all predicted δ^{11}B lie between the aqueous borate and boric acid lines within error. Thus, at this stage, the model-data misfit simply due to uncertainty in our measurements cannot be ruled out. Regardless, the model strongly supports both boron species playing a role in determining δ^{11}B of the diatom internal fluid, and subsequently δ^{11}B of diatom opal, and that at higher pH, internal total δ^{11}B tends towards δ^{11}B of borate in seawater. This model check therefore cannot fully explain the trend observed in the culture experiment, but it can recreate a negative δ^{11}B-pH relationship up to a pH of approximately

8.5, alongside a positive [B]-pH relationship (Figure 3.14).

3.4.4 Implications for boron palaeo-pH proxy development

The δ^{11}B-pH$_{sw}$ and B/Si-pH$_{sw}$ calibrations achieved for *T. weissflogii* diatoms are essentially empirical, and as pH$_{sw}$ determined by pCO$_2$ bubbling was the only variable investigated in this study, further investigation should determine as to what extent other environmental variables influence the established relationships observed here (*e.g.* irradiance, temperature, nutrient limitation). Although there is variation between the triplicate batch culture samples, the δ^{11}B-pH$_{sw}$ calibration is precise to ± 0.83 ‰, and the B/Si-pH$_{sw}$ calibration is precise to ± 1.20 ppm based on the residuals from the linear regression gradients. These could be improved upon by repeating the culturing experiment but harvesting the diatoms at 72 hours instead of 96 hours to avoid the drift in carbonate parameters observed as a result of diatom growth. This may ensure less variation between culture flasks, and therefore a better precision of calibration.

Even though δ^{11}B and B/Si of the diatom frustule are not correlated with each other, these two independent proxies indicate diatoms have good potential as a palaeo-pH archive, as both are sensitive to pH$_{sw}$. This is an especially important development in terms of areas where the majority of marine sediments are composed of biogenic opal, such as at high latitudes, as these areas are in great need of further investigation. Being able to measure boron isotopes in fossilised diatom frustules would therefore expand the marine core locations that boron isotopes can be measured from, and potentially contribute to a clearer understanding of past pCO$_2$ reconstructed from marine sediment fossils.

3.5 Conclusions

In order to further elucidate mechanisms contributing to glacial-interglacial pCO$_2$ change in the high latitude oceans, the δ^{11}B-pH$_{sw}$ relationship was examined in *T. weissflogii* diatoms. This calibration was completed using culture treatments maintained at a range of pH$_{sw}$ using bubbled pCO$_2$. Elevated pCO$_2$ had little effect

on the diatom growth rates, carbon acquisition, or degree of silicification, but it led to slightly smaller cells over 1.2 pH units, and most notably an increased cellular nitrogen content. This may therefore have implications for the oceanic nitrogen cycle in the face of pH_{sw} reduction. However, this should be further investigated in a study combining all environmental factors influencing diatom growth as well as those that may change due to an increase in pCO_2, such as temperature and nutrient availability, in order to provide better predictions for diatom response in the face of ocean acidification.

Boron content within *T. weissflogii* diatoms increased with increasing pH_{sw}, supporting the only other study completed investigating boron in diatoms (Mejía et al 2013), suggesting that borate is incorporated into the diatom frustule. The first $\delta^{11}B$ measured using MC-ICP-MS in cultured diatoms are extremely isotopically light and exhibit a negative trend with pH_{sw} a relationship never seen before in other substrates. Preliminary model results suggest that a combination of boric acid and borate species could enter the diatom, but only borate is incorporated into the diatom frustule matrix at low internal pH to produce such a negative trend in $\delta^{11}B$.

The observation that pH_{sw} (and therefore pCO_2) exhibits an influence on $\delta^{11}B$ and boron content of the diatoms confirms that diatoms may therefore be a suitable archive for palaeo-pH studies. Culture studies on further diatom species should be undertaken, in order to assess the viability of diatoms in the boron proxy as a whole, and further analytical investigation should be carried out to unequivocally determine the co-ordination of boron in the frustule. For instance, ^{11}B NMR could give vital clues as to how boron is co-ordinated in the matrix, although even NMR cannot identify the origin of the boron species co-ordinated within the frustule. Regardless, this study suggests that extending the boron-based proxies into diatom opal is possible, and therefore holds considerable promise in the future.

Chapter 4

Boron isotopes in sedimentary diatoms (*Coscinodiscus marginatus* and *C. radiatus*) from 2.85 - 2.52 Ma in the subarctic Northwest Pacific (ODP Site 882)

Intended co-authors:

George Swann (provided samples, expertise, and all diatom-sediment separation training)

Gavin Foster (general discussion and feedback)

The subarctic Northwest Pacific Ocean is important to investigate in the context of palaeoceanographic changes, as significant upwelling of deep ocean waters occurs here, yet this area is understudied in comparison to other high latitude regions (*i.e.* the Southern Ocean and North Atlantic). The intensification of Northern Hemisphere glaciation (iNHG) at 2.73 Ma is associated at ODP Site 882 with an abrupt drop in opal mass accumulation rates, reduction of $\delta^{18}O_{diatom}$ and $\delta^{30}Si_{diatom}$, and an increase in $\delta^{15}N_{diatom}$. These changes have been attributed to the development of stratification in the subarctic Pacific subsequent to global cooling over this time period. This stratification caused the upwelling of nutrient- and CO_2-rich waters to dramatically reduce, likely contributing

to the decline in atmospheric CO_2 observed at this time (Martínez-Botí et al., 2015). One way of testing this scenario is by using the boron isotope pH proxy to quantify local ocean pH change, which will reflect the CO_2 content of the surface water. Following the development of a new method to measure $\delta^{11}B$ and B/Si in diatom frustules by MC-ICP-MS, and the calibration of the $\delta^{11}B$-pH and B/Si-pH relationships in cultured diatoms, new diatom records for ODP Site 882 are presented here alongside the existing palaeoceanographic records. Both new boron proxies enhance the current understanding of the ocean changes occurring during iNHG, indicating a general increase in seawater pH (and hence pCO_2 content reduction) from 2.85 - 2.52 Ma. Brief intervals of low pH water following iNHG match the periods of stratification weakening identified by other proxies. The increase in pH inferred from the boron proxies are also comparable to modern Pacific pH change as a result of seasonal stratification, strengthening the hypothesis that iNHG led to stratification in the subarctic North Pacific, and this acted as a positive feedback on atmospheric CO_2 content.

4.1 Introduction

The subarctic Northwest Pacific has gained increased attention recently, and this research has revealed the importance of this region in global climate changes, especially over the Pliocene-Pleistocene transition and the intensification of Northern Hemisphere Glaciation (iNHG). During this period (2.85 - 2.52 Ma), productivity in the Northwest Pacific declined rapidly at 2.73 Ma, inferred from biogenic opal mass accumulation rates (MAR) (Maslin et al., 1995; Haug et al., 1999; Cortese et al., 2004; Sigman et al., 2004; Swann et al., 2006). Potential mechanisms for this large drop in productivity have been discussed including light limitation due to sea ice extension (Hillenbrand and Cortese, 2006), decline in nutrient supply to the surface ocean (Haug et al., 1999; Sigman et al., 2004) possibly linked to gradual increased freshwater input and stratification change (Haug et al., 2005), or a change in aeolian dust deposition and associated iron limitation (Bailey et al., 2011). This abrupt change has however been widely accepted as being coincident with iNHG, and has been the subject of considerable study.

Regardless of the exact cause of the drop in opal MAR at 2.73 Ma, the presence

of year-round ice sheets from this time and globally cooler temperatures are likely to have shifted the polar front southwards in the Northwest Pacific, suggesting a change in ocean circulation (Maslin et al., 1995). Furthermore, since the stability of the water column is controlled by a balance between temperature and salinity, and as global cooling occurred in the late Pliocene, the ocean density structure stability provided by temperature is thought to have deteriorated in the North Pacific to the point where salinity began to dominate (Sigman et al., 2004; Swann, 2010). Salinity was also lowered by the gradual increase in freshwater input from increased ice cover due to these cooler temperatures (Haug et al., 2005). Together these factors are thought to contribute to the abrupt onset of stratification at 2.73 Ma in this region. This would not only have also caused deep waters to be isolated from the atmosphere as is the situation today during some times of the year (Haug et al., 1999; Takahashi et al., 2014). Recent model results from Burls et al. (2017) suggest that the elevated Pliocene productivity can indeed be

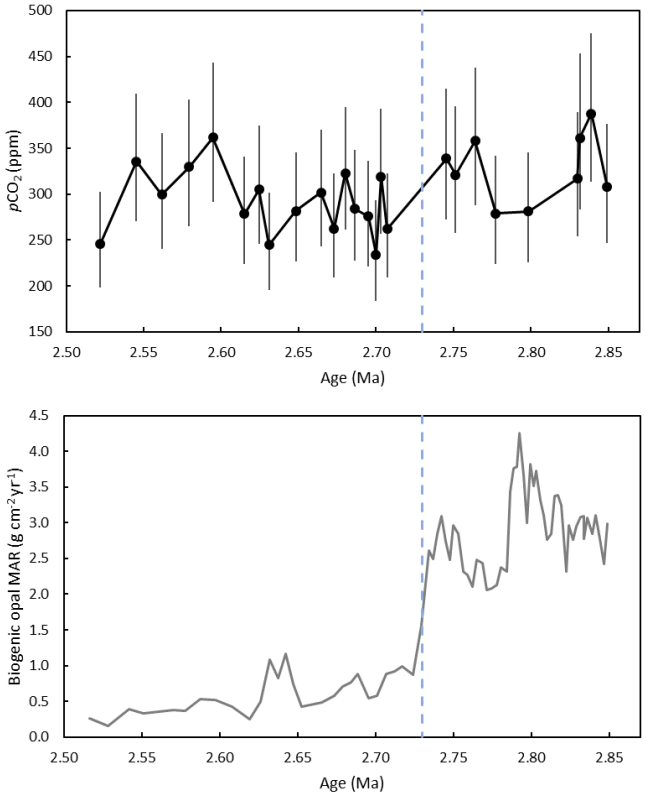

Figure 4.1: Biogenic opal mass accumulation rates (MAR; Maslin et al., 1995) for ODP Site 882 in the North Pacific and global pCO_2 derived from $\delta^{11}B$ in *G. ruber* foraminifera (Martínez-Botí et al., 2015) over the time period 2.85 - 2.52 Ma. The blue dotted line indicates iNHG at 2.73 Ma.

explained by the lack of a halocline in the subarctic North Pacific, which in turn implies deep ocean winter convection until its weakening during iNHG.

Ultimately, a shift from a well-mixed to a strongly stratified ocean would have led to the reduction of CO_2 ventilation to the atmosphere in the polar ocean, potentially acting as a positive feedback on the cooling associated with iNHG to contribute to the drawdown of CO_2 at this time (Figures 4.1 and 4.2; Haug et al., 1999; Sigman et al., 2004).

Despite the importance of the North Pacific during iNHG, the absence of sufficient numbers of foraminifera at Ocean Drilling Program (ODP) Site 882 have prevented further geochemical analyses (Swann, 2010) using boron isotopes to examine the influence of stratification and water column stability changes on surface water pH and hence air-sea CO_2 flux (*e.g.* Foster and Sexton, 2014; Martínez-Botí et al., 2015). Despite the reduction in opal MAR in the sedimentary record of an average of 2.93 g cm^{-2} yr^{-1} pre-2.73 Ma to an average of 0.64 g cm^{-2} yr^{-1} post-2.73 Ma (Figure 4.1), there is still an abundance of preserved diatoms at this site throughout the core, making it very suitable for diatom-based proxies (*e.g.* Maslin et al., 1995; Haug et al., 1999; Sigman et al., 2004; Haug et al., 2005; Jaccard, 2005; Swann et al., 2007; Reynolds et al., 2008; Swann, 2010; Bailey et al., 2011; Studer et al., 2012).

In the modern Northwest Pacific, Takahashi et al. (2014) observed an annual

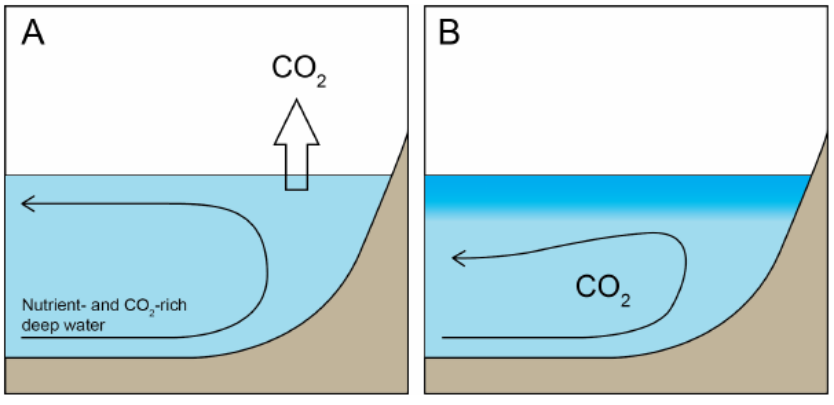

Figure 4.2: Schematic illustrating the effect changes in stratification has on pCO_2 based on Haug et al. (1999) and Rae et al. (2014). A) represents a Pliocene well-mixed, ventilated ocean allowing CO_2-rich deep waters to upwell to the surface, reducing surface pH_{sw} and ventilating CO_2 to the atmosphere, and b) depicts a Pleistocene stratified Pacific, showing the trapping of nutrient-rich water in the deep ocean.

surface pH change of ca. 0.38 pH units associated with seasonal stratification and change in ocean source/sink of CO_2 (ca. 7.74 ventilated, ca. 8.12 stratified; Figure 4.3). When stratification seasonally weakens, CO_2-rich deep waters upwell to the surface and pH_{sw} here is reduced as the ocean ventilates CO_2 to the atmosphere. It would therefore be useful to be able to elucidate the approximate palaeo-pH change in the Northwest Pacific between the ventilated Pliocene and the stratified Pleistocene during iNHG using boron isotopes, and use the understanding of ODP Site 882 and this expectation of likely pH change as an indicator of the robustness of the boron proxy in sedimentary diatoms.

This study aims to apply the methods developed and described in Chapter 2, and the calibration elucidated in Chapter 3, to explore the applicability and utility of these novel boron-based proxies, and also to provide insights into the role of the North Pacific during iNHG.

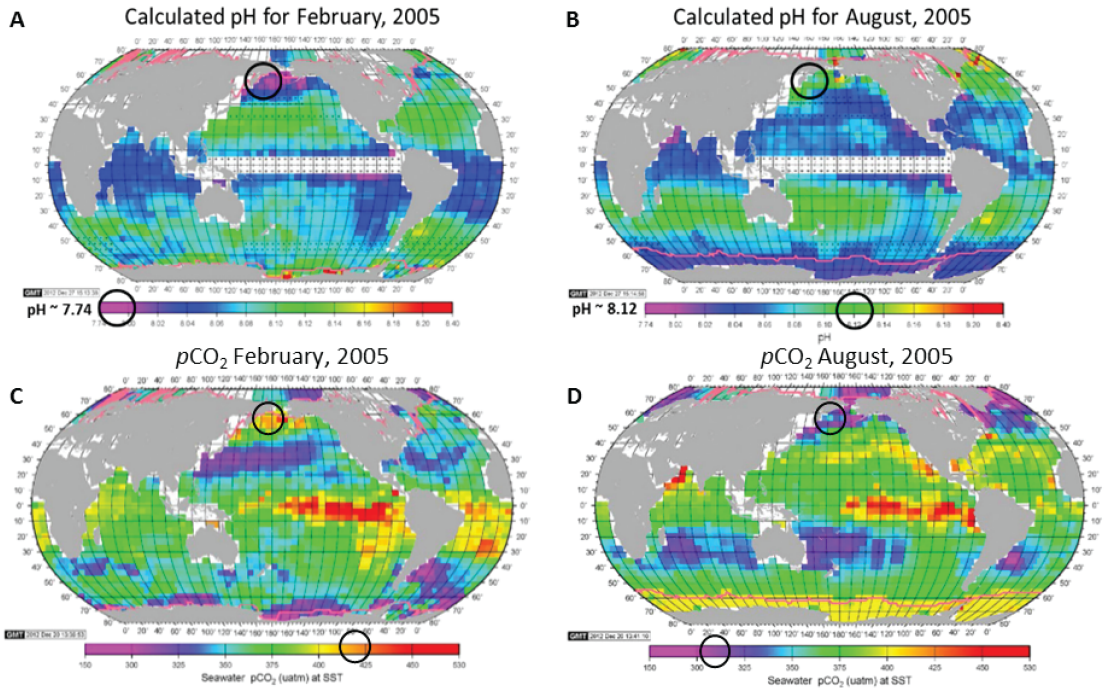

Figure 4.3: Modern annual surface pH_{sw} and pCO_2 change in the Northwest Pacific Ocean (adapted from Takahashi et al., 2014), indicating a shift from low surface pH_{sw} (A; purple) during CO_2 ventilation (C; orange) to high surface pH_{sw} (B; green) during stratification (D; purple).

4.2 Methods

4.2.1 Sample selection

Samples were obtained from ODP Site 882, from 2.85 to 2.52 Ma covering the period at the end of the Pliocene and beginning of the Pleistocene. The age model used is derived from Tiedemann and Haug (1995) and Weeks et al. (1995) This core is situated in the high latitudes of the subarctic Northwest Pacific (50°21' N, 167°35' E, water depth 3244 m; Figure 4.4) next to Detroit Seamount, and these samples have been previously used in studies recording various geochemical and isotope records including δ^{30}Si, δ^{18}O, δ^{15}N, and opal MAR (Maslin et al., 1995; Haug et al., 1999; Sigman et al., 2004; Reynolds et al., 2008; Swann, 2010; Bailey et al., 2011; Studer et al., 2012).

These samples consisted of two closely related diatom species, *Coscinodiscus marginatus* (dominant pre-iNHG) and *Coscinodiscus radiatus* (dominant post-iNHG), and greater than 96% of the samples were 100% pure diatom, determined by SEM and light microscopy (Swann et al., 2006; Swann, 2010).

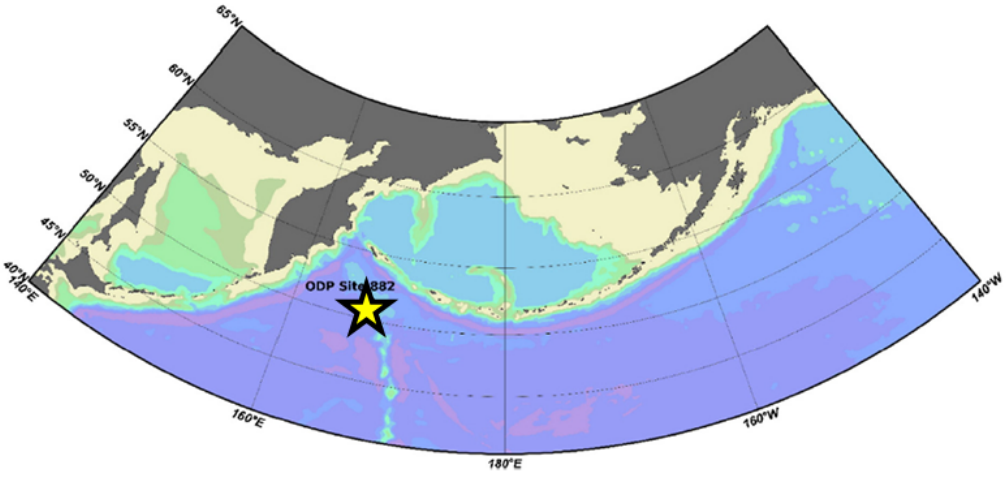

Figure 4.4: Location of ODP Site 882 in the subarctic Northwest Pacific (Ocean Data View 4.1.3; Swann, 2010).

4.2.2 Analysis

Methods for cleaning, dissolving and analysing these sediment diatom samples were identical to those described in Chapter 2 for the sediment diatom standard TC460. Briefly, 32 samples from ODP Site 882 spanning the time period 2.85 - 2.52 Ma were oxidised to remove all traces of organics using a rigorous two-step oxidation process (Horn et al., 2011; Mejía et al., 2013). In the boron-free HEPA filtered clean laboratory at the University of Southampton, each sample was dissolved completely in a gravimetrically known amount of NaOH (0.5 M) at 140°C for 48 - 72 hours. Each dissolved sample was then passed through an anion exchange column containing Amberlite IRA 743 resin in order to provide a purified boron sample (collected in 550 μL of 0.5 M HNO_3) and a matrix fraction (collected in 1800 μL MilliQ).

The δ^{11}B of the eluted pure B fraction was determined using 10^{12} Ω resistors and Faraday detectors on a Thermo Scientific Neptune MC-ICP-MS following an established method from Foster (2008). Instrument-induced fractionation of the $^{11}B/^{10}B$ ratio was corrected using a sample-standard bracketing sequence with NIST SRM 951 boric acid, allowing a direct determination of δ^{11}B using the following equation, where $^{11}B/^{10}B_{standard}$ is the mean $^{11}B/^{10}B$ ratio of the bracketing standards adjacent to the sample of interest.

$$\delta^{11}B(‰) = \left[\left(\frac{(^{11}B/^{10}B_{sample})}{(^{11}B/^{10}B_{standard})} \right) - 1 \right] \times 1000 \tag{4.1}$$

For B/Si analysis, an aliquot (ca. 4%) of the boron fraction was taken and diluted 25-fold with 0.5 M HNO_3, and analysed using a Thermo Fisher Scientific Element 2XR ICP-MS to determine B concentration. The Si concentration of the matrix fraction was determined by measuring the Si/Na ratio using a Thermo Scientific X-Series 2 ICP-MS and the known volume of 0.5 M NaOH used to dissolve the sample. Both concentrations were determined using comparison to a gravimetric standard containing boron, silicon, sodium and aluminium. Statistical analysis on all variables was undertaken using R (version 3.4.0).

4.2.3 Boron proxies in diatoms

The boron proxy arises because boron is present in aqueous environments as two pH-dependent species; boric acid (trigonal planar; $B(OH)_3$) dominates at low pH_{sw} and the borate anion (tetrahedral; $B(OH)_4^-$) is the major species at pH_{sw} above 8.6. The two stable isotopes of boron (^{10}B and ^{11}B) occur in a 1:4 ratio respectively, and an enrichment of ^{11}B is observed in boric acid of approximately 27.2 ‰ (Klochko et al., 2006) over borate due to their structural differences. Therefore, due to this isotopic fractionation and because the $\delta^{11}B$ of seawater (39.61 ± 0.04 ‰; Foster et al., 2010) is constant, as the proportions of boric acid and borate change with pH_{sw}, the $\delta^{11}B$ of each species also varies depending on pH_{sw}. Borate is also likely to be the boron species incorporated into marine carbonates, and so boron concentration tends to increase with increasing pH_{sw}.

B/Si has been investigated in diatom opal in the species *T. weissflogii* (see Chapter 3; Mejía et al., 2013) and *T. pseudonana* (Mejía et al., 2013), and both species had similar B/Si ratios that also increase with increasing pH_{sw}. This relationship has been previously suggested to result from borate entering the diatom cell *via* bicarbonate transporters during active uptake (Mejía et al., 2013) that is elevated at low pCO_2 (and hence at high pH_{sw}). This mechanism is also thought to be important in determining the $\delta^{11}B$ of diatom frustules, and in Chapter 3 a $\delta^{11}B$-pH_{sw} calibration of *T. weissflogii* is presented and discussed further.

4.3 Results

Results of the newly measured $\delta^{11}B$ and B/Si of the sedimentary diatom samples from ODP Site 882 are shown in Figure 4.5.

The $\delta^{11}B$ range from 4.68 ‰ to 7.20 ‰, but shift from a mean of 6.47 ± 0.58 ‰ (± 2σ) between 2.85 - 2.73 Ma, to a mean of 5.83 ± 2.07 ‰ between 2.73 - 2.52 Ma. Whilst $\delta^{11}B$ exhibits little variation pre-2.73 Ma, increased variability characterises the data post-2.73 Ma. This is exhibited as a more cyclic pattern post-2.73 Ma, with $\delta^{11}B$ values alternating between the heavier pre-iNHG values in warmer periods and

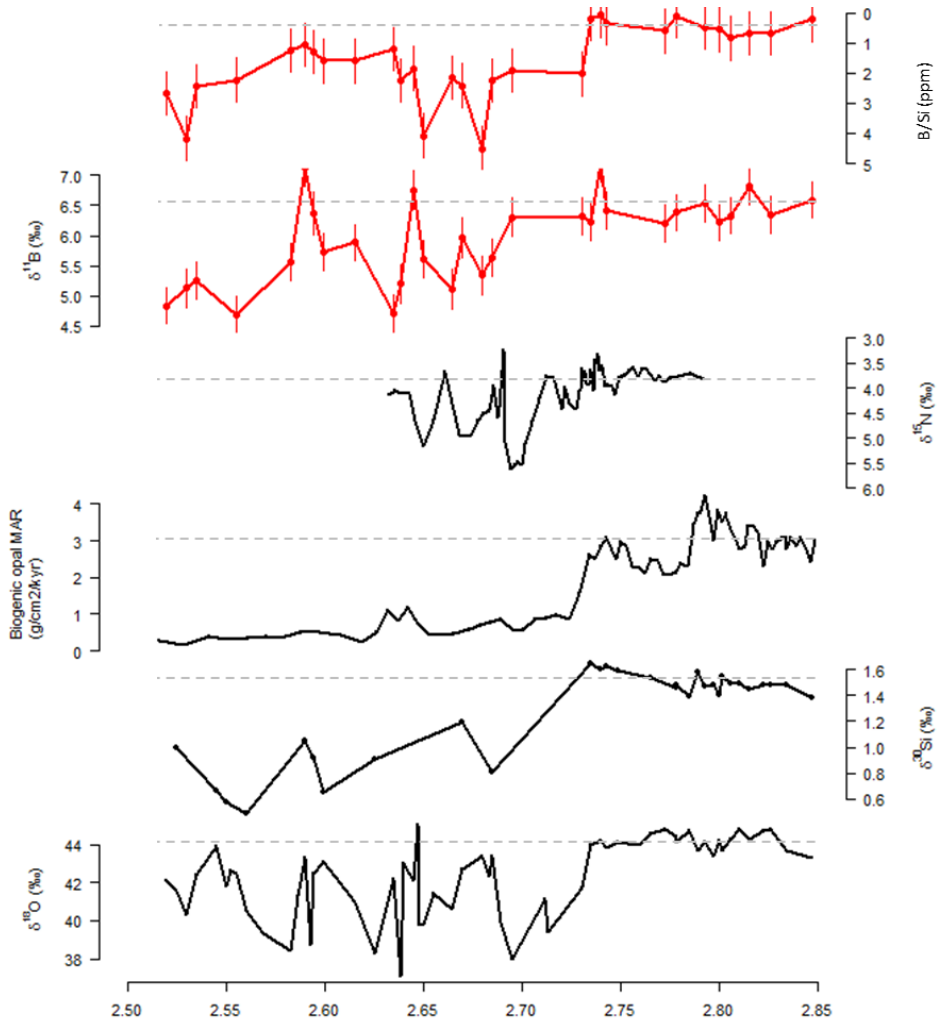

Figure 4.5: Records comparing δ^{18}O, δ^{30}Si, δ^{15}N (Sigman et al., 2004; Swann et al., 2006; Reynolds et al., 2008; Swann, 2010), opal MAR (Maslin et al., 1995) and the new δ^{11}B and B/Si data (red records; this study). There is a marked shift in all records at 2.73 Ma, except for δ^{11}B, but this is likely due to the lack of sample material available for boron analysis after this point until 2.695 Ma, as these samples have been used in a multitude of studies specifically investigating the period around 2.73 Ma. The grey dashed lines indicate the average value pre-2.73 Ma to more easily compare these records pre- and post-iNHG, and identify periods where stratification weakens and values move towards pre-2.73 Ma values.

approximately 5 ‰ in cooler periods (as defined by diatom δ^{18}O and UK'$_{37}$ SST; Haug et al., 2005; Swann, 2010).

B/Si ratios measured range from 0.08 ppm to 4.51 ppm, and exhibit a marked increase at 2.73 Ma, shifting from a mean B/Si of 0.43 ± 0.52 ppm pre-iNHG, to a mean of 2.26 ± 2.00 ppm post-iNHG (Figure 4.5).

There are obvious δ^{11}B and B/Si excursions that correspond to time periods

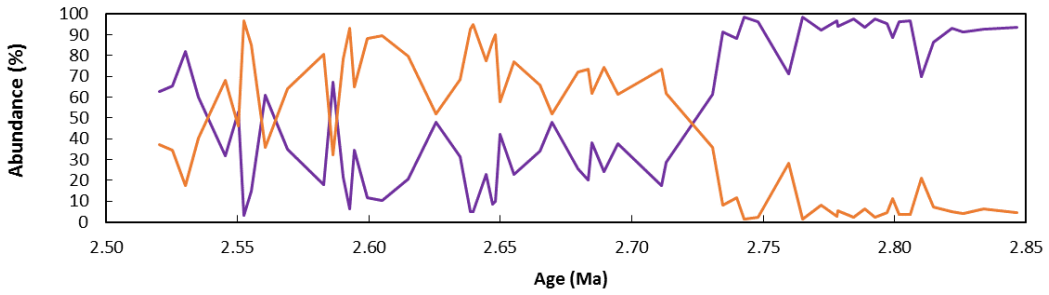

Figure 4.6: Abundance of diatom species found in the sedimentary samples of ODP Site 882 shown shifting at 2.73 Ma from *C. marginatus* (purple) to *C. radiatus* (orange).

where peaks in δ^{18}O, δ^{30}Si, δ^{15}N and biogenic opal MAR are also observed (Figure 4.5). By applying the culture calibration derived in Chapter 3 (*i.e.* a negative δ^{11}B-pH$_{sw}$ relationship), a trend towards an increase in surface pH$_{sw}$ is shown in the δ^{11}B record from 2.85 to 2.52 Ma, including the period of iNHG. This suggested increase in pH$_{sw}$ is also promoted by the B/Si record, using the elucidated B/Si-pH$_{sw}$ relationship from Chapter 3.

The change in dominant species begins at 2.73 Ma, and is complete by 2.71 Ma (Figure 4.6). At an average of 92% of the sedimentary samples, *C. marginatus* is the dominant diatom species present at ODP Site 882 pre-2.73 Ma, and whilst dominance shifts to *C. radiatus* post-2.73 Ma, the abundance of the two species is more balanced after iNHG (*C. radiatus* present at an average of 67%). The species abundance change is not associated with a significant change in δ^{11}B, but is perhaps synchronous with a step in B/Si.

Despite the low R^2 values, there is significant positive calibration between δ^{11}B and δ^{30}Si, and δ^{11}B and $\delta^{18}O_{diatom}$ (Figure 4.7; $R^2 = 0.47$, $p < 0.01$, and $R^2 = 0.14$, $p < 0.05$ respectively).

The negative correlation observed between δ^{11}B and B/Si is significant at the 99.9% level (Figure 4.8; $R^2 = 0.28$, $p < 0.01$). This negative correlation implies that with higher pH$_{sw}$, more borate is available to the diatoms based on the pH-dependent equilibrium of aqueous boron species. However, as a negative correlation is also observed between B/Si and δ^{30}Si (Figure 4.8; $R^2 = 0.60$, $p < 0.001$), this change in B/Si could also be influenced by changes in the utilisation and availability of silicic acid during

iNHG.

Despite the similarities between *C. marginatus* and *C. radiatus*, the change in B/Si could also be influenced by the change in species dominance observed around 2.73 Ma.

4.4 Discussion

4.4.1 Calibration (cultured diatoms) *vs.* application (sedimentary diatoms)

4.4.1.1 Absolute δ^{11}B comparison

A key caveat for using the calibration described for the diatom *Thalassiosira weissflogii* (*T. weissflogii*) is that they are not only a different species, but also are much smaller than the *C. marginatus* and *C. radiatus* diatoms found at ODP Site 882 (ca. 15 μm *vs.* ca. 150 μm respectively). Potentially as a result, the absolute δ^{11}B values measured by MC-ICP-MS indicated that the cultured *T. weissflogii* exhibited light δ^{11}B values of around -2 to -6 ‰, whereas the *C. marginatus* and *C. radiatus* revealed heavier δ^{11}B of between 4.6 and 7.2 ‰ (Figure 4.9), which is more similar to the bulk sedimentary diatom in-house standard TC460 (5.98 ± 0.28 ‰; discussed in Chapter 2). This indicates further calibrations for different diatom species are required before the δ^{11}B-pH proxy can be applied in a quantitative fashion.

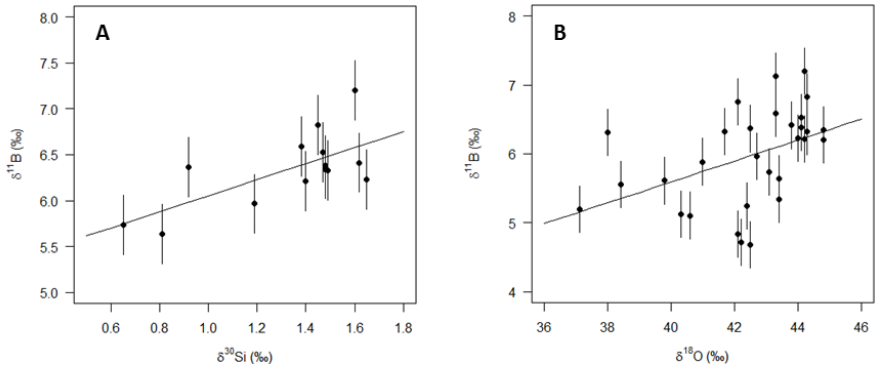

Figure 4.7: Correlations between δ^{11}B and δ^{30}Si (A; $R^2 = 0.47$, $p < 0.01$), and δ^{11}B and δ^{18}O (B; $R^2 = 0.14$, $p < 0.05$) are both significantly positive.

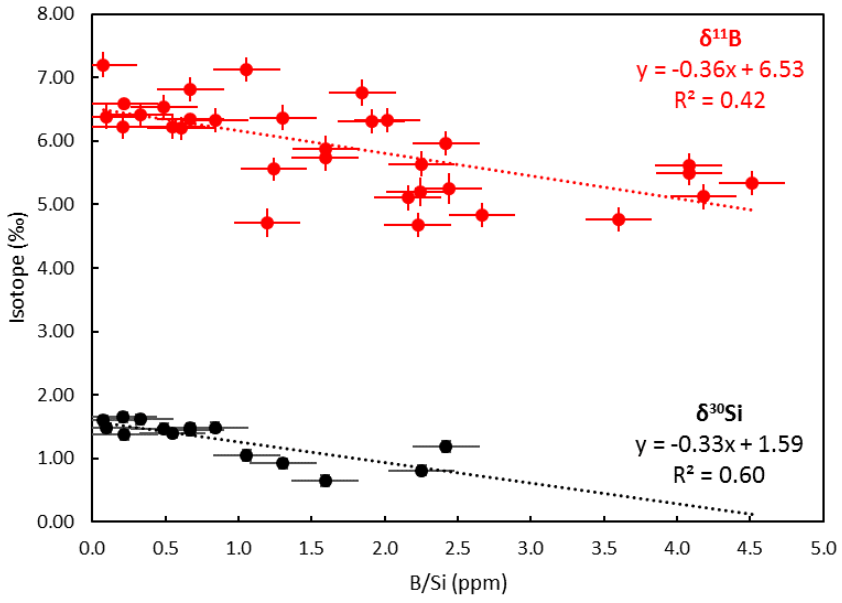

Figure 4.8: Correlations between δ^{11}B and B/Si ($R^2 = 0.42$, $p < 0.001$) and δ^{30}Si and B/Si ($R^2 = 0.60$, $p < 0.001$) are both significantly negative.

Despite the differences observed in these absolute δ^{11}B values, when δ^{11}B from cultured *T. weissflogii* diatoms (Chapter 3) and measured in sedimentary *C. marginatus* and *C. radiatus* (this study) are plotted against their B/Si ratios, both show a negative correlation with identical gradients (Figure 4.10). This suggests that despite uncertain

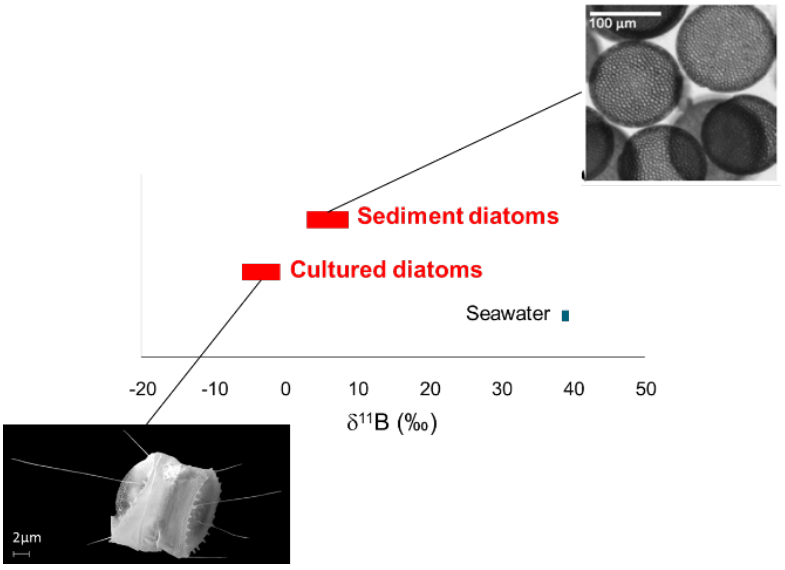

Figure 4.9: Difference between δ^{11}B between cultured and sediment diatoms could simply be due to species effects, as *T. weissflogii* is ca. 15 μm, whereas *Coscinodiscus* spp. are ca. 150 μm (Swann et al., 2006).

species differences, there is a similar mechanism of boron uptake and δ^{11}B-pH$_{sw}$ relationship in all diatoms examined in this thesis.

Further to this, the single-species calibration is applied to sedimentary samples containing two species. The species' abundance also changes at 2.73 Ma (Figure 4.6), which may be related to a step change in B/Si ratios, but this change does not appear to affect δ^{11}B. However, Mejía et al. (2013) also demonstrated that two species of diatom of the same genus (*T. weissflogii* and *T. pseudonana*) displayed similar B/Si ratios, so it is likely that the change in B/Si observed in ODP Site 882 is more influenced by pH$_{sw}$

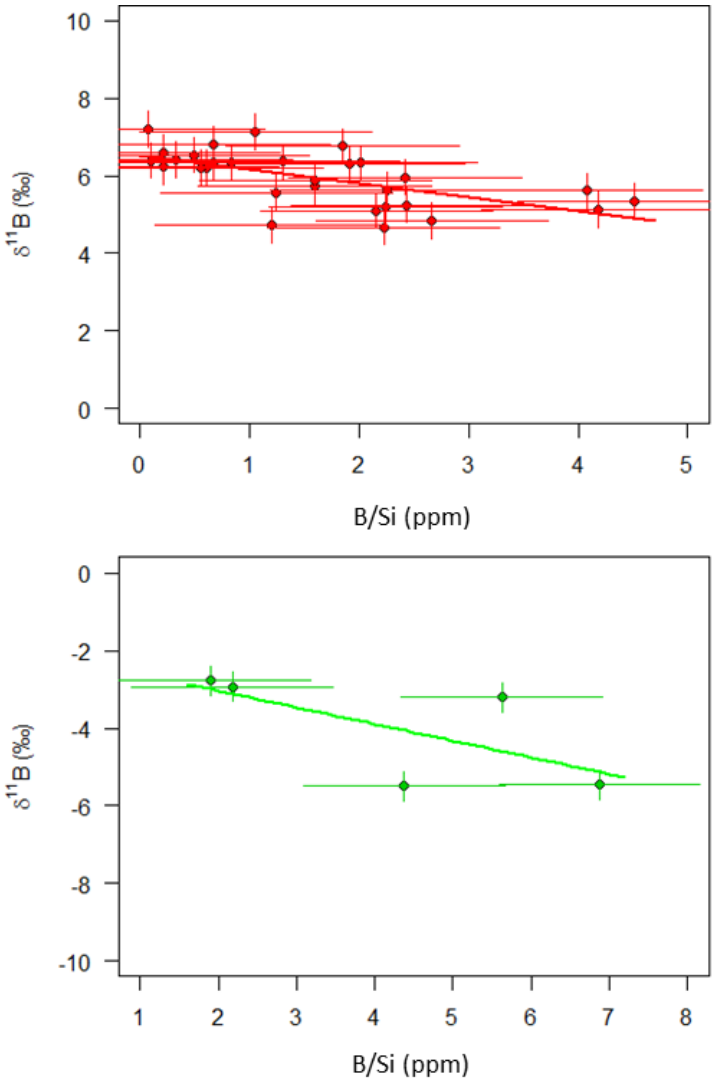

Figure 4.10: Difference between δ^{11}B *vs.* B/Si measured in cultured (green) and sedimentary (red) diatoms. Whilst the absolute values differ, the gradients of the slopes are identical (-0.37), and the R^2 values are similar (0.39 and 0.24 respectively).

than by a change in abundance of closely related diatom species.

4.4.1.2 Contamination check

Sedimentary diatom samples are potentially of a different matrix to the cultured diatom *T. weissflogii*. Indeed, we found that the Al content of the B fraction in sedimentary diatoms was consistently elevated compared to the cultured diatoms (albeit at the <100 ppb level; Figure 4.11).

It has been shown that diatom biogenic silica contains Al, potentially for structural purposes (Stoffyn, 1979; Van Bennekom et al., 1991), and whilst there may be the potential for inorganic adsorption of Al to diatom surfaces (Hydes, 1979), it has also been emphasised that Al is undoubtedly incorporated into the biogenic silica lattice of living cultured diatoms (Gehlen et al., 2002). For the cultured and sedimentary diatom analysed here, no Al was detected in the matrix fraction, but this was likely due to the extreme dilutions applied for the measurement of Si and Na. The presence of Al in the

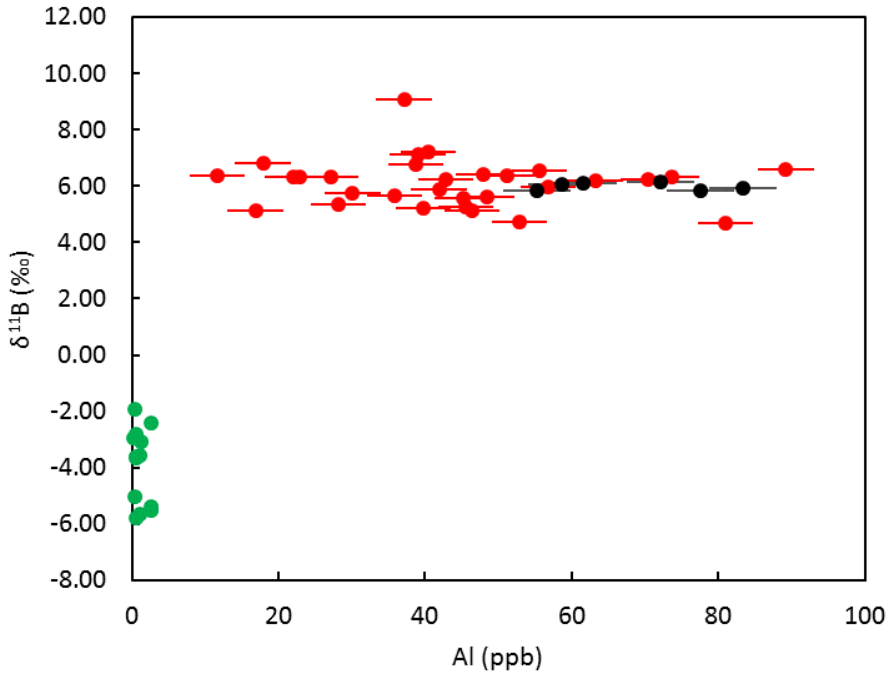

Figure 4.11: The Al concentration and δ^{11}B in both sedimentary (red) and cultured (green) diatoms. The diatom in-house standard TC460 is also shown (black) for comparison. The lack of any trend with δ^{11}B suggests these Al concentrations have no mass bias effect on δ^{11}B during MC-ICP-MS measurement.

boron fraction is nonetheless indicative of enhanced matrix contamination. There was, however, no obvious mass bias effect during analysis and there is a lack of correlation between [Al] and δ^{11}B in Figure 4.10, suggesting the level of Al contamination is not sufficient to influence the accuracy of the measured δ^{11}B. This is confirmed by the lack of correlation also displayed in the diatom in-house standard (TC460) that was used in the standard addition experiments described in Chapter 2, which indicated these samples do not experience a matrix effect during MC-ICP-MS measurement despite the presence of elevated Al.

4.4.2 Changes in the North Pacific between 2.85 and 2.52 Ma

From the Pliocene to the Pleistocene, a general cooling trend in the Northwest Pacific has been observed (*e.g.* Haug et al., 2005), and δ^{18}O measured in diatoms (Swann et al., 2006) and UK'$_{37}$ SST (Haug, et al., 2005) measured at ODP Site 882 reveal this to be the case locally over this time period. Between 2.85 - 2.73 Ma, the Northwest Pacific Ocean was well mixed and well ventilated in both glacials and interglacials, shown by minimal variation in isotope systems measured (Figure 4.5). Between 2.73 - 2.52 Ma, an abrupt drop in opal MAR is observed, and this combined with the shifts that also appear in the measured isotope systems suggest that stratification occurred at 2.73 Ma (Maslin et al., 1995; Haug et al., 1999; Sigman et al., 2004; Swann et al., 2006; Reynolds et al., 2008; Bailey et al., 2011; Studer et al., 2012; Rae et al., 2014). At certain points, stratification appears to weaken, as most isotope tracer values almost return to those exhibited pre-2.73 Ma, indicating upwelling of deep nutrient-rich waters that promote productivity. However, even though sedimentation rates increase at these points, no full recovery of the system is observed in the opal MAR record (Maslin et al., 1995).

The δ^{11}B and B/Si measured in this study appear entirely consistent with stratification occurring in the Northwest Pacific at 2.73 Ma. The δ^{11}B data indicate a trend towards increasing surface pH$_{sw}$, and there are obvious excursions in the data that correlate to excursions observed in other systems (*e.g.* biogenic opal MAR peaks at the same points that peaks are observed in the δ^{11}B record; Figure 4.5). These excursions occur where values in most systems measured nearly return to pre-stratification conditions,

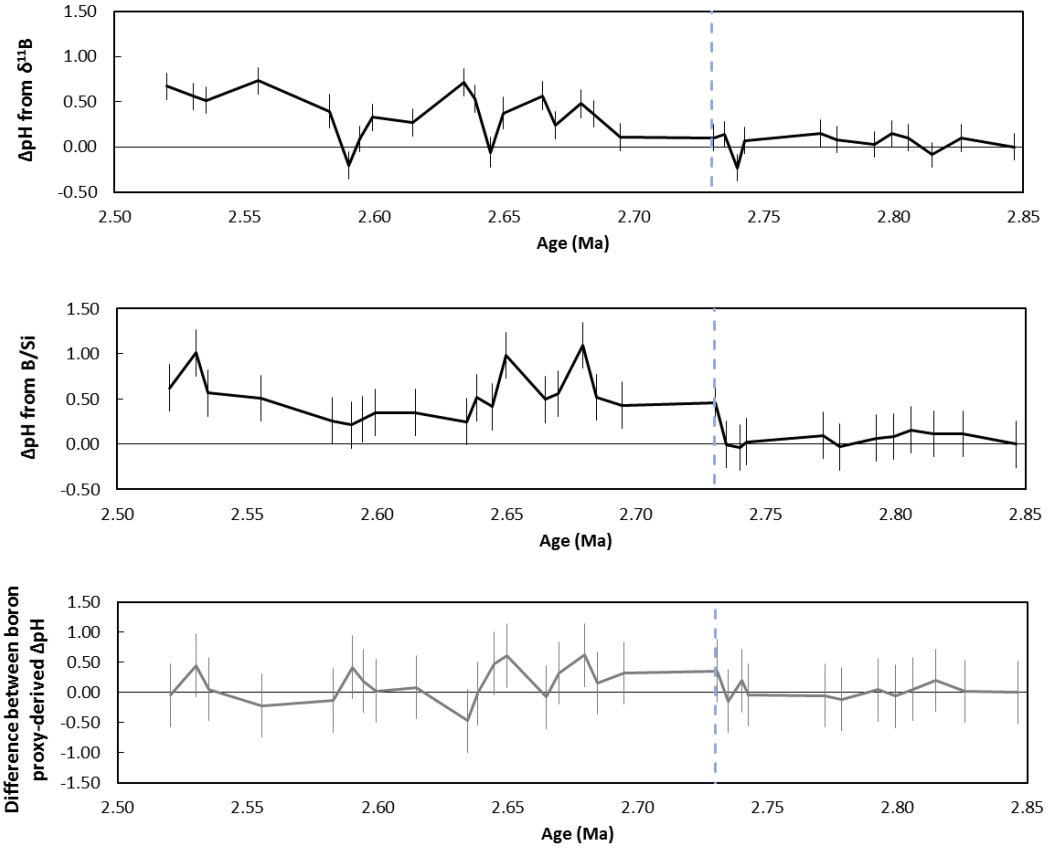

Figure 4.12: The estimated ΔpH_{sw} in the Northwest Pacific from 2.85 to 2.52 Ma derived from boron-based proxies measured in diatoms at ODP Site 882. The change in pH_{sw} is relative to the oldest sample at 2.85 Ma. A) shows the relative ΔpH_{sw} calculated from the calibration between $\delta^{11}B$ and pH_{sw} in the diatom *T. weissflogii* (calibration gradient = -2.62 ± 0.83, intercept = 17.25 ± 6.74), whilst B) shows the same but based on the calibration between B/Si and pH_{sw} (calibration gradient = 3.92 ± 1.20, intercept = -26.92 ± 9.65). C) shows the level of agreement between these two proxies, with the horizontal line at y = 0 indicating a match between the two different methods of calculating ΔpH_{sw}. The blue dotted line indicates iNHG at 2.73 Ma.

suggesting these points are where stratification weakens and ventilation of CO_2 occurs from deep waters to the surface in the Northwest Pacific (*e.g.* ca. 2.65 Ma and ca. 2.59 Ma). This upwelling also increases productivity and reduces surface pH_{sw} *via* the introduction of nutrient- and CO_2-rich deep waters to the euphotic zone. Although the biogenic opal MAR record indicates that productivity never reaches its pre-iNHG flux after 2.73 Ma, the new boron-based record supports this hypothesis by showing peaks at these points, and nutrient utilisation is increased as observed in the $\delta^{30}Si$ and $\delta^{15}N$ records.

Whilst the $\delta^{11}B$ data is unfortunately limited between 2.73 and 2.695 Ma by

lack of available samples, the B/Si data clearly show a large increase from a mean value of 0.43 ± 0.52 ppm to 2.26 ± 2.00 ppm during iNHG, simultaneous to the inferred drop in productivity, and reduction in SST. Further to indicating increasing pH_{sw}, an increase in B/Si suggests either an increase in the amount of boron incorporated into the frustules, or a reduction in the amount of silica in the surface water. In this case, the amount of silicic acid in surface seawater would have to increase over iNHG (Reynolds et al., 2008), but the utilisation of silicic acid (inferred from δ^{30}Si) reduces, suggesting that changes in Si would likely amplify the B/Si change here.

As discussed above, the difference in the species at Site ODP 882 and those cultured in Chapter 3 preclude a direct quantitative reconstruction of pH_{sw} using the boron based proxies. However, given the similar character of δ^{11}B *vs.* B/Si seen here and in the cultures of *T. weissflogii*, we attempt to calculate relative change in pH, assuming the sensitivity of δ^{11}B and B/Si in *C. marginatus* and *C. radiatus* are the same as *T. wessflogii* (Chapter 3). This treatment reveals the total range of all calculated pH_{sw} from δ^{11}B was 0.96 pH units, and from B/Si was 1.13 pH units. This then allowed a ΔpH_{sw} to be calculated for each boron-based system, using the oldest sample measured (2.8465 Ma) as an anchor point for observing the approximate change in pH_{sw} throughout the time period 2.85 - 2.52 Ma (Figure 4.12).

Figure 4.12 reveals very minor variation in pH_{sw} pre-iNHG, but after 2.73 Ma, the ΔpH_{sw} becomes larger, with a general trend towards increasing pH_{sw}. This is true of both ΔpH_{sw} derived from the δ^{11}B-pH_{sw} relationship as well as that derived from the B/Si-pH_{sw} relationship, albeit a larger general increase in pH_{sw} is observed in ΔpH_{sw} from B/Si (perhaps reflecting the additional effect of reduced seawater Si on B/Si). The mean ΔpH_{sw} from samples before 2.73 Ma was calculated as 0.04, and the mean of ΔpH_{sw} in all samples after 2.73 Ma was 0.35, resulting in a mean ΔpH_{sw} over iNHG of 0.31 pH units based on the δ^{11}B-pH_{sw} calibration. These average values were similar using the B/Si-pH_{sw} calibration, with a pre-iNHG mean of 0.05, but a larger post-iNHG mean of 0.52, leading to a mean ΔpH_{sw} over iNHG of 0.47 pH units. The ΔpH_{sw} derived from the B/Si record may include influence from the change in δ^{30}Si, but the pH_{sw} change over iNHG of approximately 0.31 - 0.47 pH units is comparable to the modern annual stratification-induced pH_{sw} change in the Northwest Pacific of 0.38 pH units.

4.4.3 Implications for the role of the North Pacific in global pCO_2 change

Martínez-Botí et al. (2015) discussed ocean-air CO_2 exchange from the Pliocene to Pleistocene using a high resolution $\delta^{11}B$ record from *G. ruber* foraminifera to reconstruct pH_{sw} and pCO_2. A comparison between the diatom-derived $\delta^{11}B$ from this study and the foraminifera-based data from Martínez-Botí et al. (2015) most notably reveals an increase in pH_{sw} from 2.85 - 2.52 Ma exhibited in both data sets (Figure 4.13), although a larger pH_{sw} increase is observed in the diatom-based data. The onset of a halocline in the subarctic Northwest Pacific coincident with iNHG would appear to suggest that this region is a key driver of global climatic change (Haug et al., 1999; Haug et al., 2005; Swann, 2010). This crucial role includes the isolation of CO_2 in the deep ocean by preventing ventilation in this northern polar ocean (Haug et al., 1999). The new δ^{11} and B/Si data from diatom frustules analysed here strongly supports a role for this process in causing pCO_2 decline observed at this time.

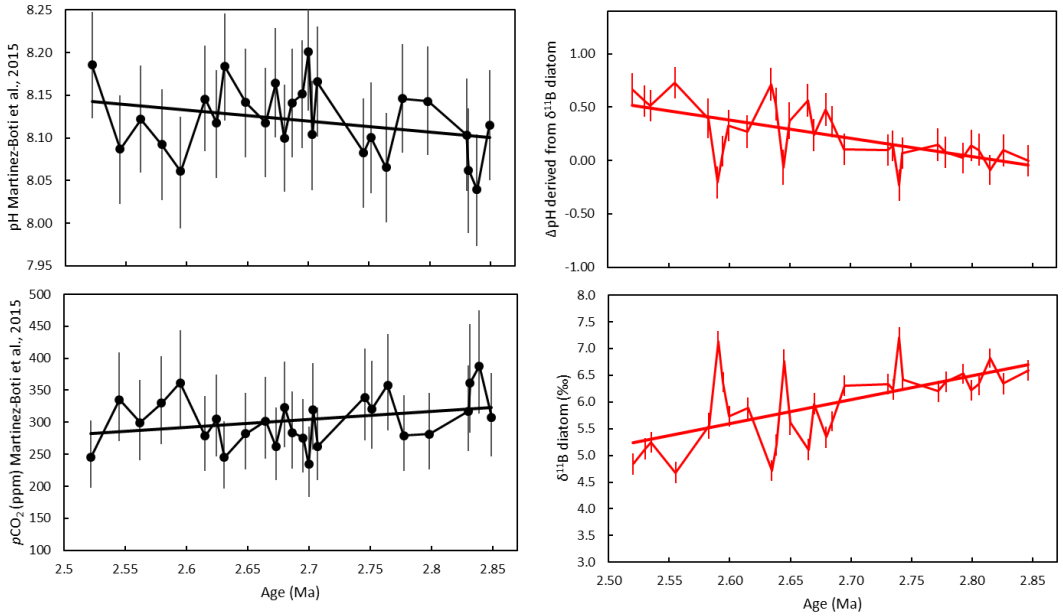

Figure 4.13: Comparison between ΔpH derived from $\delta^{11}B_{diatom}$ in this study and global pH_{sw} change from Martínez-Botí et al. (2015), and between $\delta^{11}B_{diatom}$ and pCO_2 from Martínez-Botí et al. (2015) for the time period 2.85 - 2.52 Ma. Data from this study are shown in red, and those from Martínez-Botí et al. (2015) are shown in black.

4.5 Conclusions

Sedimentary diatoms found at ODP Site 882 situated in the subarctic Northwest Pacific have been extensively studied over the time period 2.85 - 2.52 Ma, including a number of different isotope systems and opal accumulation rates. Following the development of a novel method to measure δ^{11}B in diatoms, and the exploration of δ^{11}B change with pH_{sw} in diatom frustules, this calibration has been applied to the diatoms found at ODP Site 882 to elucidate the very first boron isotope record for sedimentary diatoms. Correlations between δ^{11}B and δ^{18}O, and δ^{30}Si are positive, whilst δ^{11}B and B/Si, and δ^{15}N have an inverse relationship. These results uphold and reinforce the suggestion that a halocline is established in the Northwest Pacific at 2.73 Ma, during iNHG. The excursions in δ^{11}B and B/Si match the same periods where δ^{18}O almost returns to pre-2.73 Ma values, and where an increase in opal MAR and nutrient utilisation occur, indicating a weakening of stratification and a reduction in surface pH_{sw}. The new boron records also trace the pCO_2 record from Martínez-Botí et al. (2015), implying the subarctic North Pacific plays a large role in global pCO_2 change during iNHG.

By using the culture calibrations derived in Chapter 3, an estimate of pH_{sw} change in the Northwest Pacific between the ventilated Pliocene and the variably stratified Pleistocene could be calculated as ca. 0.31 - 0.47 pH units. This is not dissimilar to the modern stratification-induced annual pH_{sw} change of 0.38 units in the Northwest Pacific, which in turn increases confidence in the development of the boron proxies in diatoms. The timing of the change in surface water pH and pCO_2 in the Northwest Pacific correlates well with the timing of atmospheric CO_2 change revealed by Martínez-Botí et al. (2015), confirming the role of positive feedbacks in this region in the overall decline of CO_2 across iNHG. In summary, this suggests that the boron-based proxies in diatoms have considerable potential as a palaeo-pH archive, greatly expanding the palaeoceanographic proxy toolbox.

Chapter 5

Boron isotope sensitivity to seawater pH change in a species of *Neogoniolithon* coralline red alga

This chapter has been published in *Geochimica et Cosmochimica Acta* .

Donald, H.K., Ries, J.B., Stewart, J.A., Fowell, S.E., and Foster, G.L. (2017) Boron isotope sensitivity to seawater pH change in a species of *Neogoniolithon* coralline red alga. *Geochimica et Cosmochimica Acta* **217**, 240-253.

Justin Ries (provided cultured coralline algal samples, discussion and feedback)

Joseph Stewart (analysed preliminary samples for boron content and isotopes, discussion and feedback)

Sara Fowell (assisted J. A. S. with boron analysis)

Gavin Foster (general discussion and feedback)

The increase in atmospheric carbon dioxide (CO_2) observed since the industrial revolution has reduced surface ocean pH by ∼0.1 pH units, with further change in the oceanic system predicted in the coming decades. Calcareous organisms can be negatively affected by extreme changes in seawater pH (pH_{sw}) such as this due to the associated changes in the oceanic carbonate system. The boron isotopic composition ($\delta^{11}B$) of biogenic carbonates has been previously used to monitor pH at the calcification site (pH_{cf}) in scleractinian corals, providing mechanistic insights into coral biomineralisation and the impact of variable pH_{sw} on this process. Motivated by these investigations, this

study examines the δ^{11}B of the high-Mg calcite skeleton of the coralline red alga *Neogoniolithon* sp. to constrain pH_{cf}, and investigates how this taxon's pH_{cf} is impacted by ocean acidification. δ^{11}B was measured in multiple algal replicates (n = 4 to 5) cultured at four different pCO_2 scenarios averaging (± 1σ) 409 (± 6), 606 (± 7), 903 (± 12) and 2856 (± 54) μatm, corresponding to average pH_{sw} (± 1σ) of 8.19 (± 0.03), 8.05 (± 0.06), 7.91 (± 0.03) and 7.49 (± 0.02) respectively. Results show that skeletal δ^{11}B is elevated relative to the δ^{11}B of seawater borate at all pH_{sw} treatments by up to 18 ‰. Although substantial variability in δ^{11}B exists between replicate samples cultured at a given pH_{sw} (smallest range = 2.32 ‰ at pH_{sw} 8.19, largest range = 6.08 ‰ at pH_{sw} 7.91), strong correlations are identified between δ^{11}B and pH_{sw} ($R^2 = 0.72$, $p < 0.0001$, n = 16) and between δ^{11}B and B/Ca ($R^2 = 0.72$, $p < 0.0001$, n = 16). Assuming that skeletal δ^{11}B reflects pH_{cf} as previously observed for scleractinian corals, the average pH_{cf} across all experiments was 1.20 pH units (0.79 to 1.56) higher than pH_{sw}, with the magnitude of this offset varying parabolically with decreasing pH_{sw}, with a maximum difference between pH_{sw} and pH_{cf} at a pH_{sw} of 7.91. Observed relationships between pH_{sw} and calcification rate, and between pH_{sw} and pH_{cf}, suggest that coralline algae exhibit some resilience to moderate ocean acidification *via* increase of pH_{cf} relative to pH_{sw} in a similar manner to scleractinian corals. However, these results also indicate that pH_{cf} cannot be sufficiently increased by algae exposed to a larger reduction in pH_{sw}, adversely impacting calcification rates of coralline red algae.

5.1 Introduction

Atmospheric CO_2 has been increasing since the Industrial Revolution, from 280 ppm to more than 400 ppm today (Tans and Keeling, 2016). This increase has led to changes in ocean carbon chemistry, ultimately lowering seawater pH (pH_{sw}) by 0.1 pH units. Climate models predict that by 2100, a high-end "business as usual" emission scenario (*i.e.* Intergovernmental Panel on Climate Change: Representative Concentration Pathway 8.5) will result in a global average surface pH_{sw} of ca. 7.8, potentially reaching even lower levels at high latitudes. This large and rapid reduction in global pH_{sw} will result in an environment that is potentially challenging to marine organisms that rely

on biogenically produced $CaCO_3$ (Doney et al., 2009).

Ocean acidification affects biogenic calcification by reducing the $CaCO_3$ saturation state of seawater ($\Omega = [Ca^{2+}][CO_3^{3-}]/K^*_{sp}$; where K^*_{sp} is the stoichiometric solubility product of $CaCO_3$ at in situ conditions of temperature, salinity and pressure). Reductions in Ω of seawater have been shown to reduce calcification rates and, in some cases, cause net dissolution of the calcareous shells and skeletons of marine organisms (Gattuso et al., 1998; Riebesell et al., 2000; Death et al., 2009; Ries et al., 2009; Ries et al., 2016). Indeed, a recent study investigating a sub-marine volcanic CO_2 seep as an analogue for the effects of ocean acidification found that, over time, the nearby coral reef system was largely replaced by fleshy algae-covered rocks (Enochs et al., 2015). This, and a wealth of other studies (Gattuso et al., 2015; and references therein), indicate that ocean acidification can directly affect calcareous organisms through changing ocean carbonate chemistry, as well as indirectly *via* inter-species competition and modification of species interactions (*e.g.* Dodd et al., 2015).

Coralline algae are important $CaCO_3$ producers and are often found in high latitude waters. They also comprise a large component of modern coral reefs, confer stability to the reef crest, and are a vital food source for marine grazers such as sea urchins (McCoy and Kamenos, 2015). Hence, coralline algae play an important role in the marine food web, but also act as ecosystem engineers by providing defence against coastal erosion. Coralline algae are predominantly composed of high-Mg calcite ($>$ 15 mol % $MgCO_3$), which is more soluble than aragonite or low-Mg calcite found in other calcareous organisms such as corals, scallops and oysters (Ries et al., 2016). Since CO_2 is more soluble in colder water, it is likely that global high latitude regions are more vulnerable to ocean acidification than lower latitude regions (Gattuso et al., 2015). Thus, ocean acidification poses a severe threat to coralline algae and their interdependent ecosystems (Kuffner et al., 2008; Gao and Zheng, 2009; Ragazzola et al., 2012).

Coralline red algae calcify by depositing calcite within their cell walls, but exterior to their cell membrane. This is in contrast to foraminifera that calcify within seawater vacuoles (Erez, 2003), scleractinian corals that calcify in a fluid between their skeleton and calicoblastic epithelium (Cohen and McConnaughey, 2003; Gagnon et al., 2012), and coccolithophores that calcify in an intracellular vesicle (Mackinder et al.,

2010), but is similar to calcification within *Bryopsidalean* calcareous green algae, which occurs extracellularly within interutricular space (Ries, 2009).

Several studies have examined the influence of ocean acidification on the nature and rate of calcification in a variety of coralline red algae (Hall-Spencer et al., 2008; Martin and Gattuso, 2009; Roleda et al., 2015; Cornwall et al., 2017). For instance, Ries et al. (2009) and Smith and Roth (1979) documented a parabolic response in calcification rate of the coralline red algae to decreasing pH_{sw}, suggesting that the algal calcification increases in response to moderate elevations in pCO_2, but decreases in response to extreme increases. However, Ries et al. (2009) observed maximum calcification between pH_{sw} 7.9 and 8.1 ($\Omega_A \sim$ 2.0 to 2.3; where Ω_A is the saturation state for the aragonite $CaCO_3$ polymorph), while Smith and Roth (1979) observed maximum calcification between pH_{sw} 7.6 and 8.3 (Figure 5.1). These non-linear relationships suggest that coralline algae utilise biological processes to confer resilience to moderate-to-extreme changes in pH_{sw}.

The calcification response of coralline algae to ocean acidification has been shown to vary between species (Borowitzka, 1981; Semesi et al., 2009; Comeau et al., 2013). Despite this, a result common to the various species investigated in the different experiments is their ability to continue calcifying, albeit at slower rates, even under extremely reduced pH_{sw}. This mitigation of extreme ocean acidification has been shown to translate into coralline algae survival in low pH_{sw} environments across a range of natural ecosystems (Kamenos et al., 2016). Coralline red algae perform both calcification and photosynthesis (*e.g.* Buitenhuis et al., 1999), and the balance between these two key biological processes is important for coralline algae survival. Many marine organisms utilise carbon concentrating mechanisms intracellularly to ensure calcification can still occur under CO_2-limited conditions. Experimental work has shown that photosynthesis in some marine algae is CO_2-limited up to ca. 1000 μatm pCO_2 (Bowes, 1993). Therefore, the additional energy from photosynthesis as pCO_2 becomes elevated up to ca. 1000 μatm may stimulate calcification within calcifying marine algae, despite the associated decrease in pH_{sw}. This effect has previously been observed for zooxanthellate scleractinian corals (*e.g.* Castillo et al., 2014). Furthermore, photosynthesis increases local pH through the removal of dissolved CO_2 from seawater proximal to the algae (Gao

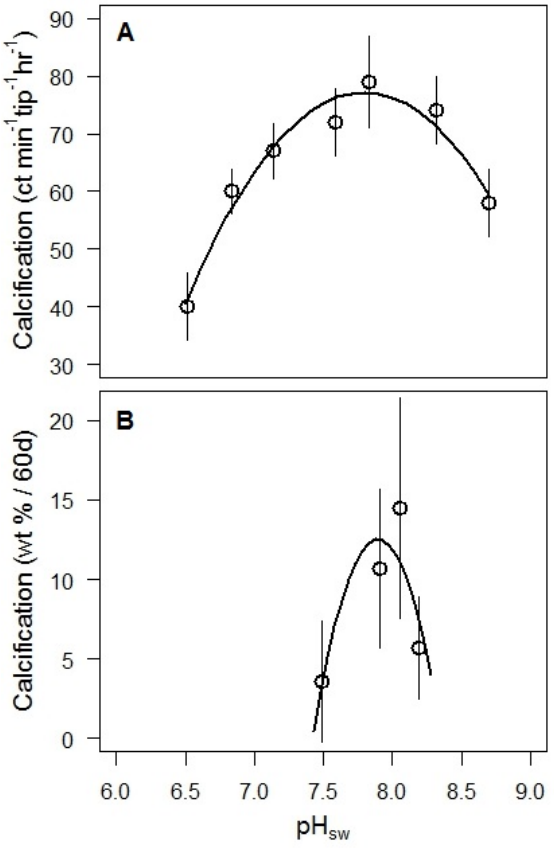

Figure 5.1: Calcification rates of coralline red algae plotted against pH_{sw}. Comparison between calcification trends in coralline red algae descried in Smith and Roth (1979; *Bossiella orbigniana*) (A) and Ries et al. (2009; *Neogoniolithon* sp.) (B). Although calcification rates are reported in different units, both studies suggest that coralline algae exhibit a parabolic calcification response to CO_2-induced ocean acidification, with an optimum near pH_{sw}sw 7.9.

et al., 1993), and respiration may reduce calcification rates by decreasing local pH as a consequence of CO_2 release (De Beer and Larkum, 2001). Calcification in coralline algae is therefore likely regulated by a number of important metabolic activities that influence the carbonate system within and around the algal cell (Smith and Roth, 1979; Gao et al., 1993; Hurd et al., 2011; Martin et al., 2013).

The impact of pH_{sw} and $CaCO_3$ saturation state on inorganic calcification differs from their impact on biogenic calcification (Ries et al., 2009; McCulloch et al., 2012a). The IpHRAC model by McCulloch et al. (2012b) ascribes the reduced sensitivity of scleractinian coral calcification in response to changing seawater aragonite saturation state to the increase of the calcification site pH (pH_{cf}), as determined from the boron isotopic composition of the coral skeleton, proton-sensitive microelectrodes (Ries, 2011a), and pH-sensitive dyes (Venn et al., 2013). Recent studies investigating

δ^{11}B of the coralline algae *Clathromorphum nereostratum via* laser ablation inductively coupled plasma mass spectrometry (LA-ICPMS) reveal that skeletal δ^{11}B within this species is also consistent with a pH_{cf} that is significantly higher than measured ambient pH_{sw} (by ca. 0.6 pH units; ΔpH = pH_{cf} - pH_{sw}), suggesting an increase of pH_{cf} may play a similarly important role in coralline algal calcification (Fietzke et al., 2015). However, skeletal δ^{11}B data for coralline algae species cultured under a range of controlled pH_{sw} conditions that demonstrate the response of pH_{cf} to changes in pH_{sw} are currently sparse (*e.g.* the only other such study is Cornwall et al., 2017). Here, the boron isotope approach to estimating pH_{cf} is applied to a branched *Neogoniolithon* sp. cultured under four pCO_2 conditions that allow us to assess the potential impacts of ocean acidification on pH_{cf} regulation in coralline red algae.

5.2 Methods

5.2.1 Boron isotopes

Numerous papers have presented detailed discussions about the basis for the boron isotope proxy of pH_{sw} (Hemming and Hanson, 1992; Zeebe and Wolf-Gladrow, 2001; Foster and Rae, 2016). Briefly, the proxy arises because (1) the abundance of the two major aqueous forms of boron in seawater are pH dependent and (2) there is boron isotope fractionation between these two boron species (Dickson, 1990). Trigonal planar boric acid ($B(OH)_3$) dominates at low pH, and the tetrahedral tetrahydroxyborate anion ($B(OH)_4^-$; henceforth referred to as borate) dominates when pH exceeds 8.6 in typical surface ocean conditions. The two stable isotopes of boron (^{10}B and ^{11}B) occur roughly in a 1:4 ratio, and the structural difference between the aqueous species leads to an enrichment of ^{11}B in boric acid of approximately 27.2 ‰ (Klochko et al., 2006; Nir et al., 2015) because the more stable trigonal structure has the stronger B-O bonds. Boron isotopic composition is described using the delta notation δ^{11}B relative to a boric acid standard (NIST SRM 951 boric acid according to Catanzaro et al., 1970) shown in

equation (5.1).

$$\delta^{11}B(‰) = \left[\left(\frac{(^{11}B/^{10}B_{sample})}{(^{11}B/^{10}B_{standard})}\right) - 1\right] \times 1000 \tag{5.1}$$

Since the δ^{11}B of total boron in seawater (boric acid and borate) is constant at 39.61 $\pm$ 0.04 ‰ (Foster et al., 2010), as the proportions of boric acid and borate change with pH_{sw}, the δ^{11}B composition of each species also varies as a function of pH, with borate δ^{11}B increasing with pH_{sw} as described in equation (5.2).

$$\delta^{11}B_{B(OH)_4^-} = \frac{\delta^{11}B_{sw} + \left(\delta^{11}B_{sw} - 1000(\alpha_B - 1)\right)10^{pK*_B - pH}}{1 + \alpha_B 10^{pK*_B - pH}} \tag{5.2}$$

Where pK^*_B is the dissociation constant (dependent on temperature and salinity; Dickson, 1990), $\delta^{11}B_{sw}$ is the δ^{11}B composition of total boron in seawater, $\delta^{11}B_{B(OH)_4^-}$ is the δ^{11}B composition of aqueous borate, and α_B is a constant (1.0272; Klochko et al., 2006) describing the equilibrium mass dependent boron isotope fractionation between boric acid and borate.

Although borate is assumed to be the most likely form of aqueous boron incorporated into $CaCO_3$, the δ^{11}B of many biogenic carbonates is elevated relative to the δ^{11}B of seawater borate (Figure 5.2 and references therein; see also Vengosh et al., 1991; Gaillardet and Allégre, 1995). As noted above, this increase in the δ^{11}B of scleractinian deep-sea and tropical corals is thought to be predominantly caused by the elevation of pH_{cf} *via* enzymatic activity (*e.g.* Ca-ATPase; McConnaughey and Falk, 1991). In this case, pH_{cf} can be calculated using boron isotopes by substituting δ^{11}B of the coral sample for δ^{11}B of aqueous borate in equation (5.3).

$$pH = pK^*_B - log\left(-\frac{\delta^{11}B_{sw} - \delta^{11}B_{B(OH)_4^-}}{\delta^{11}B_{sw} - \alpha_B\delta^{11}B_{B(OH)_4^-}1000(\alpha_B - 1)}\right) \tag{5.3}$$

Figure 5.2 shows δ^{11}B data from previous studies for several coral taxa grown over a range of pH_{sw} conditions (Hönisch et al., 2004; Reynaud et al., 2004; Krief et al., 2010; Anagnostou et al., 2012; McCulloch et al., 2012b; Holcomb et al., 2014). In all cases pH_{cf} is elevated by around 0.5 pH units at pH_{sw} 8, which is similar to observations

of the calcifying fluid from micro-electrodes (Al-Horani et al., 2003; Krief et al., 2010; Ries, 2011a; Trotter et al., 2011; McCulloch et al., 2012b) and pH sensitive dyes (Venn et al., 2011; Venn et al., 2013; Holcomb et al., 2014). Furthermore, the majority of corals examined thus far show that as ambient pH_{sw} decreases, pH_{cf} declines at a reduced rate (Venn et al., 2011; Venn et al., 2013; Holcomb et al., 2014).

5.2.2 Algal culture

A single species of tropical coralline red alga, *Neogoniolithon* sp., was cultured at four pCO_2 ($\pm$ 1σ) levels: 409 ($\pm$ 6), 606 ($\pm$ 7), 903 ($\pm$ 12) and 2856 ($\pm$ 54) μatm, resulting in pH_{sw} values ($\pm$ 1σ) of 8.19 ($\pm$ 0.03), 8.05 ($\pm$ 0.06), 7.91 ($\pm$ 0.03) and 7.49 ($\pm$ 0.02), respectively (Ries et al., 2009). The algae were grown for 60 days in 38 L aquaria in filtered Atlantic Ocean seawater (0.2 μm; Cape Cod, Massachusetts). The cultures were maintained at average aragonite saturation states ($\pm$ 1σ) of 3.12 ($\pm$ 0.22), 2.40 ($\pm$ 0.42), 1.84 ($\pm$ 0.13) and 0.90 ($\pm$ 0.05), and temperatures of 25°C using 50 W electric heaters, and illuminated on a 10hr:14hr light:dark cycle. This species of coralline red algae exhibited an apparent parabolic calcification response to increasing pCO_2, with net calcification rate increasing with an increase in pCO_2 from 409 to 606 μatm, and declining with an increase in pCO_2 to 903 and 2856 μatm (see Ries et al., 2009 and Table B1 in the supplementary materials for further details; Figure 5.1).

5.2.3 Sample preparation

Neogoniolithon sp. is a non-geniculate branched rhodolith form of coralline red algae. Replicate specimens were analysed for boron isotope composition at each culture pH_{sw} (n = 5 for pH_{sw} 7.91, and n = 4 for pH_{sw} 8.19, 8.05 and 7.49). Duplicate analyses were performed on all replicate specimens except those from the pH_{sw} 7.49 treatment, due to the small mass of $CaCO_3$ mineralised under these high-pCO_2 conditions. Skeletal material produced exclusively under the experimental treatments was identified relative to a ^{137}Ba isotope marker emplaced in the skeletons at the start of the experiment (Ries, 2011b). Branches of the specimens were powdered using a pestle and mortar in a clean laboratory fitted with boron-free HEPA filters at the University of Southampton

to produce homogenous bulk sample replicates for each specimen. Following previous studies (Foster, 2008; Krief et al., 2010), approximately 3 mg of each sample was cleaned using 500 μl of an oxidative mixture of 10% hydrogen peroxide (H_2O_2) buffered with 0.1 M ammonium hydroxide (NH_4OH). The samples were heated in a water bath and briefly ultra-sonicated a total of six times. The oxidative mixture was removed, and the samples were rinsed and transferred to clean plastic vials. The samples were leached in 0.0005 M nitric acid (HNO_3) and then dissolved in a minimal volume of 0.5 M HNO_3.

5.2.4 Trace element and isotopic analysis

Oxidatively cleaned and dissolved samples were transferred to Teflon vials and a 7% aliquot was removed for trace element analysis. Elemental analysis (B/Ca and Sr/Ca) of matrix-matched sample solutions was performed using ICP-MS on a *Thermo Scientific Element 2* mass spectrometer following the protocol of Henehan et al. (2015). Replicates of well-characterised solution consistency standards measured during this study are precise to ±5.6% and ±2.0% for B/Ca and Sr/Ca (95% confidence), respectively.

The remainder of each dissolved sample was reserved for boron isotope analysis and processed at the University of Southampton according to well-established methods (Foster, 2008). Samples were passed through micro-columns containing the boron-specific anion exchange resin Amberlite IRA-743 and boron was eluted in Teflon distilled 0.5 M HNO_3. Boron isotopic composition of each purified sample was then measured using a *Thermo Scientific Neptune* multi-collector ICP-MS (MC-ICP-MS) using two Faraday detectors fitted with 10^{12} Ω resistors at the University of Southampton following methods detailed in Henehan et al. (2013) and Foster et al. (2013). Samples were bracketed with NIST SRM 951 standard boric acid to correct for variability in instrument induced mass fractionation. The long-term reproducibility of standards is approximately ± 0.2 ‰ for 20 ng of boron (95% confidence), and analytical uncertainty is described by equation (5.4), where [^{11}B] is the voltage measured on the H3 faraday detector with one of the 10^{12} Ω resistors.

$$2\sigma = 12960e^{(-212[^{11}B])} + 0.3385e^{(-1.544[^{11}B])} \tag{5.4}$$

5.3 Results

The coralline algae across all pH treatments yield ^{11}B values ranging from 24.42 ($\pm$ 0.22) ‰ to 36.26 ($\pm$ 0.10) (Table 5.1). One sample replicate at pH_{sw} 8.19 was deemed anomalous, as duplicate analyses differed by 1.4 ‰ compared with an average difference between other duplicate analyses of 0.18 ‰. This outlying sample is therefore excluded from the discussion, and n = 16 for all subsequent regression analyses.

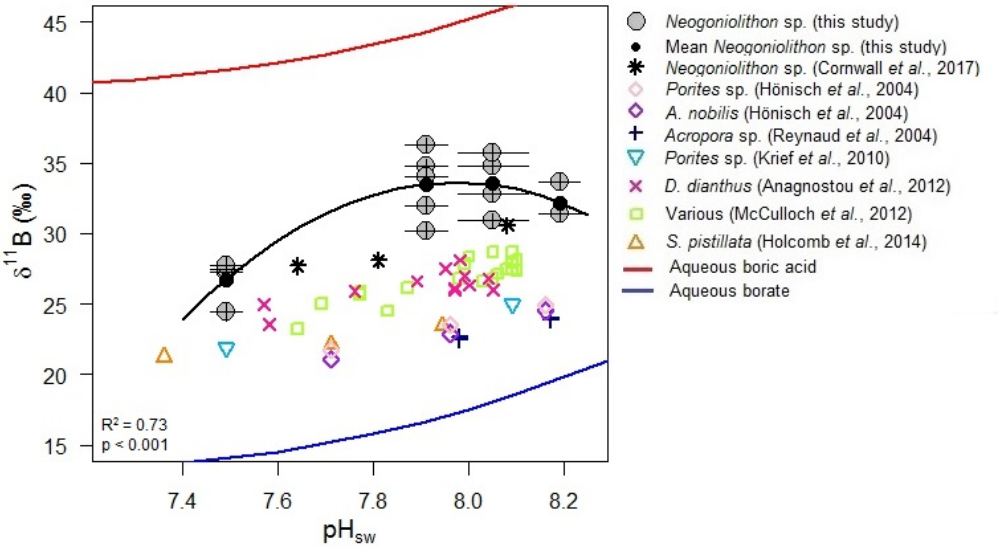

Figure 5.2: δ^{11}B of the coralline red algae *Neogoniolithon* sp. measured using MC-ICP-MS, plotted against pH_{sw}. Black circles filled with grey represent replicates measured at each pH_{sw}, and the mean δ^{11}B of each culture experiment is shown as a filled black circle. The δ^{11}B of all measured samples are elevated relative to aqueous borate (blue line) by +12 ‰ on average. δ^{11}B compositions of a crustose species of *Neogoniolithon* coralline red alga and various scleractinian corals grown at different pH_{sw} are plotted in open coloured symbols (Cornwall et al., 2017; Honisch et al., 2004; Reynaud et al., 2004; Krief et al., 2010; Anagnostou et al., 2012; McCulloch et al., 2012a; Holcomb et al., 2014).

pCO_2	pH	δ^{11}B ‰				B/Ca μmol mol^{-1}				^{11}B nmol				Sr/Ca μmol mol^{-1}			
μatm		Replicate	Duplicate	Average	Experiment mean	Replicate	Duplicate	Average	Experiment mean	Replicate	Duplicate	Average	Experiment mean	Replicate	Duplicate	Average	Experiment mean
409 (6)	8.19 (0.03)	*40.61 (0.10)*	*39.18 (0.11)*	*39.90*	**32.17 (1.33)**	*815 (41)*	*686 (34)*	*751*	**511 (78)**	*800 (132)*	*533 (57)*	*667*	415 (62)	*2.89 (0.14)*	*2.99 (0.15)*	*2.94*	**3.02 (0.11)**
		31.44 (0.13)	31.38 (0.11)	**31.41**		454 (29)	439 (39)	**447**		353 (84)	415 (40)	395		2.85 (0.10)	2.93 (0.04)	**2.89**	
		33.70 (0.11)				**598 (73)**				**590 (83)**				**3.10 (0.08)**			
		31.40 (0.12)				**488 (5)**				**530 (41)**				**3.07 (0.06)**			
606 (7)	8.05 (0.06)	35.02 (0.10)	34.60 (0.11)	**34.81**	**35.58 (2.16)**	628 (52)	521 (24)	**575**	**550 (26)**	545 (24)	440 (50)	**493**	**516 (36)**	2.99 (0.01)	2.95 (0.04)	**2.97**	**3.01 (0.13)**
		30.90 (0.10)				**516 (27)**				**466 (32)**				**2.91 (0.07)**			
		32.83 (0.14)				**565 (8)**				**500 (8)**				**3.20 (0.14)**			
		35.77 (0.11)				**542 (9)**				**603 (65)**				**2.95 (0.03)**			
903 (12)	7.91 (0.03)	32.05 (0.16)	31.99 (0.10)	**32.02**	**33.45 (2.38)**	488 (44)	572 (15)	**530**	**555 (66)**	452 (18)	513 (25)	**483**	**477 (49)**	3.02 (0.09)	3.19 (0.03)	**3.11**	**3.15 (0.11)**
		34.75 (0.11)				**547 (3)**				**371 (75)**				**3.15 (0.00)**			
		30.18 (0.15)				**506 (32)**				**488 (7)**				**3.32 (0.12)**			
		36.26 (0.10)				**670 (84)**				**641 (115)**				**3.16 (0.01)**			
		34.03 (0.10)				**524 (19)**				**401 (54)**				**3.03 (0.08)**			
2856 (54)	7.49 (0.02)	**27.31 (0.18)**			**26.75 (1.56)**	**352 (18)**			**377 (29)**	**69 (66)**			**163 (74)**	**3.31 (0.03)**			**3.36 (0.14)**
		27.47 (0.18)				**404 (19)**				**373 (149)**				**3.54 (0.13)**			
		27.78 (0.21)				**352 (18)**				**100 (44)**				**3.38 (0.02)**			
		24.42 (0.22)				**401 (17)**				**108 (39)**				**3.20 (0.11)**			

Table 5.1: Summary of each experimental treatment showing measured element ratios and δ^{11}B composition. The mean of each variable measured is shown in bold, 1σ are shown in parentheses. The sample shown in italic is anomalous and is therefore excluded from subsequent discussion (also excluded from means). Therefore n = 16 for all regression analyses.

The range of δ^{11}B for each pH treatment varies from 2.3 at pH_{sw} 8.19 to 6.1 ‰ at pH_{sw} 7.91. The relationship between δ^{11}B of *Neogoniolithon* sp. calcite and pH_{sw} (Figure 5.2) demonstrates that all δ^{11}B measurements in this study lie considerably above the pH_{sw} vs. aqueous borate δ^{11}B curve (Klochko et al., 2006), and are also elevated compared to other examples of biogenic carbonates thus far quantified (McCulloch et al., 2012b), with the exception of some deep-sea scleractinian corals (*e.g.* Blamart et al., 2007). The high δ^{11}B compositions observed in this study of a branching species of *Neogoniolithon* are also similar to those found in a crustose species of the same genus (Cornwall et al., 2017), suggesting that closely related species of coralline algae exhibit similar boron isotope systematics and pH_{cf}, and that growth form (*i.e.* crustose vs. branching) alone does not necessarily impart large differences in these systems. Although the offset of the algae's pH_{sw} vs. δ^{11}B curve from the pH_{sw} vs. aqueous borate δ^{11}B curve is generally consistent with the offset previously observed for corals grown at various pH_{sw} (Hönisch et al., 2004; Reynaud et al., 2004; Krief et al., 2010; Anagnostou et al., 2012; McCulloch et al., 2012a; Holcomb et al., 2014), the pH_{sw} vs. δ^{11}B relationship for the algae is better fit (with respect to minimising residuals) with a parabolic model ($R^2 = 0.73$ and $p < 0.001$, vs. $R^2 = 0.53$ and $p < 0.01$ for linear fit) while the pH_{sw} vs. δ^{11}B relationships for corals are better fit with linear models (Trotter et al., 2011; McCulloch et al., 2012b; Holcomb et al., 2014). Details of all regressions, gradients and intercepts can be found in Table B2 in the supplementary materials.

The measured B/Ca and δ^{11}B compositions are also highly linearly correlated ($R^2 = 0.77$, $p < 0.0001$; Figure 5.3A), a trend that is predicted from boron isotope systematics yet rarely observed so clearly in biogenic carbonates (Foster, 2008; Henehan et al., 2015) with the possible exception of recent work with deep-sea corals (Stewart et al., 2016). Sr/Ca has significant negative correlation with δ^{11}B ($R^2 = 0.33$, $p < 0.05$; Figure 5.3B).

Following the interpretations of ^{11}B in corals (Hemming et al., 1998; Rollion-Bard et al., 2003; Allison and Finch, 2010; Rollion-Bard et al., 2011; McCulloch et al., 2012b), pH_{cf} calculated using equation 3 (assuming boron in the algal calcite is sourced solely from seawater borate) reveals an elevation of pH_{cf} relative to pH_{sw} by an average of 1.20 ($\pm$ 0.22) pH units (Figure 5.4A). There is a statistically significant linear

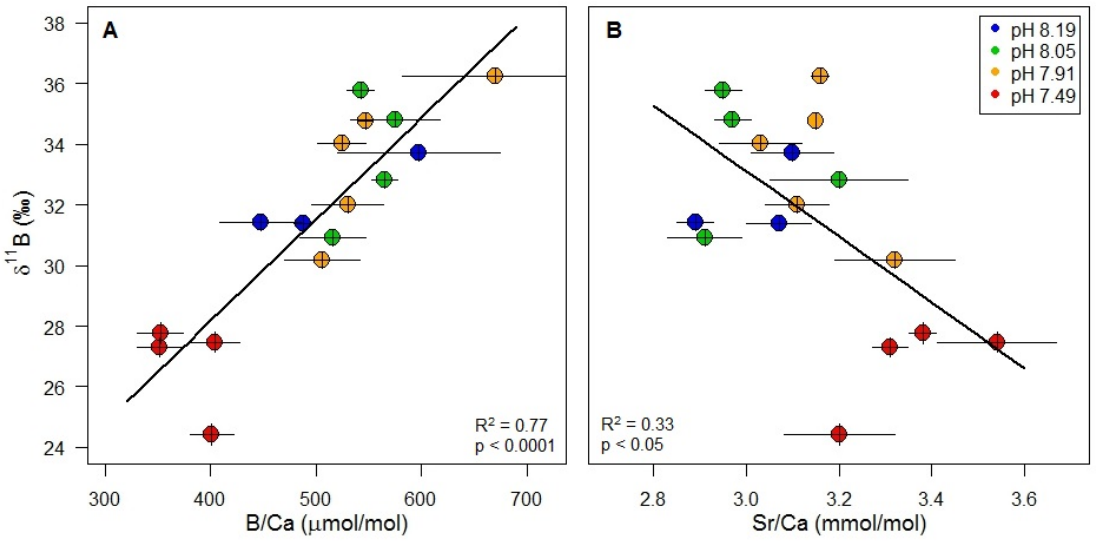

Figure 5.3: Least squares linear regression of B/Ca and Sr/Ca against δ^{11}B composition. (A) B/Ca ratios in *Neogoniolithon* sp. show a strong positive correlation when regressed against δ^{11}B composition. (B) Sr/Ca ratios show slightly less well-defined trends when regressed against δ^{11}B composition, although both reveal statistically significant correlations.

positive correlation ($R^2 = 0.45$, $p < 0.01$) between pH_{cf} and pH_{sw}, although once again a second-order polynomial model with an optimum near pH_{sw} 7.95 better describes the data ($R^2 = 0.66$, $p < 0.001$). If this model of boron incorporation is correct, ΔpH plotted against pH_{sw} exhibits an apparent parabolic relationship with pH_{sw} ($R^2 = 0.46$, $p < 0.01$; Figure 5.4B). ΔpH approaches a maximum mean of 1.26 pH units under the second most acidic treatment, and although these measurements fall within 1σ of each mean, there is a significant reduction of ΔpH at the most acidic treatment (pH_{sw} 7.49). For instance, t-tests reveal there is a significant difference between the mean δ^{11}B composition of the algae cultured at pH_{sw} 8.19, 8.05 and 7.91 when compared to the algae cultured at pH_{sw} 7.49, confirming that a reduction in pH_{sw} causes a decrease in pH_{cf} of coralline red algae.

The B/Ca of the algal specimens range from 352 ($\pm$ 18) to 670 ($\pm$ 84) μmol mol^{-1} (Figure 5.5B), and is therefore comparable to B/Ca in scleractinian corals, but exceeds that found in coccolithophores (Stoll et al., 2012) and foraminifera (Henehan et al., 2015). Although both linear ($R^2 = 0.49$, $p < 0.01$) and second-order polynomial regressions ($R^2 = 0.72$, $p < 0.001$) of the B/Ca *vs.* pH_{sw} data are statistically significant, the polynomial model better describes the data (lower p-value and higher R^2). Ranges

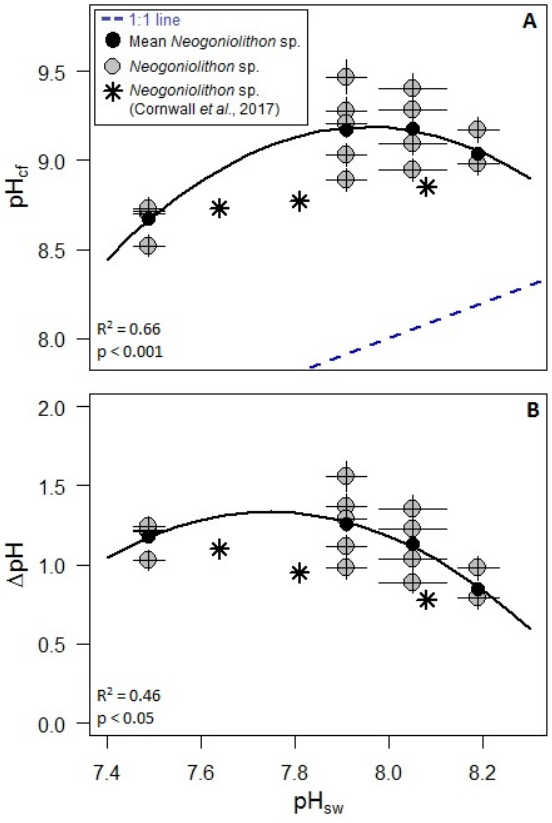

Figure 5.4: pH_{cf} vs. pH_{sw} (A) and ΔpH (pH_{cf} - pH_{sw}) vs. pH_{sw} (B). An apparent parabolic relationship is observed in A, with a maximum at pH_{cf} ~7.95. In B, ΔpH also exhibits a similar relationship with pH_{sw} suggesting that coralline red algae increase their pH_{cf} by increasingly larger amounts under acidified conditions to support biogenic calcification. At extremely low pH_{sw}, the shape of the curve suggests that coralline red algae have reached the limit of the extent to which they can elevate pH_{cf} relative to pH_{sw}. The filled black circles indicate mean values. This branching species of *Neogoniolithon* coralline red algae is compared with a crustose species of *Neogoniolithon* (stars) from Cornwall et al. (2017).

within treatments vary from 182 μmol mol^{-1} at pH_{sw} 7.91 to 52 μmol mol-$^{-1}$ at pH_{sw} 7.49.

Calcite Sr/Ca ranges from 2.85 ($\pm$ 0.10) to 3.54 ($\pm$ 0.13) mmol mol^{-1} and exhibits a statistically significant negative linear correlation with pH_{sw} (R^2 = 0.59, p < 0.001; Figure 5.5A). A negative trend is also observed between Sr/Ca and B/Ca, although it is just outside of significance at the 95% level (R^2 = 0.22, p = 0.06; Figure 5.5C).

5.4 Discussion

5.4.1 δ^{11}B and B/Ca as tracers of pH

The boron isotope palaeo-pH proxy has been primarily applied to foraminifera, and tropical and deep-sea corals (*e.g.* Spivack et al., 1993; Sanyal et al., 1996; Palmer, 1998; Krief et al., 2010; Rae et al., 2011; Anagnostou et al., 2012; Henehan et al., 2013). Calcification in foraminifera occurs *via* vacuolisation of seawater (Erez, 2003; de Nooijer et al., 2014), while corals are thought to biomineralise from a discrete fluid between their calicoblastic epithelium and skeleton (Cohen and McConnaughey, 2003). As outlined above, calcification in coralline algae occurs extracellularly within and between the cell walls of the algae yet external to their cell membrane (Ries, 2009). The application of the foraminifera or coral model for the δ^{11}B proxy in coralline algae therefore requires

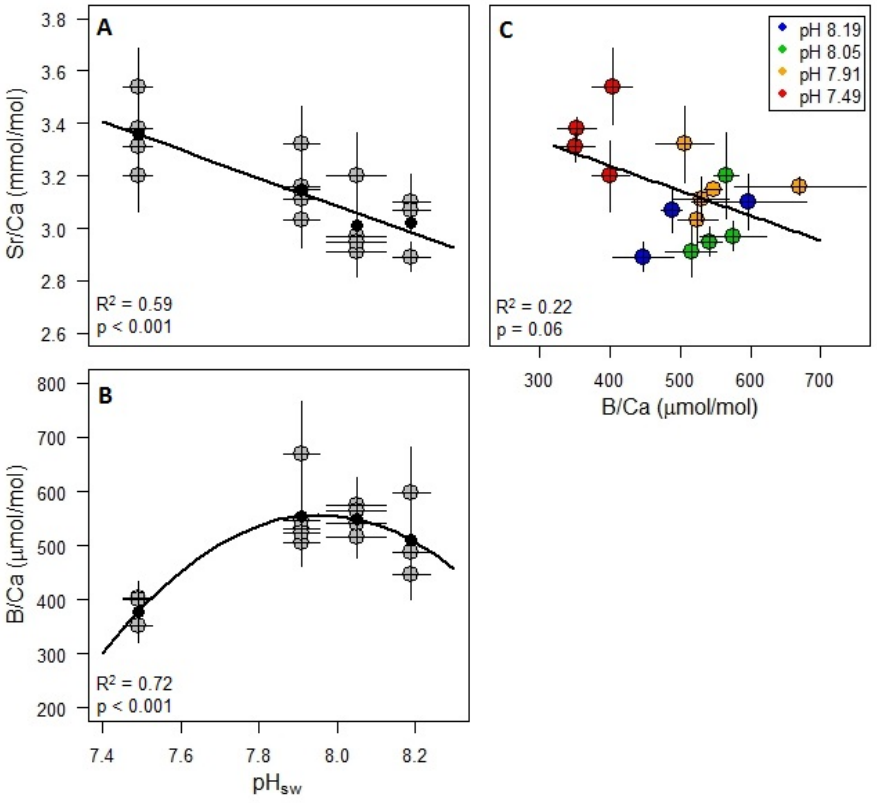

Figure 5.5: B/Ca and Sr/Ca regressed against pH$_{sw}$. Sr/Ca ratios (A) of *Neogoniolithon* sp. are strongly linearly correlated with pH$_{sw}$, while B/Ca is strongly correlated with an apparent parabolic relationship with pH$_{sw}$ (B). Sr/Ca (C) is not significantly correlated with B/Ca, although the trend is nearly significant. The filled black circles indicate mean values.

some key assumptions, including in particular that the algal calcification fluid has a total δ^{11}B and salinity similar to that of ambient seawater. Nonetheless, recent studies have shown that calcein, which cannot be transported across cellular membranes, is incorporated into the skeleton of the coralline algae *Lithothamnion glaciale* (Pauly et al., 2015), supporting the assumption that the site of calcification in coralline algae is at least partially open to seawater exchange (Comeau et al., 2012; Adey et al., 2013).

Regardless of the precise mechanism of calcification within this species, the strong positive correlations observed here between δ^{11}B composition, B/Ca ratio and pH_{sw} indicate that boron systematics of coralline algae do vary with respect to pH_{sw}. As expected from the existing understanding of the proxy, cultures at lower pH_{sw} have lower δ^{11}B and B/Ca; both, in theory, resulting from a reduction in borate concentration relative to boric acid at lower pH_{sw}. Nonetheless, the δ^{11}B data for the coralline algae presented here plot well above the borate δ^{11}B *vs.* pH_{sw} curve. Therefore, following the model for boron isotopes in corals proposed by McCulloch et al., (2012a), the results of our study suggest that coralline algae substantially increase pH_{cf} to promote calcification. Indeed pH_{cf} has been shown to increase during seasonal variations in ΔpH of 0.5 to 0.7 pH units within the coralline algae species *Clathromorphum nereostratum* (Fietzke et al., 2015), and the more recent study by Cornwall et al. (2017) shows that a crustose species of the *Neogoniolithon* genus exhibits a ΔpH of ca. 0.8 - 1.1 pH units, depending on pH_{sw}.

Interpreting the results of the boron isotope data presented here following standard boron isotope pH proxy assumptions that (1) boron enters the algal calcification site unfractionated from seawater, (2) boron isotope fractionation in coralline algae is controlled only by pH_{cf}, and (3) only seawater borate is incorporated into the coralline algal skeleton, suggests that *Neogoniolithon* sp. undergoes a large pH_{cf} increase of, on average, 1.20 units (Figure 5.4). In light of these findings, and the unique calcification mechanism in coralline algae compared to other marine calcifiers, some alternative models of boron systematics within coralline algae should be explored to ensure that these standard assumptions are met in coralline algae. The impact of possible boric acid incorporation, and Rayleigh fractionation of the calcifying medium and other processes affecting coralline algal skeletal chemistry are discussed in the following sections.

5.4.2 Boric acid incorporation

Isotopically heavy boric acid has a similar size and the same trigonal planar structure as the carbonate ion (CO_3^{2-}) found in the algal calcite lattice and, whilst boric acid holds no charge, it may be incorporated as an impurity. Solid state ^{11}B nuclear magnetic resonance (NMR) spectroscopy on coralline algal calcite has revealed that approximately 30% of boron is present in a trigonal geometry, and Cusack et al. (2015) suggested that boric acid may therefore be directly incorporated into the high-Mg calcite of *Neogoniolithon* sp. The incorporation of ^{11}B enriched boric acid into the calcite lattice would result in higher skeletal $\delta^{11}B$. Therefore, boric acid incorporation may partially explain the positive shift in skeletal $\delta^{11}B$ compositions (relative to $\delta^{11}B$ of seawater borate) that we report here (Figure 5.2).

Assuming that both seawater borate and boric acid are incorporated into coralline algal calcite, the proportion of boric acid required to match the mean skeletal $\delta^{11}B$ compositions of the algae is between 44 and 60% (Table 5.2), thereby greatly exceeding the ~30% suggested from in situ ^{11}B MAS (magic angle spinning) NMR studies (Cusack et al., 2015), yet it should also be noted that Cusack et al. (2015) examined a different species of coralline algae (*Lithothamnion glaciale*). Furthermore, given that the abundance of boric acid is pH dependent, it would be expected that the percentage of boric acid incorporated should increase with decreasing pH_{sw} (*i.e.* with increasing boric acid in solution; Noireaux et al., 2015). This was not observed for the specimens of *Neogoniolithon* sp. investigated here, as the percentage of boric acid incorporation required to explain the ^{11}B enrichment levels off for the two lowest pH_{sw} treatments.

^{11}B NMR studies by Mavromatis et al. (2015) and Noireaux et al. (2015) have recently shown that inorganically precipitated calcite contains up to 65% trigonal boron, although a linear relationship between pH_{sw}, and measured $\delta^{11}B$ of the calcite was maintained. However, these studies did identify a significant relationship between the percentage of trigonal boron in the lattice and calcite growth rate. Noireaux et al. (2015) observed that slow growth rate led to a higher percentage of trigonal boron in the calcite lattice, and suggested that this indicates an increase in boric acid incorporation

pCO_2 μatm	pH_{sw}	$\delta^{11}B$ ‰	$B(OH)_3$ %	Net calcification wt%/60 days	pH_{cf}	ΔpH
409 (6)	8.19 (0.03)	32.17 (1.33)	44 (4)	5.7 (2.9)	9.04 (0.11)	0.85 (0.11)
606 (7)	8.05 (0.06)	33.58 (2.16)	57 (7)	14.5 (6.6)	9.18 (0.20)	1.13 (0.20)
901 (12)	7.91 (0.03)	33.45 (2.38)	60 (8)	10.7 (4.7)	9.17 (0.22)	1.26 (0.22)
2856 (54)	7.49 (0.02)	26.75 (1.56)	46 (6)	3.6 (3.5)	8.67 (0.10)	1.18 (0.10)

Table 5.2: Mean skeletal $\delta^{11}B$ compositions for each experimental treatment, along with percentage of boric acid (enriched in ^{11}B by 27.2 ‰) required to be incorporated into the algal calcite to generate the measured ^{11}B composition, assuming that $\delta^{11}B$ of the borate portion of the algal calcite is equal to seawater borate. Net calcification indicates that algae from the pH_{sw} 8.19 and 7.49 treatments have the slowest calcification rates, yet also require the smallest apparent proportion of boric acid. pH_{cf} indicates mean calcification site pH for each treatment, and ΔpH describes the change in pH according to the equation $\Delta pH = pH_{cf}$ - pH_{sw}. 1σ are shown in parentheses.

(see also Mavromatis et al., 2015). The slowest growth rates in our cultured *Neogoniolithon* sp. are found at pH_{sw} 8.19 and 7.49, where in contrast, our boron isotope data suggests the smallest boric acid incorporation (Table 5.2). In light of these findings, it seems unlikely that boric acid incorporation is a dominant driver of the heavy $\delta^{11}B$ (relative to $\delta^{11}B$ of aqueous borate expected at that pH_{sw}) observed in cultured *Neogoniolithon* sp., or has a significant influence on the relationship between skeletal $\delta^{11}B$ and pH_{sw} in this species. Furthermore, although ^{11}B NMR studies may reveal that trigonal boron is present in the calcite lattice, this may be a result of geometry change of the borate molecule during incorporation into the calcite lattice, rather than direct incorporation of boric acid (Balan et al., 2016).

5.4.3 Rayleigh fractionation

Coralline algae calcification occurs intercellularly within the cell walls of the algae, which are semi-isolated from seawater by adjacent cells. Nevertheless, these extracellular restricted environments are likely to be permeable to seawater and maintained at elevated pH and calcite saturation state to promote calcification. Rayleigh fractionation describes the process by which molecules or ions are continuously removed from a

closed or semi-closed system, leading to progressive change in the elemental and/or isotopic composition of the residual fluid. The precipitation of $CaCO_3$ in this semi-isolated calcification space may therefore lead to changes in the elemental and isotopic composition of the algal calcite (as proposed for corals by Gaetani and Cohen, 2006; Gagnon et al., 2007). For example, assuming that borate (isotopically lighter than total seawater boron) is solely incorporated into coralline algal calcite, the remaining fluid would become enriched in ^{11}B, imposing a heavier $\delta^{11}B$ composition on the later forming calcite.

The partition coefficient (K_D) of boron into calcite is described by equation (5.5).

$$K_D = \frac{[B/Ca]_{CaCO_3}}{[B/Ca]_{seawater}} \tag{5.5}$$

There are several estimates for the K_D of boron, and all are much less than one (ca. 0.0005; Yu et al., 2007; Stoll et al., 2012). Consequently, as calcification progresses, Rayleigh fractionation drives an increase in the B/Ca ratio of the residual fluid, thereby increasing B/Ca of the latterly precipitated $CaCO_3$. In theory, therefore, Rayleigh fractionation may be sufficient to describe both the observed enrichment in ^{11}B in coralline algae calcite relative to seawater borate (Figure 5.2), the observed relationships between pH_{sw} and both coralline algal B/Ca (Figure 5.5) and $\delta^{11}B$ (Figure 5.2), as well as the observed correlation between coralline algal B/Ca and $\delta^{11}B$ (Figure 5.3).

However, the study of boron incorporation into deep sea scleractinian corals by Stewart et al. (2016) shows that Rayleigh fractionation is unable to drive significant changes in skeletal $\delta^{11}B$ and B/Ca from unmodified seawater (*i.e.* [B] of 432 μmol kg^{-1}; [Ca] of 10.3 mmol kg^{-1}; salinity 35 psu) given a typical biogenic carbonate B/Ca of $\sim$600 μmol mol^{-1} because insufficient borate is removed at each incremental step of precipitation to drive the observed change in $CaCO_3$ $\delta^{11}B$. Thus Rayleigh fractionation can only explain the relationship observed in Figure 5.3 between B/Ca and $\delta^{11}B$ if the B/Ca ratio of the calcifying fluid is very much reduced relative to that of seawater and the partition coefficient is higher than estimates from inorganic experiments (in order to maintain the observed B/Ca ratio). For instance, a Rayleigh model fitted to the $\delta^{11}B$ and B/Ca data in this study suggests a high K_D of 0.5, and a 98.5% reduction in seawater boron content at the site of calcification. While this is a possibility in coralline

algae as calcification occurs within a semi-restricted space, the inverse correlation between Sr/Ca and B/Ca when both elements have a K_D of <1 within calcite (defined in equation 5.5; Figure 5.5), suggests that Rayleigh fractionation is unlikely to account for the entirety of the observed ^{11}B enrichment in *Neogoniolithon* sp. relative to seawater borate, as well as the observed relationships between pH_{sw} and $\delta^{11}B$, and B/Ca.

5.4.4 Calcification rate and implications for coralline red algae in a high-CO_2 world

Boron isotope characteristics of *Neogoniolithon* coralline red algae are unlikely to result from boric acid incorporation or Rayleigh fractionation. Recent inorganic precipitation experiments have highlighted the importance of calcification rate in controlling B/Ca in calcite (Gabitov et al., 2014; Mavromatis et al., 2015; Noireaux et al., 2015; Uchikawa et al., 2015). Here we find strong correlation between calcification rate and B/Ca ($R^2 = 0.40$, $p < 0.01$), which is therefore entirely consistent with pH_{cf} elevation increasing Ω and borate concentration at the site of calcification, thereby driving increased boron incorporation into the algal calcite. Although this might be expected to also increase Sr/Ca given inorganic experiments (*e.g.* Böhm et al., 2012), the Sr/Ca in the cultured coralline algae exhibits a positive correlation with DIC (μmol $kgsw^{-1}$; Figure B2); a relationship recently documented in foraminifera (Keul et al., 2017). This points towards a new proxy in coralline algae that has potential to fully resolve the carbonate system.

We are then left with the possibility that $\delta^{11}B$ of the algal calcite reflects pH_{cf} pursuant to the $\delta^{11}B$-pH_{sw} relationship, as proposed for scleractinian corals (*e.g.* McCulloch et al., 2012b). Since pH_{cf} will largely control calcite saturation state (Ω) at the site of calcification, calcification rate should exhibit a strong relationship with $\delta^{11}B$ and pH_{cf}. This is apparent when calcification rates of individual algal specimens (Ries et al., 2009) are plotted against their respective $\delta^{11}B$-derived values of pH_{cf} (Figure 5.6A). The observed relationship between coralline algal calcification rate and pH_{sw} (Figure 5.6B; *i.e.* increased calcification under slightly elevated pCO_2, reduced calcification at

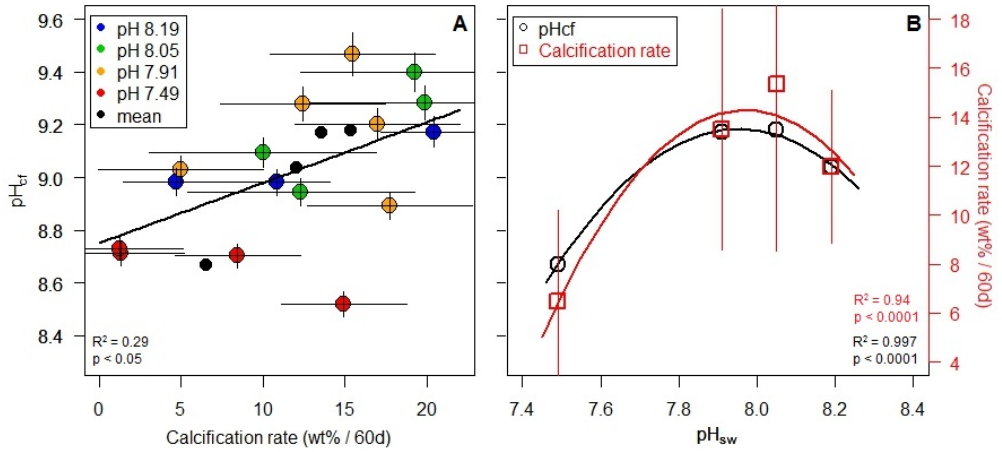

Figure 5.6: The relationship between the pH_{cf} and net calcification of *Neogoniolithon* sp. (A) This positive correlation between the mean pH_{cf} and mean calcification rate indicates a reduction in calcification rate with decreasing pH_{cf}. (B) Across treatments, pH_{cf} (black circles) is influenced by pH_{sw}, which also affects net calcification (red squares). The similarity between the two negative curves highlights the link between calcification rate and pH_{sw}, but also reveals the resilience of coralline red algae to moderate ocean acidification. The algae are able to mitigate moderate pH_{sw} reduction, but are unable to calcify efficiently at extremely low pH_{sw} values.

extremely elevated pCO_2; Ries et al., 2009) may thus arise from the relationship between pH_{sw} and pH_{cf} (Figure 5.4). Furthermore, the ability of *Neogoniolithon* algae to raise pH_{cf} relative to pH_{sw} increases under more acidified conditions, with ΔpH increasing from 0.85 ($\pm$ 0.11) to 1.26 ($\pm$ 0.22) between pH_{sw} of 8.19 to 7.91. These results are consistent with three coralline algae species (including a crustose *Neogoniolithon* sp.) cultured at variable pH_{sw} by Cornwall et al. (2017), which also exhibit a similar increase in ΔpH from ca. 0.8 to ca. 1.1 between pH_{sw} of 8.08 to 7.64 (Cornwall et al., 2017). However, our observation that ΔpH levelled off under the two most acidic treatments suggests that there is a limit to the extent to which the branching species of *Neogoniolithon* can elevate pH_{cf} relative to pH_{sw}. This limit may also exist for those species examined by Cornwall et al. (2017) but is not resolvable because their pH_{cf} data are confined to a narrower pH_{sw} range, with only three pH_{sw} treatments examined that fall within the linear portion of our pH_{cf} *vs.* pH_{sw} relationship. Nonetheless, taken together, our study and that of Cornwall et al. (2017) illustrate that pH_{cf} in coralline algal therefore appears to promote calcification in moderately acidified seawater (down to pH_{sw} 7.95), which is most likely due to CO_2-fertilisation of photosynthesis. This supports

the previous observation that photosynthesis in some marine algae is CO_2-limited up to ca. 1000 atm pCO_2 (Bowes, 1993). Our new data at low pH_{sw}, however, reveals that no additional benefit for photosynthesis in this coralline alga appears to be conferred by increasing pCO_2 from 903 to 2856 μatm pCO_2, while the accompanying increase in acidity and resulting decrease in Ω of the culture solution has a clear detrimental effect on the calcification rate of the algae.

As has been demonstrated for scleractinian corals (McCulloch et al., 2012b), the ability of coralline algae to elevate pH_{cf} may confer resilience to the deleterious effects of ocean acidification, thereby giving them an advantage over calcifying taxa competing for space on the seafloor that lack this ability. Specifically, our data suggest that species-specific pH_{sw} optima exist at pH_{sw} ca. 8 for maximising both pH_{cf} and calcification rates of *Neogoniolithon* sp. However, that pH_{cf} and algal calcification rates begin to dramatically decline as pH_{sw} is decreased from 7.9 to 7.5 indicates that there are limits to the extent that coralline algae can mitigate the effects of more extreme ocean acidification. Indeed, at extremely low pH_{sw}, mineralogical changes (high Mg calcite to gypsum ratio) are induced in other species of coralline algae (Kamenos et al., 2016). Together, these findings have implications for how *Neogoniolithon* sp. will cope with increasing ocean acidification in the future.

5.4.5 Intra-treatment variability and implications for the boron isotope proxy

One notable feature of the $\delta^{11}B$ presented here for *Neogoniolithon* sp. is the degree of variability between specimen replicates within pH_{sw} treatments. Although some degree of scatter between replicates is often observed in other culture studies, in this case it reached ca. 6 ‰. Some of this scatter may be influenced by the heterogeneity of the bulk samples, as microstructural differences have been shown to affect $\delta^{11}B$ in aragonitic corals by up to 10 ‰ (Blamart et al., 2007), and laser ablation $\delta^{11}B$ has revealed variations of up to 6 ‰ in other species of coralline algae (Fietzke et al., 2015). That the spread in $\delta^{11}B$ is still fairly large at the pH_{sw} closest to ambient confirms this is not a methodological artefact where pre-experimental skeleton is inadvertently

sampled, but rather is a primary feature of this species of coralline red algae. This is also confirmed by the lack of correlation between the scatter from the mean $\delta^{11}B$ for each treatment and the mass of $CaCO_3$ measured (Figure B1).

Despite this spread in $\delta^{11}B$ for a given treatment, there remains good correlation between B/Ca and ^{11}B (Figure 5.3). Although the strength of this correlation is perhaps unexpected given some related studies (*e.g.* Douville et al., 2010; Henehan et al., 2015), this further supports the assertion that coralline algal calcification rate, $\delta^{11}B$ and B/Ca are controlled by pH_{cf} of the algae, and that there is considerable variability in pH_{cf} amongst individuals.

The finding that coralline red algal $\delta^{11}B$ responds to pH_{sw} suggests that this is a potential taxon for reconstructing palaeo-pH_{sw}; a conclusion that is particularly noteworthy given coralline algaes ability to produce long growth records in high-latitude oceans, where palaeo-pH_{sw} records are sparse (Fietzke et al., 2015). Despite these encouraging results, further work on *Neogoniolithon* is clearly required to determine whether the $\delta^{11}B$ of this genus of coralline algae offers the precision and accuracy needed to reliably reconstruct past changes in pH_{sw}, particularly in light of their strong inter-specimen variability in boron geochemistry.

5.5 Conclusion

We find that statistically significant relationships exist in cultures of the coralline red algae *Neogoniolithon* sp. between $\delta^{11}B$ and pH_{sw}, $\delta^{11}B$ and skeletal B/Ca, and pH_{cf} and net calcification rate. Skeletal $\delta^{11}B$ in this species is considerably elevated compared to $\delta^{11}B$ of both seawater borate and most other examples of biogenic carbonate, suggesting an average pH_{cf} increase of more than 1 pH unit relative to pH_{sw}. An observed correlation between calcification rate and pH_{cf} suggests that the algae promote calcification by elevating pH_{cf}. Furthermore, the observation that ΔpH increased as pH_{sw} decreased from 8.2 to 7.9 suggests that this species of coralline red algae is able to mitigate the effects of moderate ocean acidification *via* pH regulation at the site of calcification. However, the observation that pH_{cf} and calcification rates decreased when

pH_{sw} was reduced to 7.5 suggest that there is a limit to the extent to which this species can mitigate the effects of extreme ocean acidification.

Acknowledgements

Financial support for this study was provided by the Natural Environmental Research Council (UK) to H.K.D. (grant number 1362080) and G.L.F. (NE/H017356/1). J.B.R. acknowledges funding from NSF-BIO-OCE 1437371 and NSF-BIO-OCE 1459706 and acknowledges Northeastern University's Marine Science Center. We thank J. A. Milton and M. J. Cooper (University of Southampton) for their assistance during MC-ICPMS work. Discussions with A. J. Poulton and C. M. Moore are gratefully acknowledged. The authors also thank associate editor Claire Rollion-Bard, and three reviewers (Nick Kamenos and two anonymous) for their constructive feedback that led to an improved version of this manuscript.

Chapter 6

Conclusions

6.1 Thesis synopsis and key conclusions

This thesis has sought to advance current knowledge of boron geochemistry by measuring boron isotopes in diatoms and coralline algae. This was achieved by developing analytical protocols to measure δ^{11}B and B/Si in biogenic silica by MC-ICP-MS, and assessing the relationship between δ^{11}B of *T. weissflogii* diatoms and seawater pH for the first time. This protocol and calibration were applied to preserved diatoms for the first time, from ODP Site 882 in the subarctic Northwest Pacific in order to establish the palaeo-archive potential of boron in diatoms. The pH sensitivity in δ^{11}B of *Neogniolithon* sp. coralline algae was also assessed, providing insights into how these algae mitigate negative effects from ocean acidification, and their potential as a palaeo-archive was also examined. The key questions addressed in Chapter 1 are revisited below.

6.1.1 Chapter 2

Q1. Can boron isotopes be measured in diatoms using MC-ICP-MS?

A method to measure boron isotope in diatoms by MC-ICP-MS was developed using existing carbonate-based analytical protocols. This method was developed using a bulk

sediment diatom in-house standard (TC460), and involved several steps including cleaning, dissolution, matrix separation and the analysis of δ^{11}B using a Thermo Fisher Neptune MC-ICP-MS. Boron isotopes can therefore indeed be measured in diatoms using MC-ICP-MS (Figure 6.1). Complementary to δ^{11}B is the development of a successful method to measure B/Si in diatoms by solution based ICP-MS.

Q2. If so, can δ^{11}B be measured in diatoms accurately and with comparable reproducibility to marine carbonates?

The method detailed in Chapter 2 was shown to be accurate by the standard addition method (2σ ± 0.29 ‰), and reproducible from 11 - 34 ng boron (± 0.28 ‰). This precision is comparable to existing carbonate methods, where δ^{11}B can be measured to ± 0.20 ‰ at 95% confidence. This shows that measuring δ^{11}B in diatoms holds great potential for expanding the use of the boron palaeo-pH proxy in oceanic areas where sediment is dominated by siliceous material.

6.1.2 Chapter 3

Q3. How could ocean acidification affect *T. weissflogii* diatoms?

The study carried out in Chapter 3 focuses solely on variable seawater pH and, under

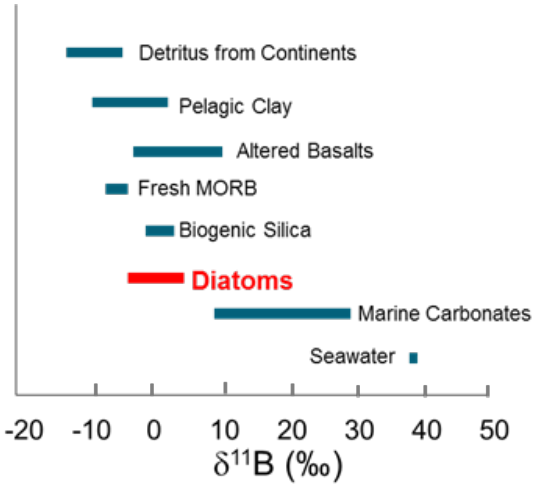

Figure 6.1: δ^{11}B measured in other marine-sourced organisms and sediments. Diatom δ^{11}B from this thesis has been added in red. Adapted from Zeebe and Wolf-Gladrow (2001).

nutrient replete conditions, *T. weissflogii* diatoms appear to be unaffected by the detrimental effects of ocean acidification often observed in marine carbonates. The diatoms grown under low seawater pH (high pCO_2) were smaller by 1.5% over 1.2 pH units, although silica content remained constant, implying the diatoms grew slightly thicker frustules at low seawater pH. It also appeared that CCMs in *T. weissflogii* were efficient enough to adapt to a large change in pCO_2, as carbon content of the diatoms remained constant at every pH treatment. The smaller diatoms did, however, exhibit an increased nitrogen uptake rate, indicating that a higher amount of nitrogen fixation occurred at lower seawater pH. This may therefore have implications for the oceanic nitrogen cycle, if diatoms are ultimately more resilient to ocean acidification than marine carbonates, and can outcompete calcifying organisms in the face of higher pCO_2.

Q4. What is the relationship between δ^{11}B in diatoms and seawater pH?

The statistically significant negative correlation between δ^{11}B in *T. weissflogii* diatoms and seawater pH is defined as:

$$\delta^{11}B_{diatom} = [(-2.62 \pm 0.83) \times pH_{sw}] + (17.25 \pm 6.74) \tag{6.1}$$

($R^2 = 0.43$, $p < 0.01$). This negative correlation indicates that lighter δ^{11}B in diatoms corresponds to higher seawater pH, which is the opposite relationship observed in previously measured carbonates. B/Si measured in these *T. weissflogii* diatoms increased with increasing seawater pH ($R^2 = 0.71$, $p < 0.05$), suggesting that the assumption that the boron species incorporated into the carbonate lattice is borate can be maintained for the diatom opal polymer.

Q5. By what mechanism could this relationship occur?

Preliminary attempts at modelling have been able to explain the δ^{11}B *vs.* seawater pH relationship shown above. As diatoms are marine algae, and boron has been shown to be an essential nutrient for plants, boric acid from seawater likely passively diffuses into the diatom in order to meet these biological requirements. The positive correlation between boron content and seawater pH suggests that borate also enters the diatom by

active uptake through bicarbonate transporters, and therefore boron uptake is linked to ambient pCO_2. As pCO_2 in seawater drops with increasing pH, diatoms utilise CCMs to obtain enough CO_2 to perform photosynthesis, and increase bicarbonate pumping. In doing so, more borate is pumped into the cell, and therefore more is incorporated into the frustule, indicating a positive relationship between the uptake of borate and bicarbonate. This mechanism of boron uptake by diatoms reproduces the relationship observed from the culture experiment in terms of both $\delta^{11}B$ and boron content.

6.1.3 Chapter 4

Q6. Can $\delta^{11}B$ measured in diatoms be used to accurately reconstruct past ocean pH?

$\delta^{11}B$ can be measured in both cultured and sedimentary diatoms, and in this case, the calibration identified in Chapter 3 between $\delta^{11}B$ and seawater pH was applied to the diatom samples from Site 882. One caveat for using this calibration is that the diatom species examined in Chapter 3 and 4 are different (*T. weissflogii*, and *C. marginatus* and *C. radiatus* respectively). Despite this, the calibration was able to identify a relative change in pH for the subarctic Northwest Pacific between 2.85 and 2.52 Ma, which equated to an average increase in seawater pH at 2.73 Ma of 0.31 - 0.47 pH units. In order to reconstruct absolute past seawater pH, a culture calibration study of *C. marginatus* and *C. radiatus* would need to be carried out.

The absolute $\delta^{11}B$ values between cultured and sedimentary diatoms differed, with the sedimentary diatoms appearing ca. 10 ‰ heavier than the cultured. Whilst this is likely due to species specific differences, it is encouraging that a similar relationship between $\delta^{11}B$ and B/Si was found between both the sedimentary diatoms and the cultured diatoms discussed in Chapter 3.

Q7. What can the new $\delta^{11}B_{diatom}$ data tell us about the effect of the onset and intensification of Northern Hemisphere Glaciation in the subarctic Northwest Pacific?

Adding $\delta^{11}B$ data to this extensively studied core enhanced previous conclusions drawn

that suggest that 2.73 Ma is the point at which a halocline develops in the subarctic Northwest Pacific. The general trend of increasing surface seawater pH suggests that the cooler surface temperatures led to this halocline development, trapping CO_2-rich waters in the deep ocean. The excursions observed in the new $\delta^{11}B$ trace coincide with periods of increased opal mass accumulation rates and $\delta^{30}Si$ indicating increased productivity. These observations suggest that a breakdown of stratification occurs at these points, with nutrient- and CO_2-rich deep waters upwelling and ventilating the deep ocean to the surface, leading to these temporary reductions in seawater pH.

6.1.4 Chapter 5

Q8. How could coralline algae (*Neogoniolithon* sp.) be affected by ocean acidification?

The $\delta^{11}B$ measured in the *Neogoniolithon* sp. of coralline algae examined in Chapter 5 revealed a curved relationship with seawater pH. This indicates that coralline algae can mitigate moderate ocean acidification, but succumb to the detrimental effects of extreme seawater pH reduction on their calcification.

Q9. Does $\delta^{11}B$ measured in coralline algae behave in a similar way to that measured in coral?

The coralline algae exhibit a similar mechanism to corals that increase their internal pH to aid calcification in order to confer resilience to ocean acidification. This can be inferred from the elevated $\delta^{11}B$ values, although $\delta^{11}B$ of coralline algae exceed those recorded in corals. Coralline algae differ to linear coral behaviour in the face of reduced seawater pH, however, as they display a curved relationship.

Q10. Do coralline algae hold potential as palaeo-archives?

This study is one of a handful recently investigating boron in coralline algae, and all have shown very similar results despite using different species. As $\delta^{11}B$ displays sensitivity to seawater pH, and skeletal B/Ca ratios and $\delta^{11}B$ are highly correlated, coralline algae hold great potential as palaeo-archives. However, further work is required due to the

apparent sizeable variability in $\delta^{11}B$ within a single culture treatment, and in order to ensure species-specific effects are accounted for in all future calibrations.

6.2 Future work

The following sections set out to address some limitations of the work described in this thesis, and to suggest potential avenues that directly lead on from this study.

6.2.1 Method optimisation

More work is required to optimise the method described in Chapter 2, particularly the testing of different cleaning protocols to potentially avoid the use of perchloric acid, which may make this method more accessible to labs without the correct fume-hoods in which to handle this particularly hazardous chemical. A study could examine the fine details of this preliminary method, by investigating many different options for the cleaning and dissolution of biogenic silica in order to optimise the whole process. Numerous studies have been completed in order to ground-truth the boron proxy in marine carbonates, so this is just the beginning for boron in diatoms.

The development of a diatom standard reference material in order to matrix match samples is essential. This would also allow long term reproducibility to be measured thoroughly, as well as eventually allow inter-laboratory comparisons to be achieved. Finally, in terms of systematically investigating boron uptake in diatoms, and in order to determine how boron is incorporated into a silica lattice, inorganic studies could be completed by growing SiO_2 polymer and doping with boron (similar to the calcite study performed by Sanyal et al., 2000). The $\delta^{11}B$ could then be measured, and this combined with ^{11}B NMR studies may be able to empirically determine the boron species included in inorganic silica, and elucidate any specific biogenic effects observed in siliceous organisms.

6.2.2 Calibration

Further culture studies are clearly required, and these should initially include examinations of species and size effects at a constant pH_{sw}. The calibration step is arguably the most important with regard to reconstructing past ocean pH, as culture calibration studies should be carried out for every sedimentary species of diatom utilised in the boron proxy. This could be achieved by repeating the culture study described in Chapter 3 using different diatom species, ranging in size, global location and temperature optimum. This is not only important to apply the correct calibration to sediment samples, but also to examine any temperature and size effects.

Another way to test the method and calibration would be to take both foraminifera and diatom samples from the same intervals in the same core, and measure $\delta^{11}B$ in both organisms to directly compare the robustness of the diatom method in reconstructing past ocean pH. This experiment could also explore whether diatom $\delta^{11}B$ is complementary to foraminifera $\delta^{11}B$, or whether it tells us something different about the core/location. For example, any differences in $\delta^{11}B$ could tell us that diatoms were influenced by a different growing season to foraminifera. This may therefore lead to gaining more information about existing datasets from cores, as well as being able to measure $\delta^{11}B$ in core locations previously restricted by lack of carbonate material.

Finally, culture studies could also be undertaken in other siliceous taxa, such as sponges and radiolaria. The aim of these studies could be to discern absolute $\delta^{11}B$ values, but also to ensure any mixing effects are identified if there is any contamination in sedimentary diatom samples.

6.2.3 Application

Siliceous fractions in core samples have sometimes been considered as "waste" in the past and washed away in carbonate cleaning protocols (at the University of Southampton). However, this new method ensures siliceous organisms could be utilised when specifically measuring $\delta^{11}B$ in a sediment core. This directly leads to the possibility of multiproxy approaches, for example, diatom-bound silicon and nitrogen isotope

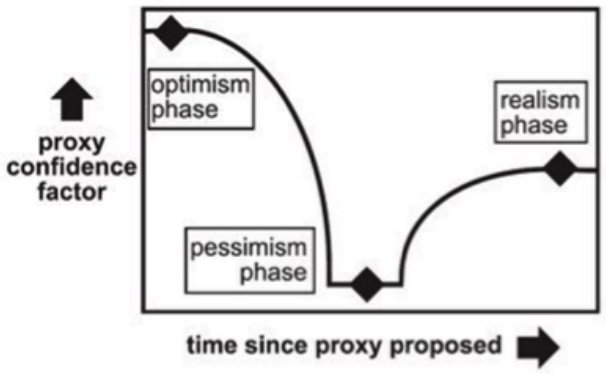

Figure 6.2: Harry Elderfield's "proxy confidence curve"

measurements could now be paired with a δ^{11}B, enabling a more thorough study of each core location, and perhaps leading to the better understanding of areas of diatom interest in terms of elucidating a direct combination of nutrient and carbon cycle information.

This new method to measure δ^{11}B in diatoms could now lead to further δ^{11}B being measured in the Southern Ocean, which is an area of high interest concerning the global carbon cycle. A further application step would also be to choose sediment samples from within the ice core record to directly compare glacial-interglacial pCO$_2$ records, and assess whether δ^{11}B in diatoms could be used to confidently reconstruct past pCO$_2$. This could potentially address what drives glacial-interglacial pCO$_2$.

6.3 Closing remarks

The work described in this thesis represents a significant advancement in the study of boron isotopes in silicifying and calcifying marine algae. With the further work described in this chapter, boron isotopes measured in diatoms could become a valuable palaeoceanographic tool, and help to provide answers to climate change questions. This work represents the preliminary stages of proxy development, and whilst there is a long way to go, this is certainly a positive start (Figure 6.2).

The ultimate aim for this thesis was to be able to measure δ^{11}B in more locations and in more organisms globally. Eventually, despite its carbonate or siliceous content, a complete marine sediment core from anywhere in the world could now undergo δ^{11}B

analysis in order to gain valuable information from our planet's climate history, which could give us vital clues about our climate future.

Appendix A

Chapter 4 - Sponge spicule analysis

During this PhD project, three types of marine sponge biogenic silica were prepared for analysis:

1. *Acoelocalyx* from the Scotia Sea
2. A demosponge from the SARS Seamount
3. A Mycalidae from Burdwood Bank

In order to ensure this observed difference in δ^{11}B between cultured and sedimentary diatoms was not due to any contamination in the sediment samples, some sponge spicule samples were also measured (Table A1). These sponges originated from the Southern Ocean and have been examined previously for silicon isotopes (Hendry et al., 2010; Hendry and Andersen, 2013).

Firstly, it was confirmed that this new method to measure δ^{11}B and B/Si in biogenic silica is able to be utilised in sponges as well as diatoms. Secondly, the lack of contamination of sponge spicules in the sediment samples was also established from both the boron concentration and δ^{11}B. Whilst the B/Si ratios of all biogenic silica samples lay within a similar range, the boron concentration of the sponges measured was an

Classification	**Location**	**T**	**S**	**pH$_{sw}$**	**[Si(OH)$_4$]**	**δ^{30}Si**	**δ^{11}B**	**B/Si**
		°C	psu		μM	‰	‰	ppm
Mycalidae	Burdwood Bank	4.3	34.17	7.96	12	-1.01	9.00	2.73
Unidentified demosponge	Burdwood Bank	3.1	34.35	7.8	56	-1.55	14.59	1.79
Acoelocalyx	SARS Seamount	1.9	34.77	7.72	94	-2.92	11.26	1.16
Acoelocalyx	Scotia Sea	1.5	35	7.7	120	-3.76	7.56	1.23
Acoelocalyx	Scotia Sea	1.5	35	7.7	110	-3.2	10.35	1.59

Table A.1: δ^{11}B and B/Si results measured in sponge samples from the Southern Ocean compared to previous analysis from Hendry and Andersen (2013).

average of 212 ppm compared to an average boron concentration in the diatom sediment samples of 0.2 - 0.5 ppm. The principal aim of studying sponge δ^{11}B was to determine the contamination potential of the sponge spicules. Clearly this large magnitude of difference in concentration means a single sponge spicule contaminating a sediment sample would be easy to identify due to a large increase in boron concentration. The average δ^{11}B measured in sponge biogenic silica here is 10.55 $\pm$ 2.66 ‰, compared to an average δ^{11}B in the sediment diatoms of 6.06 $\pm$ 0.88 ‰. The anticipated contamination of the diatom fraction by sponge spicules would therefore be large. Given that the samples examined in Chapter 4 were optically confirmed to be free of sponge spicules, plus the large hinge such contamination would have on the measured isotope ratio, this difference strongly suggests the lack of contamination from sponge biogenic silica in these samples.

There are only a handful of studies investigating boron in biogenic silica, and the δ^{11}B data presented here contribute to a small global dataset with a previous sponge-based study by Furst (1981) and the unpublished study of de Leon (2015). Figure A1 indicates the data from these sponges fits well with previously measured data (de Leon, 2015), apart from the δ^{11}B-[Si(OH)$_4$] relationship in the two *Acoelocalyx* sponges from the Scotia Sea. The lack of correlation between δ^{11}B and pH$_{sw}$ in these sponges may stem from the different species involved in this study, but this observation was also revealed by de Leon (2015), who suggested that δ^{11}B in sponges was more closely controlled by the rate of silica precipitation due to the stronger relationship between δ^{11}B and [Si(OH)$_4$]. The addition of the new data obtained here perhaps more strongly suggests that temperature has an important role to play in sponge δ^{11}B. However, future work is clearly required to examine the δ^{11}B-pH$_{sw}$ relationship in sponges more thoroughly,

and most importantly in a culture experiment to determine an appropriate calibration (if one exists).

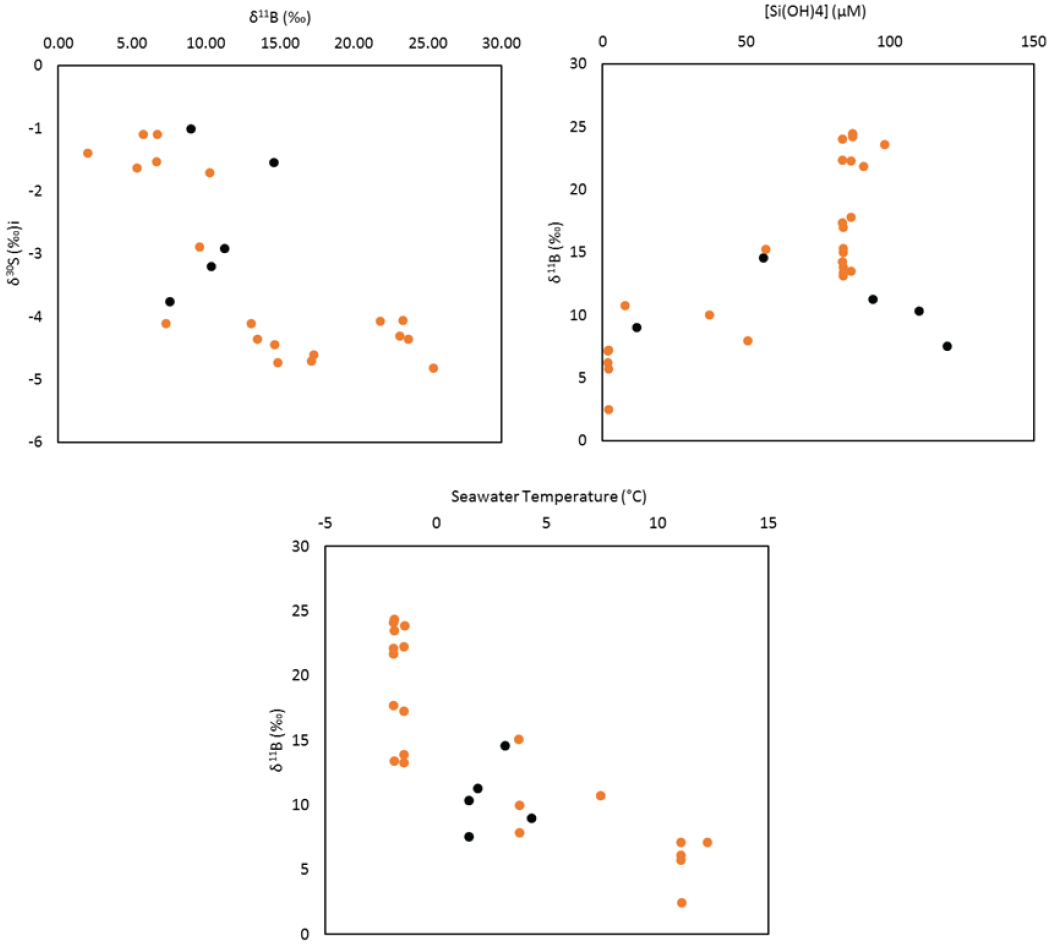

Figure A.1: Sponge data from this study (black circles) compared to a previous study (de Leon, 2015; orange circles). The data measured for this study fits well into the trends previously observed, except for two *Acoelocalyx* samples from the Scotia Sea in the δ^{11}B-[Si(OH)$_4$] relationship.

Appendix B

Chapter 5 - Supplementary material

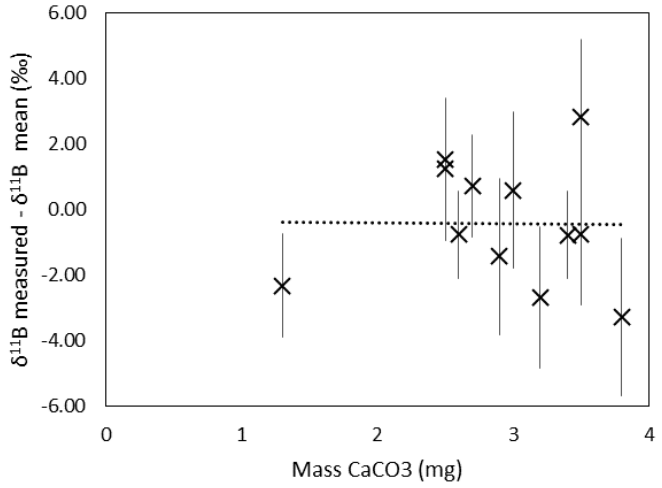

Figure B.1: Size of sample plotted against difference from mean δ^{11}B. This relationship reveals there are comparable ranges of difference between the measured δ^{11}B and the mean δ^{11}B for every pH_{sw} treatment, no matter the size of sample measured. This indicates there is no bias towards larger samples, and that δ^{11}B is unaffected by the size of the initial sample.

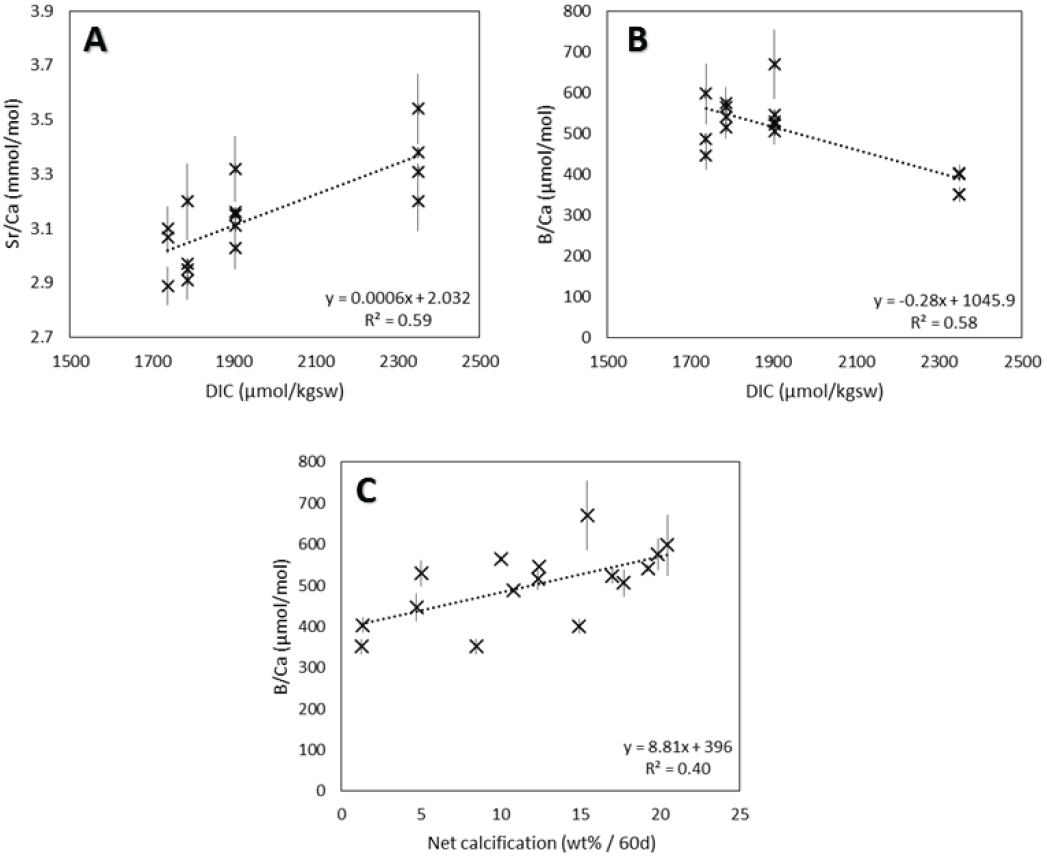

Figure B.2: Sr/Ca *vs.* DIC (A), B/Ca vs. DIC (B), and B/Ca *vs.* net calcification (C). These relationships were explored further following a recent paper investigating foraminiferal Sr/Ca as a new carbonate system proxy (Keul et al., 2017). With an enhanced DIC influx, Ω increases, and therefore Ca influx decreases, hence a positive relationship can be found between DIC and Sr/Ca. Net calcification appears to have a dominant role in determining B/Ca, as opposed to DIC determining Sr/Ca. B/Ca ratios have a strong positive correlation with net calcification, and whilst there is a negative relationship present between B/Ca and DIC, this is most likely due to typically lower calcification rates at higher DIC.

	All	**pH 8.19**	**pH 8.05**	**pH 7.91**	**pH 7.49**
Sample location	Atlantic Ocean, FL				
Number of tanks	4				
Filter rate (L/h)	600				
Irradiance (W/m^2)	426				
K_{sp}	(Mucci, 1983)				
K_1 and K_2	(Roy et al., 1993)				
Water temperature (°C)		25.0 ± 0.055	25.0 ± 0.152	25.1 ± 0.164	24.9 ± 0.130
Salinity (psu)		31.8 ± 0.207	31.7 ± 0.118	31.5 ± 0.155	31.8 ± 0.258
Ω_{arag}		3.12 ± 0.221	2.40 ± 0.420	1.84 ± 0.129	0.90 ± 0.050
DIC		1738 ± 50.35	1786 ± 100.71	1903 ± 45.91	2350 ± 33.21

Table B.1: Further details of the culture experiment from Ries et al. (2009). Values for all tanks as well as individual culture treatment tanks are shown with ± 1σ.

Parameter 1	**Parameter 2**	**Regression**	**Equation**	**R^2**	**p**
δ^{11}B	pH_{sw}	Curve	y = -30x^2 + 472x 1846	0.73	< 0.001
δ^{11}B	B/Ca	Linear	y = 0.034x + 14.8	0.77	< 0.0001
δ^{11}B	Sr/Ca	Linear	y = -10.8x + 65.6	0.33	< 0.05
pH_{cf}	pH_{sw}	Curve	y = -2.4x^2 + 38.5x 143.8	0.66	< 0.001
ΔpH	pH_{sw}	Curve	y = -2.4x^2 + 37.6x 144.3	0.46	< 0.05
Sr/Ca	pH_{sw}	Linear	y = -0.53x + 7.3	0.59	< 0.001
B/Ca	pH_{sw}	Curve	y = -833x^2 + 13258x 52173	0.72	< 0.001
Sr/Ca	B/Ca	Linear	y = -0.001x + 3.6	0.22	0.06
pH_{cf}	Calcification rate	Linear	y = 0.023x + 8.8	0.29	< 0.05
Calcification rate	pH_{sw}	Curve	y = -34x^2 + 545x 2161	0.94	< 0.0001

Table B.2: Statistical analysis of all parameters investigated in this study. Regressions, regression equations and significance values are all described in further detail.

Bibliography

Adey W. H., Halfar J. and Williams B. (2013) Biological, Physiological, and Ecological Factors Controlling Carbonate Production in an Arctic-Subarctic Climate Archive. *Smithson. Contrib. Mar. Sci.* **40**, 1-41.

Al-Ammar A. S., Gupta R. K. and Barnes R. M. (2000) Elimination of boron memory effect in inductively coupled plasma-mass spectrometry by ammonia gas injection into the spray chamber during analysis. *Spectrochim. acta, Part B At. Spectrosc.* **55**, 629-635.

Al-Horani F. A, Al-Moghrabi S. M. and De Beer D. (2003) The mechanism of calcification and its relation to photosynthesis and respiration in the scleractinian coral *Galaxea fascicularis*. *Mar. Biol.* **142**, 419-426.

Allison N. and Finch A. A. (2010) $\delta^{11}B$, Sr, Mg and B in a modern *Porites* coral: the relationship between calcification site pH and skeletal chemistry. *Geochim. Cosmochim. Acta* **74**, 1790-1800.

Del Amo Y. and Brzezinski M. A. (1999) The chemical form of dissolved Si taken up by marine diatoms. *J. Phycol.* **1170**, 1162-1170.

Anagnostou E., Huang K. F., You C. F., Sikes E. L. and Sherrell R. M. (2012) Evaluation of boron isotope ratio as a pH proxy in the deep sea coral *Desmophyllum dianthus*: Evidence of physiological pH adjustment. *Earth Planet. Sci. Lett.* **349350**, 251-260.

Anderson D. M. and Archer D. (2002) Glacialinterglacial stability of ocean pH inferred from foraminifer dissolution rates. *Nature* **416**, 70-73.

Anthony K. R. N., Kline D. I., Diaz-Pulido G., Dove S. and Hoegh-Guldberg O. (2008) Ocean acidification causes bleaching and productivity loss in coral reef builders. *Proc. Natl. Acad. Sci.* **105**, 17442-17446.

Bach L. T., Riebesell U. and Schulz K. G. (2011) Distinguishing between the effects of ocean acidification and ocean carbonation in the coccolithophore *Emiliania huxleyi*.

Limnol. Ocean. **56**, 2040-2050.

Badger M. P. S., Lear C. H., Pancost R. D., Foster G. L., Bailey T. R., Leng M. J. and Abels H. A. (2013) CO_2 drawdown following the middle Miocene expansion of the Antarctic Ice Sheet. *Paleoceanography* **28**, 42-53.

Baeuerlein E. (2000) *Biomineralization: From Biology to Biotechnology and Medical Application.*, Wiley, Weinheim.

Bailey I., Liu Q., Swann G. E. A., Jiang Z., Sun Y., Zhao X. and Roberts A. P. (2011) Iron fertilisation and biogeochemical cycles in the sub-Arctic northwest Pacific during the late Pliocene intensification of northern hemisphere glaciation. *Earth Planet. Sci. Lett.* **307**, 253-265.

Bala G. (2013) Digesting 400 ppm for global mean CO_2 concentration. *Curr. Sci.* **104**, 1471-1472.

Balan E., Pietrucci F., Gervais C., Blanchard M., Schott J. and Gaillardet J. (2016) First-principles study of boron speciation in calcite and aragonite. *Geochim. Cosmochim. Acta* **193**, 119-131.

Beaufort L., Probert I., de Garidel-Thoron T., Bendif E. M., Ruiz-Pino D., Metzl N., Goyet C., Buchet N., Coupel P., Grelaud M., Rost B., Rickaby R. E. M. and de Vargas C. (2011) Sensitivity of coccolithophores to carbonate chemistry and ocean acidification. *Nature* **476**, 80-83.

De Beer D. and Larkum A. W. D. (2001) Photosynthesis and calcification in the calcifying algae *Halimeda discoidea* studied with microsensors. *Plant, Cell Environ.* **24**, 1209-1217.

Van Bennekom A. J., Buma A. G. J. and Nolting R. F. (1991) Dissolved aluminium in the Weddell-Scotia Confluence and effect of Al on the dissolution kinetics of biogenic silica. *Mar. Chem.* **35**, 423-434.

Bickert T. (2009) Carbonate Compensation Depth. In *Encyclopedia of Paleoclimatology and Ancient Environments* (ed. V. Gornitz). Springer Netherlands, Dordrecht. pp. 136-138.

Blamart D., Rollion-Bard C., Meibom A., Cuif J. P., Juillet-Leclerc A. and Dauphin Y. (2007) Correlation of boron isotopic composition with ultrastructure in the deep-sea coral *Lophelia pertusa*: Implications for biomineralization and paleo-pH. *Geochemistry, Geophys. Geosystems* **8**, 1-11.

Böhm F., Eisenhauer A., Tang J., Dietzel M., Krabbenhft A., Kisakrek B. and Horn C. (2012) Strontium isotope fractionation of planktic foraminifera and inorganic

calcite. *Geochim. Cosmochim. Acta* **93**, 300-314.

Borowitzka M. A. (1981) Photosynthesis and calcification in the articulated coralline red algae *Amphiroa anceps* and *A. foliacea. Mar. Biol.* **62**, 17-23.

Bowes G. (1993) Facing the inevitable: Plants and increasing atmospheric CO_2. *Annu. Rev. Plant Physiol. Plant Mol. Biol.* **44**, 309-32.

Brown L., Sanders R., Savidge G. and Lucas C. H. (2003) The uptake of silica during the spring bloom in the Northeast Atlantic Ocean. *Limnol. Oceanogr.* **48**, 1831-1845.

Brown P. H., Bellaloui N., Wimmer M. A., Bassil E. S., Ruiz J., Hu H., Pfeffer H., Dannel F. and Rmheld V. (2002) Boron in plant biology. *Plant Biol.* **4**, 205-223.

Brown P. H. and Shelp B. J. (1997) Boron mobility in plants. *Physiol. Plant.* **94**, 356-361.

Brunner E., Gröger C., Lutz K., Richthammer P., Spinde K. and Sumper M. (2009) Analytical studies of silica biomineralization: towards an understanding of silica processing by diatoms. *Appl. Microbiol. Biotechnol.* **84**, 607-616.

Buitenhuis E. T., De Baar H. J. W. and Veldhuis M. J. W. (1999) Photosynthesis and calcification by *Emiliania Huxleyi* (Prymnesiophyceae) as a function of inorganic carbon species. *J. Phycol.* **35**, 949-959.

Burkhardt S., Amoroso G., Riebesell U. and Sltemeyer D. (2001) CO_2 and HCO_3^- uptake in marine diatoms acclimated to different CO_2 concentrations. *Limnol. Oceanogr.* **46**, 1378-1391.

Burkhardt S., Riebesell U. and Zondervan I. (1999) Effects of growth rate, CO_2 concentration, and cell size on the stable carbon isotope fractionation in marine phytoplankton. *Geochim. Cosmochim. Acta* **63**, 3729-3741.

Burls N. J., Fedorov A. V., Sigman D. M., Jaccard S. L., Tiedemann R. and Haug G. H. (2017) Active Pacific meridional overturning circulation (PMOC) during the warm Pliocene. *Sci. Adv.* **3**, 1-13.

Camacho-Cristóbal J. J., Rexach J. and González-Fontes A. (2008) Boron in plants: Deficiency and toxicity. *J. Integr. Plant Biol.* **50**, 1247-1255.

Castillo K. D., Ries J. B., Bruno J. F. and Westfield I. T. (2014) The reef-building coral *Siderastrea siderea* exhibits parabolic responses to ocean acidification and warming. *Proc. Biol. Sci.* **281**, 20141856-20141856.

Catanzaro E. J., Champion C. E., Garner E. L., Marinenko G., Sappenfield K. M. and

Shields W. R. (1970) *Boric Acid: Isotopic and Assay Standard Reference Materials.*, NBS (US) Special Publications, National Bureau of Standards, Institute for Materials Research, Washington, D. C.

Chen C. Y. and Durbin E. G. (1994) Effects of pH on the growth and carbon uptake of marine phytoplankton. *Mar. Ecol. Prog. Ser.* **109**, 83-94.

Cohen A. L. and McConnaughey T. A. (2003) Geochemical Perspectives on Coral Mineralization. *Rev. Mineral. Geochemistry* **54**, 151-187.

Comeau S., Carpenter R. C. and Edmunds P. J. (2012) Coral reef calcifiers buffer their response to ocean acidification using both bicarbonate and carbonate. *Proc. R. Soc. B Biol. Sci.* **280**, 20122374-20122374.

Comeau S., Edmunds P. J., Spindel N. B. and Carpenter R. C. (2013) The responses of eight coral reef calcifiers to increasing partial pressure of CO_2 do not exhibit a tipping point. *Limnol. Oceanogr.* **58**, 388-398.

Cornwall C. E., Comeau S. and Mcculloch M. T. (2017) Coralline algae elevate pH at the site of calcification under ocean acidification. *Glob. Chang. Biol.* **0**, 1-12.

Cortese G., Gersonde R., Hillenbrand C. D. and Kuhn G. (2004) Opal sedimentation shifts in the World Ocean over the last 15 Myr. *Earth Planet. Sci. Lett.* **224**, 509-527.

Cusack M., Kamenos N. A., Rollion-Bard C. and Tricot G. (2015) Red coralline algae assessed as marine pH proxies using ^{11}B MAS NMR. *Sci. Rep.* **5**, 8175.

Daniels C. J., Tyrrell T., Poulton A. J. and Pettit L. (2012) The influence of lithogenic material on particulate inorganic carbon measurements of coccolithophores in the Bay of Biscay. *Limnol. Oceanogr.* **57**, 145-153.

De'ath G., Lough J. M. and Fabricius K. E. (2009) Declining coral calcification on the Great Barrier Reef. *Science.* **323**, 116-119.

Dickson A. G. (1990) Thermodynamics of the dissociation of boric acid in synthetic seawater from 273.15 to 318.15 K. *Deep Sea Res.* **37**, 755-766.

Dodd L. F., Grabowski J. H., Piehler M. F., Westfield I. and Ries J. B. (2015) Ocean acidification impairs crab foraging behaviour. *Proc. Biol. Sci.* **282**, 20150333.

Doney S. C., Fabry V. J., Feely R. A. and Kleypas J. A. (2009) Ocean Acidification: The Other CO_2 Problem. *Ann. Rev. Mar. Sci.* **1**, 169-192.

Dordas C. and Brown P. H. (2000) Permeability of boric acid across lipid bilayers and

factors affecting it. *J. Membr. Biol.* **175**, 95-105.

Douville E., Paterne M., Cabioch G., Louvat P., Gaillardet J., Juillet-Leclerc A. and Ayliffe L. (2010) Abrupt sea surface pH change at the end of the Younger Dryas in the central sub-equatorial Pacific inferred from boron isotope abundance in corals *(Porites). Biogeosciences* **7**, 2445-2459.

Dove P. M., Han N., Wallace A. F. and De Yoreo J. J. (2008) Kinetics of amorphous silica dissolution and the paradox of the silica polymorphs. *Proc. Natl. Acad. Sci. U. S. A.* **105**, 9903-9908.

Dutkiewicz S., Follows M. J. and Bragg J. G. (2009) Modeling the coupling of ocean ecology and biogeochemistry. *Global Biogeochem. Cycles* **23**, 1-15.

Dutkiewicz S., Hickman A. E., Jahn O., Gregg W. W., Mouw C. B. and Follows M. J. (2015) Capturing optically important constituents and properties in a marine biogeochemical and ecosystem model. *Biogeosciences* **12**, 4447-4481.

Egan K. E., Rickaby R. E. M., Leng M. J., Hendry K. R., Hermoso M., Sloane H. J., Bostock H. and Halliday A. N. (2012) Diatom silicon isotopes as a proxy for silicic acid utilisation: A Southern Ocean core top calibration. *Geochim. Cosmochim. Acta* **96**, 174-192.

Enochs I. C., Manzello D. P., Donham E. M., Kolodziej G., Okano R., Johnston L., Young C., Iguel J., Edwards C. B., Fox M. D., Valentino L., Johnson S., Benavente D., Clark S. J., Carlton R., Burton T., Eynaud Y. and Price N. N. (2015) Shift from coral to macroalgae dominance on a volcanically acidified reef. *Nat. Clim. Chang.*, 1-9.

Erez J. (2003) The source of ions for biomineralization in foraminifera and their implications for paleoceanographic proxies. *Rev. Mineral. Geochemistry* **54**, 115-149.

Exley C. (1998) Silicon in life: A bioinorganic solution to bioorganic essentiality. *J. Inorg. Biochem.* **69**, 139-144.

Exley C. and Sjberg S. (2014) Silicon species in seawater. *Spectrochim. Acta. A. Mol. Biomol. Spectrosc.* **117**, 820-821.

Fietzke J., Ragazzola F., Halfar J., Dietze H., Foster L. C., Hansteen T. H., Eisenhauer A. and Steneck R. S. (2015) Century-scale trends and seasonality in pH and temperature for shallow zones of the Bering Sea. *Proc. Natl. Acad. Sci.* **112**, 2960-2965.

Fischer H., Schmitt J., Lüthi D., Stocker T. F., Tschumi T., Parekh P., Joos F., Köhler P., Vlker C., Gersonde R., Barbante C., Le Floch M., Raynaud D. and Wolff E. (2010) The role of Southern Ocean processes in orbital and millennial CO_2 variations - A synthesis. *Quat. Sci. Rev.* **29**, 193-205.

Foster G. L. (2008) Seawater pH, pCO_2 and $[CO_3]^{2-}$ variations in the Caribbean Sea over the last 130 kyr: A boron isotope and B/Ca study of planktic foraminifera. *Earth Planet. Sci. Lett.* **271**, 254-266.

Foster G. L., Hnisch B., Paris G., Dwyer G. S., Rae J. W. B., Elliott T., Gaillardet J., Hemming N. G., Louvat P. and Vengosh A. (2013) Interlaboratory comparison of boron isotope analyses of boric acid, seawater and marine $CaCO_3$ by MC-ICPMS and NTIMS. *Chem. Geol.* **358**, 1-14.

Foster G. L., Lécuyer C. and Marschall H. R. (2016) *Encyclopedia of Geochemistry - Boron Stable Isotopes.* ed. W. M. White, Springer International Publishing AG.

Foster G. L., Pogge von Strandmann P. A. E. and Rae J. W. B. (2010) Boron and magnesium isotopic composition of seawater. *Geochemistry, Geophys. Geosystems* **11**, 1-10.

Foster G. L. and Rae J. W. B. (2016) Reconstructing ocean pH with boron isotopes in foraminifera. *Annu. Rev. Earth Planet. Sci.* **44**, 207-237.

Foster G. L. and Sexton P. F. (2014) Enhanced carbon dioxide outgassing from the eastern equatorial Atlantic during the last glacial. *Geology* **42**, 1003-1006.

Freiwald A., Fossa J. H., Grehan A., Koslow T. and Roberts J. M. (2004) Cold-water coral reefs out of sight - no longer out of mind. *Environment* **22**, 84.

Furst M. J. (1981) Boron in siliceous materials as a paleosalinity indicator. *Geochim. Cosmochim. Acta* **45**, 1-13.

Gabitov R. I., Rollion-Bard C., Tripati A. and Sadekov A. (2014) In situ study of boron partitioning between calcite and fluid at different crystal growth rates. *Geochim. Cosmochim. Acta* **137**, 81-92.

Gaetani G. A. and Cohen A. L. (2006) Element partitioning during precipitation of aragonite from seawater: A framework for understanding paleoproxies. *Geochim. Cosmochim. Acta* **70**, 4617-4634.

Gagnon A. C., Adkins J. F. and Erez J. (2012) Seawater transport during coral biomineralization. *Earth Planet. Sci. Lett.* **329-330**, 150-161.

Gagnon A. C., Adkins J. F., Fernandez D. P. and Robinson L. F. (2007) Sr/Ca and Mg/Ca vital effects correlated with skeletal architecture in a scleractinian deep-sea coral and the role of Rayleigh fractionation. *Earth Planet. Sci. Lett.* **261**, 280-295.

Gaillardet J. and Allgre C. J. (1995) Boron isotopic compositions of corals: Seawater or

diagenesis record? *EPSL* **136**, 665-676.

Gao K., Aruga Y., Asada K., Ishihara T., Akano T. and Kiyohara M. (1993) Calcification in the articulated coralline alga *Corallina pilulifera*, with special reference to the effect of elevated CO_2 concentration. *Mar. Biol.* **117**, 129-132.

Gao K. and Campbell D. A. (2014) Photophysiological responses of marine diatoms to elevated CO_2 and decreased pH: a review. *Funct. Plant Biol.* **41**, 449-459.

Gao K. and Zheng Y. (2009) Combined effects of ocean acidification and solar UV radiation on photosynthesis, growth, pigmentation and calcification of the coralline alga *Corallina sessilis* (Rhodophyta). *Glob. Chang. Biol.* **16**, 2388-2398.

Gattuso J.-P., Magnan A., Bille R., Cheung W. W. L., Howes E. L., Joos F., Allemand D., Bopp L., Cooley S. R., Eakin C. M., Hoegh-Guldberg O., Kelly R. P., Portner H.-O., Rogers a. D., Baxter J. M., Laffoley D., Osborn D., Rankovic A., Rochette J., Sumaila U. R., Treyer S. and Turley C. (2015) Contrasting futures for ocean and society from different anthropogenic CO_2 emissions scenarios. *Science* **349**, 4722-1-4722-10.

Gattuso J. P., Frankignoulle M., Bourge I., Romaine S. and Buddemeier R. W. (1998) Effect of calcium carbonate saturation of seawater on coral calcification. *Glob. Planet. Change* **18**, 37-46.

Gehlen M., Beck L., Calas G., Flank A. M., Van Bennekom A. J. and Van Beusekom J. E. E. (2002) Unraveling the atomic structure of biogenic silica: Evidence of the structural association of Al and Si in diatom frustules. *Geochim. Cosmochim. Acta* **66**, 1601-1609.

Goldbach H. E. and Wimmer M. A. (2007) Boron in plants and animals: Is there a role beyond cell-wall structure? *J. Plant Nutr. Soil Sci.* **170**, 39-48.

Goldbach H. E., Yu Q., Wingender R., Schulz M., Wimmer M., Findeklee P. and Baluka F. (2001) Rapid response reactions of roots to boron deprivation. *J. Plant Nutr. Soil Sci.* **164**, 173-181.

Grasshoff K., Ehrhardt M. and Kremling K. (1983) *Methods of Seawater Analysis.* 2nd editio. ed. G. Giesler, Verlag Chemie GmbH, Basel.

Greenop R., Hain M. P., Sosdian S. M., Oliver K. I. C., Goodwin P., Chalk T. B., Lear C. H., Wilson P. A. and Foster G. L. (2017) A record of Neogene seawater $\delta^{11}B$ reconstructed from paired $\delta^{11}B$ analyses on benthic and planktic foraminifera. *Clim. Past* **13**, 149-170.

Hall-Spencer J. M., Rodolfo-Metalpa R., Martin S., Ransome E., Fine M., Turner S. M., Rowley S. J., Tedesco D. and Buia M.-C. (2008) Volcanic carbon dioxide vents

show ecosystem effects of ocean acidification. *Nature* **454**, 96-99.

Hammad D. M. and Ibrahim L. A. (2012) Influence of iron and silicon speciation on the abundance of diatoms in River Nile. *J. Appl. Sci. Res.* **8**, 556-570.

Haug G. H., Ganopolski A., Sigman D. M., Rosell-Mele A., Swann G. E. A, Tiedemann R., Jaccard S. L., Bollmann J., Maslin M. A, Leng M. J. and Eglinton G. (2005) North Pacific seasonality and the glaciation of North America 2.7 million years ago. *Nature* **433**, 821-825.

Haug G. H., Sigman D. M., Tiedemann R., Pedersen T. F. and Sarntheink M. (1999) Onset of permanent stratification in the subarctic Pacific Ocean. *Nature* **401**, 21-24.

Hemming N. G. and Hanson G. N. (1994) A procedure for the isotopic analysis of boron by negative thermal ionization mass-spectrometry. *Chem. Geol.* **114**, 147-156.

Hemming N. G. and Hanson G. N. (1992) Boron isotopic composition and concentration in modern marine carbonates. *Geochim. Cosmochim. Acta* **56**, 537-543.

Hemming N. G., Reeder R. J. and Hart S. R. (1998) Growth-step-selective incorporation of boron on the calcite surface. *Geochim. Cosmochim. Acta* **62**, 2915-2922.

Hendry K. R. and Andersen M. B. (2013) The zinc isotopic composition of siliceous marine sponges: Investigating nature's sediment traps. *Chem. Geol.* **354**, 33-41.

Hendry K. R., Bastian Georg R., Rickaby R. E. M., Robinson L. F. and Halliday A. N. (2010) Deep ocean nutrients during the Last Glacial Maximum deduced from sponge silicon isotopic compositions. *Earth Planet. Sci. Lett.* **292**, 290-300.

Hendry K. R. and Brzezinski M. A. (2014) Using silicon isotopes to understand the role of the Southern Ocean in modern and ancient biogeochemistry and climate. *Quat. Sci. Rev.* **89**, 13-26.

Hendry K. R., Robinson L. F., McManus J. F. and Hays J. D. (2014) Silicon isotopes indicate enhanced carbon efficiency in the North Atlantic during deglaciation. *Nat. Commun.* **5**, 3107.

Henehan M. J., Foster G. L., Rae J. W. B., Prentice K. C., Erez J., Bostock H. C., Marshall B. J. and Wilson P. A. (2015) Evaluating the utility of B/Ca ratios in planktic foraminifera as a proxy for the carbonate system: A case study of *Globigerinoides ruber. Geochemistry, Geophys. Geosystems,* 1052-1069.

Henehan M. J., Rae J. W. B., Foster G. L., Erez J., Prentice K. C., Kucera M., Bostock H. C., Martínez-Botí M. A., Milton J. A., Wilson P. A., Marshall B. J. and Elliott

T. (2013) Calibration of the boron isotope proxy in the planktonic foraminifera *Globigerinoides ruber* for use in palaeo-CO_2 reconstruction. *Earth Planet. Sci. Lett.* **364**, 111-122.

Hervé V., Derr J., Douady S., Quinet M., Moisan L. and Lopez P. J. (2012) Multiparametric analyses reveal the pH-dependence of silicon biomineralization in diatoms. *PLoS One* **7**, 1-12.

Van Heuven S., Pierrot D., Rae J. W. B., Lewis E. and Wallace D. W. R. (2011) MATLAB program developed for CO_2 system calculations. ORNL/CDIAC-105b.

Hillenbrand C. D. and Cortese G. (2006) Polar stratification: A critical view from the Southern Ocean. *Palaeogeogr. Palaeoclimatol. Palaeoecol.* **242**, 240-252.

Hoegh-Guldberg O., Mumby P. J., Hooten A. J., Steneck R. S., Greenfield P., Gomez E., Harvell C. D., Sale P. F., Edwards a J., Caldeira K., Knowlton N., Eakin C. M., Iglesias-Prieto R., Muthiga N., Bradbury R. H., Dubi A. and Hatziolos M. E. (2007) Coral reefs under rapid climate change and ocean acidification. *Science* **318**, 1737-1742.

Holcomb M., Venn A. A., Tambutt E., Tambutté S., Allemand D., Trotter J. and McCulloch M. (2014) Coral calcifying fluid pH dictates response to ocean acidification. *Sci. Rep.* **4**, 1-4.

Hönisch B. and Hemming N. G. (2004) Ground-truthing the boron isotope-paleo-pH proxy in planktonic foraminifera shells: Partial dissolution and shell size effects. *Paleoceanography* **19**, 1-13.

Hönisch B. and Hemming N. G. (2005) Surface ocean pH response to variations in pCO_2 through two full glacial cycles. *Earth Planet. Sci. Lett.* **236**, 305-314.

Hönisch B., Hemming N. G., Archer D., Siddall M. and McManus J. F. (2009) Atmospheric carbon dioxide concentration across the Mid-Pleistocene Transition. *Science* **324**, 1551-1554.

Hönisch B., Hemming N. G., Grottoli A. G., Amat A., Hanson G. N. and Bijma J. (2004) Assessing scleractinian corals as recorders for paleo-pH: Empirical calibration and vital effects. *Geochim. Cosmochim. Acta* **68**, 3675-3685.

Hopkinson B. M., Dupont C. L., Allen A. E. and Morel F. M. M. (2011) Efficiency of the CO_2-concentrating mechanism of diatoms. *PNAS* **108**, 3830-3837.

Horn M. G., Robinson R. S., Rynearson T. A. and Sigman D. M. (2011) Nitrogen isotopic relationship between diatom-bound and bulk organic matter of cultured polar diatoms. *Paleoceanography* **26**, 1-12.

Huergo L. F., Chandra G. and Merrick M. (2013) PII signal transduction proteins: Nitrogen regulation and beyond. *FEMS Microbiol. Rev.* **37**, 251-283.

Hurd C. L., Cornwall C. E., Currie K., Hepburn C. D., McGraw C. M., Hunter K. A. and Boyd P. W. (2011) Metabolically induced pH fluctuations by some coastal calcifiers exceed projected 22nd century ocean acidification: a mechanism for differential susceptibility? *Glob. Chang. Biol.* **17**, 3254-3262.

Hydes D. J. (1979) Aluminium in seawater: Control by inorganic processes. *Science* **4412**, 1260-1262.

Ishikawa T. and Nakamura E. (1993) Boron isotope systematics of marine sediments. *Earth Planet. Sci. Lett.* **117**, 567-580.

Isshiki K., Sohrin Y. and Nakayama E. (1991) Form of dissolved silicon in seawater. *Mar. Chem.* **32**, 1-8.

Jaccard S. L. (2005) Glacial/Interglacial Changes in Subarctic North Pacific Stratification. *Science* **308**, 1003-1006.

Kamenos N. A., Perna G., Gambi M. C., Micheli F. and Kroeker K. J. (2016) Coralline algae in a naturally acidified ecosystem persist by maintaining control of skeletal mineralogy and size. *Proc. R. Soc. B* **283**, 20161159.

Kasemann S. A., Schmidt D. N., Bijma J. and Foster G. L. (2009) In situ boron isotope analysis in marine carbonates and its application for foraminifera and palaeo-pH. *Chem. Geol.* **260**, 138-147.

Keller M. D., Selvin R. C., Claus W. and Guillard R. R. L. (1987) Media for the culture of oceanic ultraphytoplankton. *J. Phycol.* **23**, 633-638.

Keul N., Langer G., Thoms S., de Nooijer L. J., Reichart G. J. and Bijma J. (2017) Exploring foraminiferal Sr/Ca as a new carbonate system proxy. *Geochim. Cosmochim. Acta* **202**, 374-386.

Kiss E. (1988) Ion-exchange separation and spectrophotometric determination of boron in geological materials. *Anal. Chim. Acta* **211**, 243-256.

Klochko K., Cody G. D., Tossell J. A., Dera P. and Kaufman A. J. (2009) Re-evaluating boron speciation in biogenic calcite and aragonite using ^{11}B MAS NMR. *Geochim. Cosmochim. Acta* **73**, 1890-1900.

Klochko K., Kaufman A. J., Yao W., Byrne R. H. and Tossell J. A. (2006) Experimental measurement of boron isotope fractionation in seawater. *Earth Planet. Sci. Lett.* **248**, 276-285.

Krief S., Hendy E. J., Fine M., Yam R., Meibom A., Foster G. L. and Shemesh A. (2010) Physiological and isotopic responses of scleractinian corals to ocean acidification. *Geochim. Cosmochim. Acta* **74**, 4988-5001.

Kroger N. and Poulsen N. (2008) Diatoms - from cell wall biogenesis to nanotechnology. *Annu. Rev. Genet.* **42**, 83-107.

Kuffner I. B., Andersson A. J., Jokiel P. L., Rodgers K. S. and Mackenzie F. T. (2008) Decreased abundance of crustose coralline algae due to ocean acidification. *Nat. Geosci.* **1**, 114-117.

De La Rocha C. L. (2006) Opal-based isotopic proxies of paleoenvironmental conditions. *Global Biogeochem. Cycles* **20**, 1-11.

De La Rocha C. L., Brzezinski M. A., DeNiro M. J. and Shemesh A. (1998) Silicon-isotope composition of diatoms as an indicator of past oceanic change. *Nature* **395**, 680-683.

Lécuyer C., Grandjean P., Reynard B., Albaréde F. and Telouk P. (2002) $^{11}B/^{10}B$ analysis of geological materials by ICP-MS plasma 54: Application to the boron fractionation between brachiopod calcite and seawater. *Chem. Geol.* **186**, 45-55.

Lee K., Kim T.-W., Byrne R. H., Millero F. J., Feely R. A. and Liu Y.-M. (2010) The universal ratio of boron to chlorinity for the North Pacific and North Atlantic oceans. *Geochim. Cosmochim. Acta* **74**, 1801-1811.

Lemarchand D., Gaillardet J., Gopel C. and Manhes G. (2002) An optimized procedure for boron separation and mass spectrometry analysis for river samples. *Chem. Geol.*, **182**, 323-334.

Leng M. J. and Swann G. (2010) Stable Isotopes from diatom silica. *Diatoms Appl. Environ. earth Sci.*, **1**, 127-143.

Leng M. J., Swann G. E. A., Hodson M. J., Tyler J. J., Patwardhan S. V. and Sloane H. J. (2009) The potential use of silicon isotope composition of biogenic silica as a proxy for environmental change. *Silicon* **1**, 65-77.

de Leon A. (2015) The Boron Geochemistry of Biogenic Silica: Insights from Marine Sponges and Diatoms. *Thesis, unpublished*

Li F., Wu Y., Hutchins D. A., Fu F. and Gao K. (2016) Physiological responses of coastal and oceanic diatoms to diurnal fluctuations in seawater carbonate chemistry under two CO_2 concentrations. *Biogeosciences* **13**, 6247-6259.

Loucaides S., Van Cappellen P. and Behrends T. (2008) Dissolution of biogenic silica from land to ocean: Role of salinity and pH. *Limnol. Oceanogr.* **53**, 1614-1621.

Lueker T. J., Dickson A. G. and Keeling C. D. (2000) Ocean pCO_2 calculated from dissolved inorganic carbon, alkalinity, and equations for K1 and K2: Validation based on laboratory measurements of CO_2 in gas and seawater at equilibrium. *Mar. Chem.* **70**, 105-119.

Mackinder L., Wheeler G., Schroeder D., Riebesell U. and Brownlee C. (2010) Molecular mechanisms underlying calcification in coccolithophores. *Geomicrobiol. J.* **27**, 585-595.

Marschner H. (1995) *Mineral Nutrition of Higher Plants.* 2nd edn., Academic Press, San Diego, CA.

Martin J. H. (1990) Glacial-interglacial CO_2 change: the iron hypothesis. *Paleoceanography* **5**, 1-13.

Martin S., Charnoz A. and Gattuso J.-P. (2013) Photosynthesis, respiration and calcification in the Mediterranean crustose coralline alga *Lithophyllum cabiochae* (Corallinales, Rhodophyta). *Eur. J. Phycol.* **48**, 163-172.

Martin S. and Gattuso J.-P. (2009) Response of Mediterranean coralline algae to ocean acidification and elevated temperature. *Glob. Chang. Biol.* **15**, 2089-2100.

Martínez-Botí M. A., Foster G. L., Chalk T. B., Rohling E. J., Sexton P. F., Lunt D. J., Pancost R. D., Badger M. P. S. and Schmidt D. N. (2015) Plio-Pleistocene climate sensitivity evaluated using high-resolution CO_2 records. *Nature* **518**, 49-54.

Maslin M. A., Haug G. H., Sarnthein M., Tiedemann R., Erlenkeuser H. and Stax R. (1995) Northwest Pacific Site 882: the initiation of Northern Hemisphere Glaciation. *Proc. Ocean Drill. Program, Sci. Results*, **145**, 315-329.

Mavromatis V., Montouillout V., Noireaux J., Gaillardet J. and Schott J. (2015) Characterization of boron incorporation and speciation in calcite and aragonite from co-precipitation experiments under controlled pH, temperature and precipitation rate. *Geochim. Cosmochim. Acta* **150**, 299-313.

McConnaughey T. A. and Falk R. H. (1991) Calcium-proton exchange during algal calcification. *Biol. Bull.* **180**, 185-195.

McCoy S. J. and Kamenos N. A. (2015) Coralline algae (Rhodophyta) in a changing world: integrating ecological, physiological, and geochemical responses to global change. *J. Phycol.* **51**, 6-24.

McCulloch M., Falter J., Trotter J. and Montagna P. (2012a) Coral resilience to ocean acidification and global warming through pH up-regulation. *Nat. Clim. Chang.* **2**, 623-627.

McCulloch M., Trotter J., Montagna P., Falter J., Dunbar R., Freiwald A., Frsterra G., Lpez Correa M., Maier C., Rggeberg A. and Taviani M. (2012) Resilience of cold-water scleractinian corals to ocean acidification: Boron isotopic systematics of pH and saturation state up-regulation. *Geochim. Cosmochim. Acta* **87**, 21-34.

Mejía L. M., Isensee K., Méndez-Vicente A., Pisonero J., Shimizu N., González C., Monteleone B. and Stoll H. (2013) B content and Si/C ratios from cultured diatoms (*Thalassiosira pseudonana* and *Thalassiosira weissflogii*): Relationship to seawater pH and diatom carbon acquisition. *Geochim. Cosmochim. Acta* **123**, 322-337.

Miklasz K. A. and Denny M. W. (2010) Diatom sinkings speeds: Improved predictions and insight from a modified Stokes law. *Limnol. Oceanogr.* **55**, 2513-2525.

Montagnes D. J. S. and Franklin M. (2001) Effect of temperature on diatom volume, growth rate, and carbon and nitrogen content: Reconsidering some paradigms. *Limnol. Oceanogr.* **46**, 2008-2018.

Morley D. W., Leng M. J., Mackay A. W., Sloane H. J., Rioual P. and Battarbee R. W. (2004) Cleaning of lake sediment samples for diatom oxygen isotope analysis. *J. Paleolimnol.* **31**, 391-401.

Mucci A. (1983) The solubility of calcite and aragonite in seawater at various salinities, temperatures and one atmosphere total pressure. *Am. J. Sci.* **283**, 780-799.

Nakajima K., Tanaka A. and Matsuda Y. (2013) SLC4 family transporters in a marine diatom directly pump bicarbonate from seawater. *PNAS* **110**, 1767-1772.

Nelson D. M., Tréguer P., Brzezinski M. A., Leynaert A. and Quéguiner B. (1995) Production and dissolution of biogenic silica in the ocean: Revised global estimates, comparison with regional data and relationship to biogenic sedimentation. *Global Biogeochem. Cycles* **9**, 359-372.

Ni Y., Foster G. L. and Elliott T. (2010) The accuracy of $\delta^{11}B$ measurements of foraminifers. *Chem. Geol.* **274**, 187-195.

Nir O., Vengosh A., Harkness J. S., Dwyer G. S. and Lahav O. (2015) Direct measurement of the boron isotope fractionation factor: Reducing the uncertainty in reconstructing ocean paleo-pH. *Earth Planet. Sci. Lett.* **414**, 1-5.

Noireaux J., Mavromatis V., Gaillardet J., Schott J., Montouillout V., Louvat P., Rollion-Bard C. and Neuville D. R. (2015) Crystallographic control on the boron

isotope paleo-pH proxy. *Earth Planet. Sci. Lett.* **430**, 398-407.

de Nooijer L. J., Spero H. J., Erez J., Bijma J. and Reichart G. J. (2014) Biomineralization in perforate foraminifera. *Earth-Science Rev.* **135**, 48-58.

Oberhammer H. and James E. (1980) Importance of (p-d)pi-bonding in the siloxane bond. *J. Am. Chem. Soc.* **102**, 7241-7244.

Orr J. C., Fabry V. J., Aumont O., Bopp L., Doney S. C., Feely R. M., Gnanadesikan A., Gruber N., Ishida A., Key R. M., Lindsay K., Maier-reimer E., Matear R., Monfray P., Mouchet A., Najjar R. G., Plattner G. K., Rodgers K. B., Sabine C. L., Sarmiento J. L., Schlitzer R., Slater R. D., Totterdell I. J., Weirig M. F., Yamanaka Y., Yool A. and Matear R. (2005) Anthropogenic decline in high-latitude ocean carbonate by 2100. *Nature* **437**, 681-686.

Otzen D. (2012) The Role of Proteins in Biosilification. *Scientifica (Cairo)*, **2012**, 1-22.

Pagani M., Lemarchand D., Spivack A. and Gaillardet J. (2005) A critical evaluation of the boron isotope-pH proxy: The accuracy of ancient ocean pH estimates. *Geochim. Cosmochim. Acta* **69**, 953-961.

Palmer M. R. (1998) Reconstructing past ocean pH-depth profiles. *Science* **282**, 1468-1471.

Pamirsky I. E. and Golokhvast K. S. (2013) Silaffins of diatoms: from applied biotechnology to biomedicine. *Mar. Drugs* **11**, 3155-3167.

Passow U. and Laws E. A. (2015) Ocean acidification as one of multiple stressors: Growth response of *Thalassiosira weissflogii* (diatom) under temperature and light stress. *Mar. Ecol. Prog. Ser.* **541**, 75-90.

Pauly M., Kamenos N. A., Donohue P. and LeDrew E. (2015) Coralline algal Mg-O bond strength as a marine pCO_2 proxy. *Geology* **43**, 267-270.

Pearson P. N. and Palmer M. R. (2000) Atmospheric carbon dioxide concentrations over the past 60 million years. *Nature* **406**, 695-699.

Pfeffer H., Dannel F. and Rmheld V. (2001) Boron compartmentation in roots of sunflower plants of different boron status: A study using the stable isotopes ^{10}B and ^{11}11B adopting two independent approaches. *Physiol. Plant.* **113**, 346-351.

Rae J. W. B., Foster G. L., Schmidt D. N. and Elliott T. (2011) Boron isotopes and B/Ca in benthic foraminifera: Proxies for the deep ocean carbonate system. *Earth Planet. Sci. Lett.* **302**, 403-413.

Rae J. W. B., Sarnthein M., Foster G. L., Ridgewell A., Grootes P. M. and Elliott T. (2014) Deep water formation in the North Pacific and deglacial CO_2 rise. *Paleoceanography* **29**, 1-23.

Ragazzola F., Foster L. C., Form A., Anderson P. S. L., Hansteen T. H. and Fietzke J. (2012) Ocean acidification weakens the structural integrity of coralline algae. *Glob. Chang. Biol.* **18**, 2804-2812.

Ramakumar K. L., Parab A. R., Khodade P. S., Almaula A. I., Chitambar S. A. and Jain H. C. (1985) Determination of isotopic composition of boron. *J. Radioanal. Nucl. Chem.* **94**, 53-62.

Raven J. A. (1980) Short-and long-distance transport of boric acid in plants. *Snv Phytol* **84**, 231-249.

Reynaud S., Hemming N. G., Juillet-Leclerc A. and Gattuso J. P. (2004) Effect of pCO_2 and temperature on the boron isotopic composition of the zooxanthellate coral *Acropora* sp. *Coral Reefs* **23**, 539-546.

Reynolds B. C., Frank M. and Halliday A. N. (2008) Evidence for a major change in silicon cycling in the subarctic North Pacific at 2.73 Ma. *Paleoceanography* **23**, 1-10.

Richthammer P., Brmel M., Brunner E. and van Pée K.-H. (2011) Biomineralization in diatoms: the role of silacidins. *Chembiochem* **12**, 1362-1366.

Riebesell U., Wolf-Gladrow D. A. and Smetacek V. (1993) Carbon dioxide limitation of marine phytoplankton growth rates. *Nature* **361**, 249-251.

Riebesell U., Zondervan I., Rost B., Tortell P. D., Zeebe R. E. and Morel F. M. (2000) Reduced calcification of marine plankton in response to increased atmospheric CO_2. *Nature* **407**, 364-7.

Ries J. B. (2011a) A physicochemical framework for interpreting the biological calcification response to CO_2-induced ocean acidification. *Geochim. Cosmochim. Acta* **75**, 4053-4064.

Ries J. B. (2009) Effects of secular variation in seawater Mg/Ca ratio (calcite-aragonite seas) on $CaCO_3$ sediment production by the calcareous algae *Halimeda, Penicillus* and *Udotea* - Evidence from recent experiments and the geological record. *Terra Nov.* **21**, 323-339.

Ries J. B. (2011b) Skeletal mineralogy in a high-CO_2 world. *J. Exp. Mar. Bio. Ecol.* **403**, 54-64.

Ries J. B., Cohen A. L. and McCorkle D. C. (2009) Marine calcifiers exhibit mixed

responses to CO_2-induced ocean acidification. *Geology* **37**, 1131-1134.

Ries J. B., Ghazaleh M. N., Connolly B., Westfield I. and Castillo K. D. (2016) Impacts of seawater saturation state and temperature on the dissolution kinetics of whole-shell biogenic carbonates. *Geochim. Cosmochim. Acta* **192**, 318-337.

Rodolfo-Metalpa R., Houlbrque F., Tambutté É., Boisson F., Baggini C., Patti F. P., Jeffree R., Fine M., Foggo A., Gattuso J.-P. and Hall-Spencer J. M. (2011) Coral and mollusc resistance to ocean acidification adversely affected by warming. Nat. Clim. Chang. 1, 308-312.

Roleda M. Y., Cornwall C. E., Feng Y., McGraw C. M., Smith A. M. and Hurd C. L. (2015) Effect of ocean acidification and ph fluctuations on the growth and development of coralline algal recruits, and an associated benthic algal assemblage. *PLoS One* **10**, e0140394.

Rollion-Bard C., Blamart D., Trebosc J., Tricot G., Mussi A. and Cuif J. P. (2011) Boron isotopes as pH proxy: A new look at boron speciation in deep-sea corals using ^{11}B MAS NMR and EELS. *Geochim. Cosmochim. Acta* **75**, 1003-1012.

Rollion-Bard C., Chaussidon M. and France-Lanord C. (2003) pH control on oxygen isotopic composition of symbiotic corals. *Earth Planet. Sci. Lett.* **215**, 275-288.

Roy R. N., Roy L. N., Vogel K. M., Portermoore C., Pearson T., Good C. E., Millero F. J. and Campbell D. M. (1993) The dissociation constants of carbonic acid in seawater at salinities 5 to 45 and temperatures 0 degrees C to 45 degrees C. *Mar. Chem.* **44**, 249-267.

Sabine C. L., Mackenzie F. T., Winn C. and Karl D. M. (1995) Geochemistry of carbon dioxide in seawater at the Hawaii Ocean Time Series Station, ALOHA. *Global Biogeochem. Cycles* **9**, 637-651.

Sanyal A., Bijma J., Spero H. and Lea D. W. (2001) Empirical relationships between pH and the boron isotopic composition of Gloigerinoides sacculifer: Implications for the boron isotope paleo-pH proxy. Paleoceanography 16, 515-519.

Sanyal A., Hemming N. G., Broecker W. S., Lea D. W., Spero H. J. and Hanson G. N. (1996) Oceanic pH control on the boron isotopic composition of foraminifera: Evidence from culture experiments. *Paleoceanography* **11**, 513-517.

Sanyal A., Nugent M., Reeder R. J. and Bijma J. (2000) Seawater pH control on the boron isotopic composition of calcite: Evidence from inorganic calcite precipitation experiments. *Geochim. Cosmochim. Acta* **64**, 1551-1555.

Semesi I. S., Kangwe J. and Bjrk M. (2009) Alterations in seawater pH and CO_2 affect calcification and photosynthesis in the tropical coralline alga, *Hydrolithon* sp.

(Rhodophyta). *Estuar. Coast. Shelf Sci.* **84**, 337-341.

Sigman D. M. and Boyle E. A. (2000) Glacial/interglacial variations in atmospheric carbon dioxide. *Nature* **407**, 859-869.

Sigman D. M., Hain M. P. and Haug G. H. (2010) The polar ocean and glacial cycles in atmospheric CO_2 concentration. *Nature* **466**, 47-55.

Sigman D. M., Jaccard S. L. and Haug G. H. (2004) Polar ocean stratification in a cold climate. *Nature* **428**, 59-63.

Smetacek V. (1999) Diatoms and the Ocean Carbon Cycle. *Protist* **150**, 25-32.

Smith A. D. and Roth A. A. (1979) Effect of carbon dioxide concentration on calcification in the red coralline alga *Bossiella orbigniana*. *Mar. Biol.* **52**, 217-225.

Spivack A. J., You C.-F. and Smith H. J. (1993) Foraminiferal boron isotope ratios as a proxy for surface ocean pH over the past 21 Myr. *Nature* **363**, 149-151.

Stewart J. A., Anagnostou E. and Foster G. L. (2016) An improved boron isotope pH proxy calibration for the deep-sea coral *Desmophyllum dianthus* through subsampling of fibrous aragonite. *Chem. Geol.* **447**, 148-160.

Stoffyn M. (1979) Biological control of dissolved aluminium in seawater: experimental evidence. *Science* **203**, 651-653.

Stoll H., Langer G., Shimizu N. and Kanamaru K. (2012) B/Ca in coccoliths and relationship to calcification vesicle pH and dissolved inorganic carbon concentrations. *Geochim. Cosmochim. Acta* **80**, 143-157.

Studer A. S., Martínez-Garcia A., Jaccard S. L., Girault F. E., Sigman D. M. and Haug G. H. (2012) Enhanced stratification and seasonality in the Subarctic Pacific upon Northern Hemisphere Glaciation-New evidence from diatom-bound nitrogen isotopes, alkenones and archaeal tetraethers. *Earth Planet. Sci. Lett.* **351-352**, 8494.

Swann G. E. A. (2010) Salinity changes in the North West Pacific Ocean during the late Pliocene early Quaternary from 2.73 Ma to 2.52 Ma. *Earth Planet. Sci. Lett.* **297**, 332-338.

Swann G. E. A., Leng M. J., Sloane H. J., Maslin M. A. and Onodera J. (2007) Diatom oxygen isotopes: Evidence of a species effect in the sediment record. *Geochemistry, Geophys. Geosystems* **8**, 1-10.

Swann G. E. A., Maslin M. A., Leng M. J., Sloane H. J. and Haug G. H. (2006) Diatom

$\delta^{18}O$ evidence for the development of the modern halocline system in the subarctic northwest Pacific at the onset of major Northern Hemisphere glaciation. *Paleoceanography* **21**, 1-12.

Takahashi T., Olafsson J., Goddard J. G., Chipman D. W. and Sutherland S. C. (1993) Seasonal variation of CO_2 and nutrients in the highlatitude surface oceans: A comparative study. *Global Biogeochem. Cycles* **7**, 843-878.

Takahashi T., Sutherland S. C., Chipman D. W., Goddard J. G. and Ho C. (2014) Climatological distributions of pH, pCO_2, total CO_2, alkalinity, and $CaCO_3$ saturation in the global surface ocean, and temporal changes at selected locations. *Mar. Chem.* **164**, 95-125.

Tanaka M. and Fujiwara T. (2008) Physiological roles and transport mechanisms of boron: Perspectives from plants. *Pflugers Arch. Eur. J. Physiol.* **456**, 671-677.

Tanaka M., Nemoto M., Horimoto N. and Takahashi K. (2014) Letter to Editor: Concerning the comments"Silicon Species in Seawater" by Professor Exley and Professor Sjöberg. *Spectrochim. Acta. A. Mol. Biomol. Spectrosc.* **117**, 822.

Tanaka M., Takahashi K., Nemoto M. and Horimoto N. (2013) Selectivity of silica species in ocean observed from seasonal and local changes. *Spectrochim. Acta. A. Mol. Biomol. Spectrosc.* **104**, 423-427.

Tans P. (NOAA/ESRL) and Keeling R. (Scripps I. of O. (2016) ESRL Global Monitoring Division.

Thornton D. C. O. (2009) Effect of low pH on carbohydrate production by a marine planktonic diatom (*Chaetoceros muelleri*). *Res. Lett. Ecol.* **2009**, 4-7.

Tiedemann R. and Haug G. H. (1995) Astronomical calibration of cycle stratigraphy for Site 882 in the Northwest Pacific. *Proc. Ocean Drill. Program, Sci. Results* **145**, 283-292.

Tipper E. T., Louvat P., Capmas F., Galy A. and Gaillardet J. (2008) Accuracy of stable Mg and Ca isotope data obtained by MC-ICP-MS using the standard addition method. *Chem. Geol.* **257**, 65-75.

Tréguer P., Nelson D. M., Van Bennekom A. J., Demaster D. J., Leynaert A. and Quéguiner B. (1995) The silica balance in the world ocean: a re-estimate. *Science* **268**, 375-379.

Trotter J., Montagna P., McCulloch M., Silenzi S., Reynaud S., Mortimer G., Martin S., Ferrier-Pags C., Gattuso J. P. and Rodolfo-Metalpa R. (2011) Quantifying the pH "vital effect" in the temperate zooxanthellate coral *Cladocora caespitosa*: Validation of the boron seawater pH proxy. *Earth Planet. Sci. Lett.* **303**, 163-173.

Uchikawa J., Penman D. E., Zachos J. C. and Zeebe R. E. (2015) Experimental evidence for kinetic effects on B/Ca in synthetic calcite: Implications for potential $B(OH)_4$ and $B(OH)_3$ incorporation. *Geochim. Cosmochim. Acta* **150**, 171-191.

Vengosh A., Kolodny Y., Starinsky A., Chivas A. R. and McCulloch M. T. (1991) Coprecipitation and isotopic fractionation of boron in modern biogenic carbonates. *Geochim. Cosmochim. Acta* **55**, 2901-2910.

Venn A. A., Tambutté E., Holcomb M., Laurent J., Allemand D. and Tambutté S. (2013) Impact of seawater acidification on pH at the tissueskeleton interface and calcification in reef corals. *Proc. Natl. Acad. Sci.* **110**, 1634-1639.

Venn A., Tambutté E., Holcomb M., Allemand D. and Tambutt S. (2011) Live tissue imaging shows reef corals elevate pH under their calcifying tissue relative to seawater. *PLoS One* **6**, e20013.

Verity P. G., Robertson C. Y., Tronzo C. R., Andrews M. G., Nelson J. R. and Sieracki M. E. (1992) Relationships between cell volume and the carbon and nitrogen content of marine photosynthetic nanoplankton. *Limnol. Oceanogr.* **37**, 1434-1446.

Vogl J. and Rosner M. (2012) Production and certification of a unique set of isotope and delta reference materials for boron isotope determination in geochemical, environmental and industrial materials. *Geostand. Geoanalytical Res.* **36**, 161-175.

Vrieling E. G., Gieskes W. W. C. and Beelen T. P. M. (1999) Silicon deposition in diatoms: control by the pH inside the silicon deposition vesicle. *J. Phycol.* **559**, 548-559.

Weeks R. J., Roberts A. P., Verosub K. L., Okada M. and Dubuisson G. J. (1995) Magnetostratigraphy of upper cenozoic sediments from leg 145, North Pacific ocean. *Proc. Ocean Drill. Program, Sci. Results* **145**, 491-521.

Wischmeyer A. G., Del Amo Y., Brzezinski M. and Wolf-Gladrow D. A. (2003) Theoretical constraints on the uptake of silicic acid species by marine diatoms. *Mar. Chem.* **82**, 13-29.

Woods W. G. (1996) Review of possible boron speciation relating to its essentiality. *J. Trace Elem. Exp. Med.* **9**, 153-163.

Wu Y., Campbell D. A., Irwin A. J., Suggett D. J. and Finkel Z. V. (2014) Ocean acidification enhances the growth rate of larger diatoms. *Limnol. Oceanogr.* **59**, 1027-1034.

Wu Y., Gao K. and Riebesell U. (2010) CO_2-induced seawater acidification affects physiological performance of the marine diatom *Phaeodactylum tricornutum. Biogeosciences* **7**, 3855-3878.

Wu Y., Jeans J., Suggett D. J., Finkel Z. V. and Campbell D. A. (2014) Large centric diatoms allocate more cellular nitrogen to photosynthesis to counter slower RUBISCO turnover rates. *Front. Mar. Sci.* **1**, 1-11.

Yang G. and Gao K. (2012) Physiological responses of the marine diatom *Thalassiosira pseudonana* to increased pCO_2 and seawater acidity. *Mar. Environ. Res.* **79**, 142-151.

Yu J., Elderfield H. and Hnisch B. (2007) B/Ca in planktonic foraminifera as a proxy for surface seawater pH. *Paleoceanography* **22**, PA2202.

Yu J., Foster G. L., Elderfield H., Broecker W. S. and Clark E. (2010) An evaluation of benthic foraminiferal B/Ca and $\delta^{11}B$ for deep ocean carbonate ion and pH reconstructions. *Earth Planet. Sci. Lett.* **293**, 114-120.

Zeebe R. E. and Wolf-Gladrow D. (2001) *CO_2 in Seawater: Equilibrium, Kinetics, Isotopes.* Third., Elsevier Ltd, Oxford.